Control of Structures Using SMA Wires and Piezoelectric Patches

RMIT University

A thesis submitted in total fulfilment of the requirements for the degree of

Doctor of Philosophy

by

Mohammed Abdullah Hariri (BSc, MSc)

School of Aerospace, Mechanical & Manufacturing Engineering

College of Science, Engineering & Technology

RMIT University

March 2009

To my family especially my parents for their support....

DECLARATION

Except where due references are made, the work reported in this thesis is solely that of the author alone and has not been submitted or published previously, in whole or in parts, for any academic award.

The work that is reported in this thesis was carried out between the official periods of candidature at RMIT University.

Mohammed Abdullah Hariri 27 March 2009

ACKNOWLEDGEMENTS

ABSTRACT

Smart materials and structures systems are increasingly being developed to handle more complex problems. One of the main research schemes is the augmentation of the control authority of the smart actuators used in such systems. The augmentation can be obtained by constructing hybrid and multi- smart materials actuator systems and/or by the optimization of the location and orientation of those actuators. In the first part of this study, the alteration of the natural frequency of composite structures using Nitinol-based Shape Memory Alloy (SMA) wires will be presented using the analyses of strain energy perturbations on a plate. These governing strain equations were solved analytically and numerically to show the effect of point forces acting in a distributive manner and the subsequent effect it has on the plate's stiffness and hence it's natural frequency. In the second part of the thesis, a more complex loading condition is considered to investigate piezoceramic actuator control authority in relation to wing flutter control.

The advancement in the application of active material induced-strain actuation such as piezoelectric materials in suppression of structural vibrations drew wide interest in its use for wing flutter control. Higher flutter speed and hence wider operating envelope was achieved by delaying the coalescence of the eigenvalues for plunge and twist modes. . This delay is obtained by adding more strain energy to the system as a result of the activation of the piezoelectric actuators. Most of the studies done were by controlling the plunge/bending motion, where the piezoelectric actuators are bonded longitudinally to produce bending moments. In this study, the control of the pitch/twisting motion was investigated and it showed better control of flutter by using simultaneous multi-actuations compared to single piezo actuations. It was shown that within the scope of the angular orientations of the piezoelectric patches investigated in this study, piezoelectric patches oriented about $+15^0$ from the beam's longitudinal axis resulted in the most optimal piezo-configuration. This was corroborated by both the numerical flutter speed and actuator moment evaluations. In addition, the orientation of the piezoelectric patches was shown to significantly affect the pitch angle of the beam relative to each other. The damping ratio was also investigated and this showed greater instability for piezoelectric patches oriented at negative angles, thus further supporting the finding of the aforementioned optimal orientation of $+15^0$. These findings confirmed the dominance of the base (closest to the fixed portion of the beam) piezo when actuated with other piezos.

TABLE OF CONTENTS

LIST OF FIGURES

LIST OF TABLES

NOMENCLATURE

A_{ij}	Extensional stiffnesses matrix	
B_{ij}	Bending-extensional coupling stiffnesses matrix	
D_{ij}	Bending stiffnesses	
E	Modulus of elasticity.	Pa
$\mathbb{E}$	Electric field.	V/m
EPA	Effective Pitch Angle	Radian
Fa	External force due to pitching moment.	N
Fap	Torsional piezoelectric moment.	N.m
F_i	External force due to lift.	N
F_P	Piezoelectric force.	N
G	Shear modulus of elasticity.	Pa
GA	Geometric torsional stiffness due to piezoelectric	
GH	Geometric bending stiffness due to piezoelectric	
Ga	Geometric bending-torsional stiffness due to piezoelectric	
I_0, I_2	Mass moments of Inertia	
JA	Torsional stiffness/rigidity	
K	Kinetic energy.	
KA	Plane-torsional stiffness	
KH	Flexural stiffness/rigidity	
Ka	Bending-torsional stiffness	
Kh	Torsional-bending stiffness	
K_x, K_y, K_{xy}	Curvatures of the plate	
L	Aerodynamic lift	N
M	Aerodynamic pitching moment	N.m
Maa	Polar mass moment of inertia	
Mah,ha	Product mass moment of inertia	
Mhh	Mass/inertia	Kg
$M_{xx,yy}$	Structural moments	N.m
M_x	Structural moment per unit length in x-direction	N.m/m
M_y	Structural moment per unit length in y-direction	N.m/m

M_{xy}	Structural twisting moment per unit length	N.m/m
N	Plane force	N
N_x	Force per unit length in the x-direction	N/m
N_y	Force per unit length in the y-direction	N/m
N_{xy}	Shear force per unit length	N/m
$\bar{Q}$	Plane stress-reduced stiffness in system/problem coordinates	
Q_{ij}	Reduced stiffness coefficient	
Q_x, Q_y	Shear forces per unit length	N/m
T	In-plane loads induced due to Shape memory Alloy wires	
U	Potential energy	
U_∞	Free stream air velocity	m/s
V	Work done by external forces	
X,Y,Z	System/problem coordinate	
$Y_{0,1,2}$	Chord integrals	
a	Length of the composite plate	m
b	Width of the composite plate.	m
d	Piezoelectric strain coefficient.	m/V
e	Piezoelectric stress coefficient.	
h	Wing bending displacement in Z-direction	
h	Ply thickness.	m
l	Beam length	m
p	Aerodynamic pressure	
q	Induced pressure due to ply weight.	Pa
u, v, w	Plate displacements in x, y, z directions	m
x,y,z	Axes	
$\propto$	Angle of attack	
δ	Variation operator	
∂	Partial differential operator	
ε	Strain	
$\varepsilon_x, \varepsilon_y$	Strains in x, y directions of the plate,	
ε_{xy}	Shear strain of the plate,	
$\sigma_x, \sigma_y, \sigma_z$	Tensile stresses,	

σ_{xz}, σ_{yz}		Transverse shear stresses,
ρ		Density
ρ_0		Density of the composite plate
ϕ, ψ		Approximation functions
ζ_h		Flexural/Plunge damping ratio
ζ_α		Torsional/Pitch damping ratio

Chapter 1. INTRODUCTION

1.1.Background

Although the static properties such as strength and stiffness are major considerations in designing mechanical structures, the dynamic properties such as fatigue and resonance of the structure have a significant role in the design process. For example, the importance of considering the resonance comes from the fact that during the resonance, the amplitude of the vibration is magnified to levels that may lead to a catastrophic event. While the usual design process depends on the collected experiences and statistical data, a developing trend is to implement smart technologies to develop smart structures that are capable of self-monitoring, diagnostics and repair.

The technology of Smart materials and Structures has given a new face of development to the fields of Aerospace, robotics and structural engineering due to which the demand for less weight stand-alone systems is growing. Smart materials [1] represent a group of functional materials, which can sense and respond to changes in their environment in a predefined manner, they also have the flexibility to go back to their initial stage once the changes in the environment come down. Smart Structures are structures that can sense certain stimuli and respond accordingly, somewhat like Humans. They can interact with external environment and have the ability to adapt to varying loading scenarios. Research on smart structures has emphasized the incorporation of various devices in a structure to provide Smart functions like Strain sensing (for structural vibration control and traffic monitoring), Damage sensing (for Structural health monitoring), Temperature sensing (for Hazard mitigation & Structural performance control), Structural vibration control. In the process of developing Smart structures materials like piezoelectrics, Shape Memory Alloys (SMAs) and Electro Rheological Fluids (ERFs) are used for sensing the different loading conditions and actuation to deliver a required force to maintain the equilibrium.

Due to its importance and complexity, the aerospace discipline becomes one of the major developers and utilisers of the smart materials and structures technology. Several applications of smart structures were exploited such as (i) vibration and acoustic control; tail buffet suppression, flutter damping, engine vibration control and active acoustic control, (ii) shape control; adaptive smart wing, adaptive engine inlet, adaptive Micro Air Vehicles and vortex wake control, (iii) multifunctional smart structures; smart skin and antenna, structure-power

materials and (iv) morphing aircraft structures [2]. Most of these applications are to enhance the aircraft performance however the most important application is the flutter damping or control as it may lead to a catastrophic event. Traditionally, the wing flutter problem (and other Aeroelasticity phenomena) was treated in design stages via altering the stiffness of the structures, the mass distribution and the position of the flexural axes. The process outcome is an operational envelop that limit the boundaries (basically the flutter critical speed) of the operation of the aircraft to prevent catastrophic structure failure. Then in the event of the flutter, it is controlled or damped using the conventional aerodynamic control surfaces operated by servo-hydraulic actuators. To replace these heavy equipments several smart actuators were investigated such as induced helicopter blade twist, active blade tip with bending-torsion ISA actuator, rotor blade flap actuation, bimorph servo-flap actuation, C-block and recurved flap actuators, and piezostacks actuated servo-flaps [3]. In aeroelastic systems, the shape of the structure affects the aeroloading on that structure, and hence higher actuator forces are required to control aerostructures effectively.

Each of smart sensor and actuator materials has its own advantages and disadvantages. For example, SMA generates large forces but in low frequency, while the piezoelectrics generate lower forces but at higher frequencies. However, by careful selection, numerous classes of hybrid actuation systems can be synthesized to satisfy a broad range of performance requirements [4], [5], [6].

1.2. Objectives

The main theme of this study is to investigate the possible methods to augment the control authority of smart structures and their applicability in complex structural dynamic problems such as flutter suppression/control of aerostructures. Two streams were examined; hybrid actuation system of SMA and Piezoelectric materials, and multi-actuation of an advanced piezoelectric material technology, namely, the Active Fibre Composite (AFC).

The research questions are set as follows:

- Can SMA's adequately control structures?

- How can SMA's affect natural frequency?

- Can activated SMA's be properly modeled?

- Can the optimized actuation of Piezoelectrics adequately control flutter?

16

- Is torsional control more effective than bending in overall flutter response?

1.3. Thesis Structure

Figure 1 shows the overview of the work conducted in the study. The thesis is structured to follow the sequence of the research work.
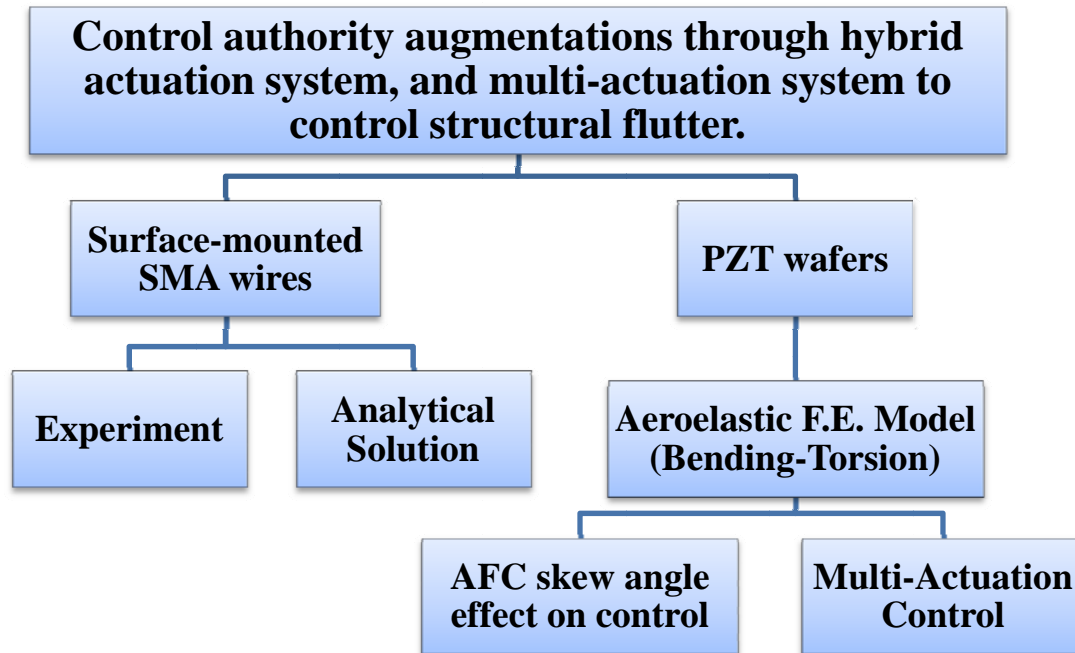
Figure 1.1: The structure of the research work.

The organization of the thesis chapters are shown below:

Chapter 1: The Introduction chapter contains the background, the objective, publications that have emerged from this work and the layout of the thesis.

Chapter 2: The literature reviews of the various disciplines of control and smart structures that form the body of knowledge are compiled in this area.

Chapter 3: Mathematical modelling, analytical solution and experiment work of the alteration of the dynamic properties of a strip using SMA wires are presented in this chapter. The mathematical formulation starts from basic solid mechanics and ends with the comparison with the experiment results.

Chapter 4: This chapter deals with the flutter phenomena and its control. The equations of motion of the aeroelastic structure incorporating piezoelectric patches are derived in this chapter. Also, this chapter contains the Finite Element model constructed to solve these equations.

Chapter 5: In this chapter the control law and the formulation of the aerodynamic forces and actuators matrices are presented. The computer program validation and the numerical simulation results and discussion are also presented in this chapter.

Chapter 6: This chapter is dedicated to the overall conclusion and the recommendations for the further work.

1.4.Publications

1.4.1. Journals

1. S John & M Hariri, (2008), 'Effect of Shape Memory Alloy Actuation on the Dynamic Response of Polymeric Composite Plates'. Composites A Journal 39, pp 769-776.

2. M Hariri, S John & P Trivailo, (2008), 'Configuration of Piezoelectric Patches in Mitigating Structural Flutter, Proceedings of the 2008 ASME conference on Smart Materials, Adaptive Structures & Intelligent Systems, Baltimore, USA, Paper 405, ISBN 978-07918-3839-6. (Submitted to a special edition of the journal of Smart Materials & Structures - 2009).

1.4.2. Conferences

3. M Hariri, S John & B Veeramachaneni , (2006), 'Vibration control of composite plates using shape memory alloys', Proceedings of the 14th International Conference on Composites/Nano Engineering Boulder, Colorado, USA, Editor D Hui, July, 2006.

4. M Hariri, B Veeramachaneni and S John (2006), ' Vibration Control of Polymeric Composite Plates using Shape Memory Alloys', Smart Structures and Materials 2006 SPIE (Society of Photo-optical & Instrumentation Engineers) publication, SPIE Vol. 6167, Paper ID -616710.

5. M Hariri, S John & P Trivailo, (2008), ' Control of structural flutter using Piezoelectric Patches, Proceedings of the 2008 ASME conference on Smart Materials, Adaptive Structures & Intelligent Systems, Baltimore, USA, Paper 405, ISBN 978-07918-3839-6.

Chapter 2.   LITERATURE REVIEW

2.1. The Concept of Smart Structures

Mechanical structures have evolved from passive load-carrying elements into interactive systems known as Smart Structures which can be defined as "structures possessing the capability to sense and actuate in a controlled manner in response to variable ambient stimuli" [7]. In the same manner, Rogers and Giurgiutiu [8] defined the smart structures as " the integration of actuators, sensors, and controls with material or structural component". These two definitions are limited to the description of the components comprise such systems but not their functionality. Takahashi (cited in [9]) defined the smart structures as "those which posses characteristics close to, and, if possible, exceeding, those found in biological structures". Such characteristics include sensing, actuation, adaptability, sustainability and survival, selectivity, stability, self-diagnosis, self-repair, multifunctionality, reproduction, memory, recognition, discrimination, etc [9]. This definition describes wide range of functionalities that can be designed and implemented in mechanical structures by mimicking biological structures. However, Rogers and Giurgiutiu [8] distinguish between the biological and smart structures in that the biological structures serve themselves, while the smart structures produce artefacts designed by human being to serve human needs. They define the adaptronic structures as those to "be designed for a given purpose; and, by the transduction of energy, must be able to modify its behaviour to create an envelope of utility." Wadhawan [9] summarized the definition of the smart structures in "Smart or adaptronic structures are structures with an ability to respond in a pre-designed useful and efficient manner to changing environmental conditions, including any changes in their own conditions."

Although the smart structure functionalities go beyond those of the biological ones, full mimicking of biological systems is still far from realization. The biological/living systems comprise several subsystems as depicted in Figure (2.1). The sophistication (smartness) of these systems depends on the level of the interaction between these subsystems. These subsystems are the host structure (body), sensors (nerves), actuators (muscles), control centre (brain), and the energy source [9]. One can add that those subsystems have the capabilities to regenerate themselves and grow.
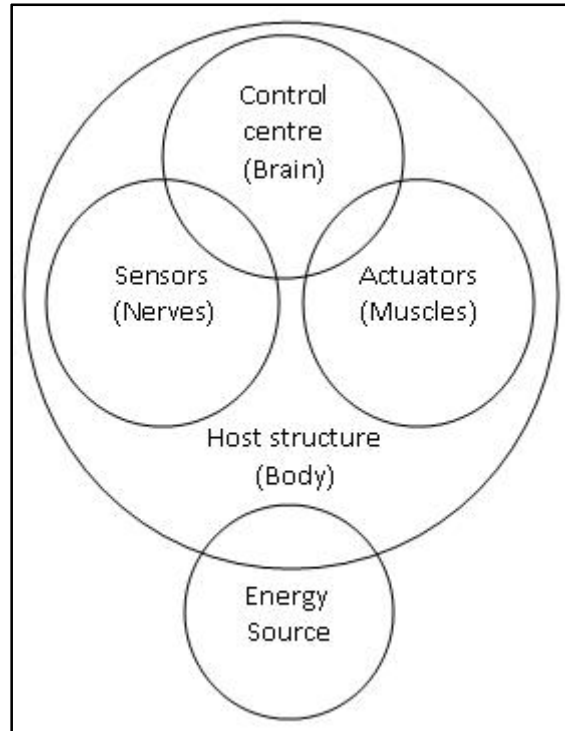
Figure 2.1: Subsystems of living/biological systems.

Likewise, the smart structures employ distributed and on-line sensors, actuators and microprocessors to measure (sense) the change in the surrounding environment and take corrective or preventive actions.

Each of the smart structure subsystems leads to different line of applications. For example, Structural Health Monitoring (SHM) which is one of the fastest emerging technologies is an application emphasizing on the sensors subsystem. In SMH, loading capacity of the structure (load carrying) is monitored and structural failure can be predicted allowing time to intervene and prevent catastrophic consequences. SHM technology is well implemented in Nuclear reactor walls and common bridges. It is also progressively used in maritime and aerospace fields where the polymeric composite structures, which are prone to cracking, are becoming dominant. Emphasizing on the muscles (actuators) leads to shape control functionalities. The concepts of morphing wing and airfoil with variable cambers are promising in developing efficient aircraft by optimizing airfoil shapes and replacing the heavy hydraulic equipments [10], [11, 12], [12] & [3]. Intelligent structures capable of learning from the surrounding environment and making decisions based on that learning are feasible by incorporating *Artificial Intelligence* techniques such as *Neural Networks, Fuzzy Logics and Genetic Algorithms*, in the control subsystem. The concept of self-healing structures, shown in Figure (2.2) [13], currently grasps significant attention from the scientific community. Energy

harvesting from vibrating structures is also an emerging technologies aiming to develop efficient and stand alone structural systems.
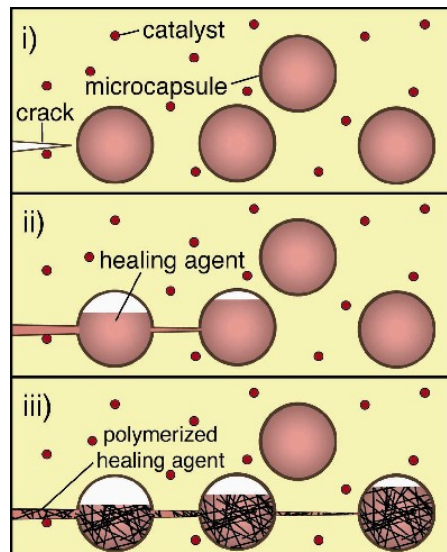
Figure 2.2: Self-healing structures concept [13].

Smart Structures is an interdisciplinary technology which includes materials science and engineering, electronics and signal processing, and control. The advancements in these disciplines have broadened the scope of smart structures and helped in the development of reliable and efficient smart structure systems. With the fundamental roles of the digital and micro-electronics and –processors technologies in realizing of the smart structures, nanotechnology will get these structures into unprecedented levels.

2.2. Smart Materials

2.2.1. Overview

In most of the literatures the materials used in smart structures and systems are called *smart materials*. However, this term is debatable; "Is the material smart by itself?" In engineering, smart systems basically turn complex and surplus information into useful outcomes. In this sense, Culshaw viewed that *smartness* requires some sort of entropy reduction [14]. First of all, for the entropy reduction to take place an outside energy source is required, in other words, "all smart system have some form of energy source associated with them" [14]. Another important aspect in defining the *smartness* is the requirement of information reduction, where the complex information is refined to produce useful function(s). This requirement is known as *Information-reduction criterion* [9]. These two requirements are clear when comparing between the simple pressure transducer and the pressure transmitter. The pressure transducer could not be regarded as smart because the input pressure produces a

voltage in one-to-one relationship. In contrast, the pressure transmitter incorporating a thermocouple that measures both the pressure and the temperature reduces this (surplus) information to a single value of temperature-corrected pressure. Here, the temperature fluctuation acts as a source of energy which is converted into mechanical forces and corrects the apparent pressure [14]. The pressure transmitter satisfies both the energy and information-reduction requirement of the *smartness*.

The materials used in smart systems come under the generic classification known as *functional materials* which are those "can perform certain functions when triggered by environmental stimuli or control signal" [15]. The functional materials can be categorized in to passive and active groups. The passive functional materials are characterized by the existence of anomalies in one or more of their physical properties or phase transition that can be used as a function. For example, the fact that the volume of the mercury changes with temperature is used in thermometer to measure the temperature. The active functional materials are characterized by their capability to convert energy from one form to another such as shape memory alloys, piezoelectric, magnetostrictive and electrostrictive materials [15]. Wadhawan [9] redefined the smart materials as "that subset of functional materials which satisfy Culshaw's *information-reduction* criterion."

2.2.2. Shape Memory Materials

Shape memory effect in alloys dates back to the 1930s, however it was the discovery of Nickel Titanium alloy by Buehler and Wiley from the Naval Ordinance Laboratory in 1962 which proved that Shape Memory Alloys exhibit unique mechanical memory [16]. SMAs have the ability to return to their predefined shape from large strains without undergoing plastic deformation. This ability of recovering its shape after undergoing a shape change with the help of a rise in temperature is called Shape Memory Effect (SME). This shape change occurs due to changes in the atomic crystal structure as shown in Figure (2.3).

The chemical composition of Ni-Ti alloys is 50%Ni / 50% Ti, with small additions of copper, iron, cobalt, or chromium. The crystal structure of SMAs for example Ni-Ti is cubic when the temperature is high, this cubic crystal structure is called austenite. When the SMA is cooled the material then transforms to a monoclinic lattice structure, which looks like parallelogram in two dimensions, and is called martensite. When the SMA, which contains many atoms, is cooled the rows of atoms alternatively tilt in left and right directions. This property of arrangement of atoms is called "twinning" as the atoms form mirror images of themselves

through a symmetrical plane. Any four connected atoms in the low temperature structure have martensite parallelogram shape. The stress required to rearrange the twinned SMA is relatively low. Thus, the application of sufficient stress to deform the SMA leads to the atoms being reoriented so that they all lie in the same direction. This property is called "detwinning". If the SMA is heated the deformed martensite will revert back to austenite phase and the original shape of the piece will be obtained. This occurs as a result of atomic positions always being maintained in the austenitic phase [17].
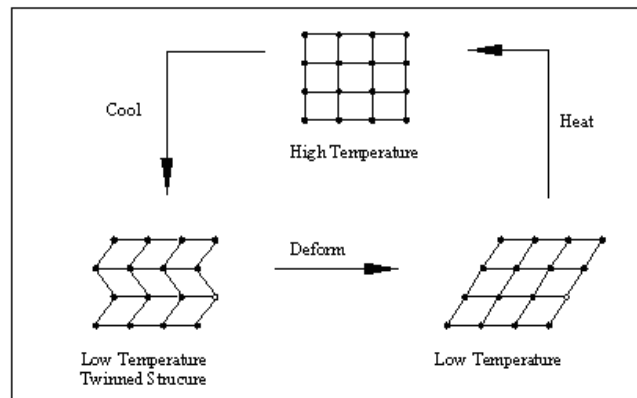
Figure 2.3 Description of Shape Memory effect [17].

The SMA's have very good corrosion resistance and biocompatibility, which enable them to be widely used in the biomedical field. Plastic strains of 6-8 % may be completely recovered by heating SMA, which can also change its properties reversibly especially Young's Modulus during the phase transformation. As a result of the Ti-Ni alloys being readily fabricated into various forms or sizes, it is technically feasible to make them an active element in various composites. In particular, Ti-Ni thin films, fibres, particles and porous bulks have been successfully fabricated in recent years, hence these materials, either in the monolithic form or in combination with other materials, have exhibited some exciting application potentials in Micro-Electro-Mechanical systems (MEMs), medical implants, intelligent materials and structural systems. Shape memory alloys have proven to be successful in many commercial applications such as Hitachi's Robotic Hand, radiator valves, greenhouse vents etc. In every application, SMA has demonstrated large force and displacement capabilities and low power consumption with lightweight added to the operating device [17].

C.A. Rogers et al. [18], [19] embedded SMA wires into composite plates and demonstrated the ability to alter the effective stiffness, natural frequencies and mode shapes of the plates. Two concepts were used; Active Strain Energy Tuning (ASET) and Active Modal

Modification (AMM) or Active Property Tuning (APT). Using Rayleigh-Ritz method several structural cases were analysed; bending deflection, buckling and acoustic transmission loss.

In the ASET technique the SMA wires are plastically elongated and embedded in to the composite material at its neutral axis. By curing the composite material at high temperature the SMA wires are constrained from contracting to their normal length. When the fibres are heated, the SMA fibres try to contract to their memorized length generating a recovery force. The resultant force will therefore adaptively change the structural response of the plate. On the other hand the Active Property Tuning (APT) method avoids inducing large internal stresses in a SMA composite plate. This method embeds the SMA wires to the composite plate without plastic elongation. As the Young's modulus of the embedded SMA fibres will change from 4 to 12 Mpsi during the phase transformation, the embedded SMA fibres will change the overall stiffness of the plate resulting in a change of structural response of the plate [19].

In 1990, A Baz et al. [20] demonstrated both theoretically and experimentally, the feasibility of utilizing SMA in controlling the flexural vibrations of a flexible cantilever beam. Unlike the work done by Rogers *et al*, the SMA wires are placed external to the beams, in order to enhance the cooling and dynamic response characteristics of the SMA.

Chaudhry et al. [21] demonstrated experimentally the ability to induce large bending displacements of beams using SMA wire actuators. The SMA wires are placed externally in two different configurations.

Two experiments were carried out by Srinivasan [22] (cited in [16]) to explore the use of the SMAs in passive and active vibration control of structures. In the first experiment the vibration control was obtained by using SMA wire fastened to the beam in V-configuration and a forcing piezoelectric patch. Both actuators are located at the root of the beam. Multiple SMA wires were used in the second experiment to demonstrate the ability to control the beam in different frequencies.

2.2.3. Piezoelectric Materials

The piezoelectricity (piezein in Greek means press) goes back to the behaviour of the Tourmaline stone which if it were put into hot ash, the ash particles are attracted to one side and are rejected from the other side [23]. During their experiments on several crystals (Tourmaline, Quartz, Topaz ...etc.), Pierre and Jacques Curie in 1880 discovered the direct

piezoelectric effect; mechanical deformation in certain directions causes proportional electrical charges at opposite faces of the crystals. Later the brothers Curie, through experimentation, were able to confirm the converse effect (electrical charges cause deformation) which is deduced mathematically by Lippmann in 1881 [23], [24]. The work on piezoelectricity continued until the publication of '*Lerbuch der Kristallphysik*' (1910); a standard reference defining the natural crystal classes associated with the piezoelectricity effects and the macroscopic piezoelectricity coefficients. In 1917 and during World War I, P. Langevin and French co-workers succeeded in developing an ultrasonic submarine detector (sonar) using thin quartz crystals. Intense activities in developing piezoelectric devices were motivated by the success of the sonar. During World War II, easily manufactured ceramic materials, known as *ferroelectrics*, exhibiting astonishing dielectric characteristics (100 times higher than common crystals) were discovered in isolated research groups in U.S., Japan and Soviet Union [24]. The barium titanate and lead zirconate titanate piezoceramic families were developed during this period. The commercial use of the piezoelectric materials grew especially in Japan where several devices employing piezoceramics had been produced such as signal filters used in televisions and communication equipments, audio buzzers in (smoke alarms). Piezoelectricity has become the heart of solid-state motion technology aiming to replace solenoid actuators with electrostatic actuators.

The generation of the piezoelectric effect in certain crystals is due to the nature of their atomic structure where the positive and negative ions are bonded in asymmetric structure. This asymmetry induces an electrical dipole (Polar). For example, the α-quartz crystal structure shown in Figure (2.4) has a neutral electric charge.
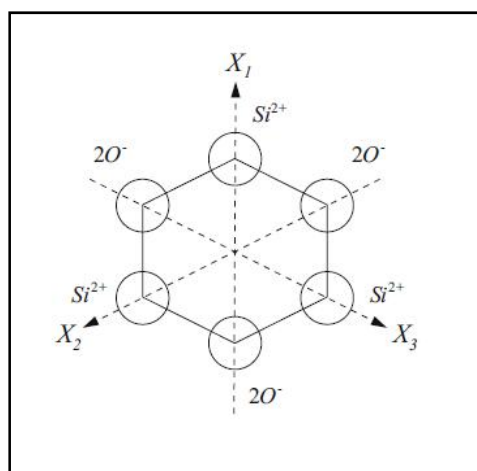
Figure 2.4: Quartz crystal structure [23].

Under deformation the positive and negative ions are displaced against each other causing the electric polarization as in Figure (2.5) [23].
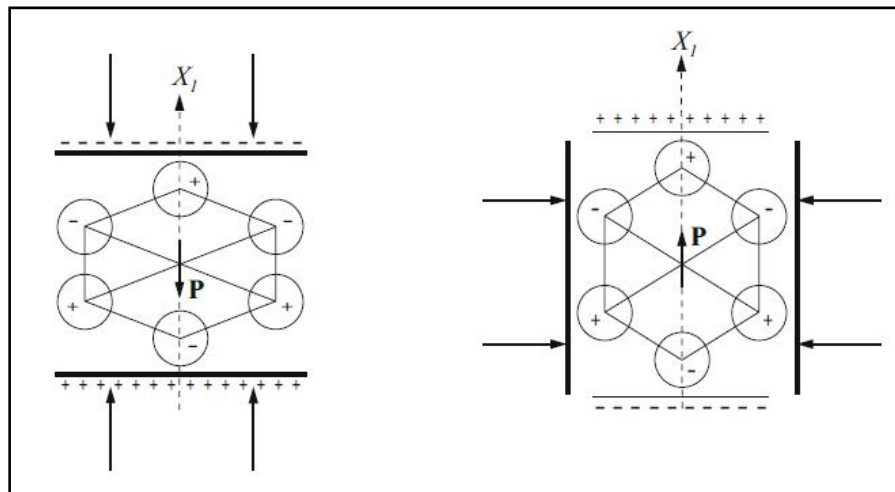
Figure 2.5: Direct piezoelectric effect of quartz cell due to applied deformation [23].

For the case of the piezoceramic (*ferroelectric*) materials, the crystal grain structure is symmetrical (cube texture) above a certain temperature T_C known as *Curie temperature* whereas below this temperature the structure is distorted into tetragonal texture as in Figure (2.6). This distortion is known as *spontaneous deformation* [23].
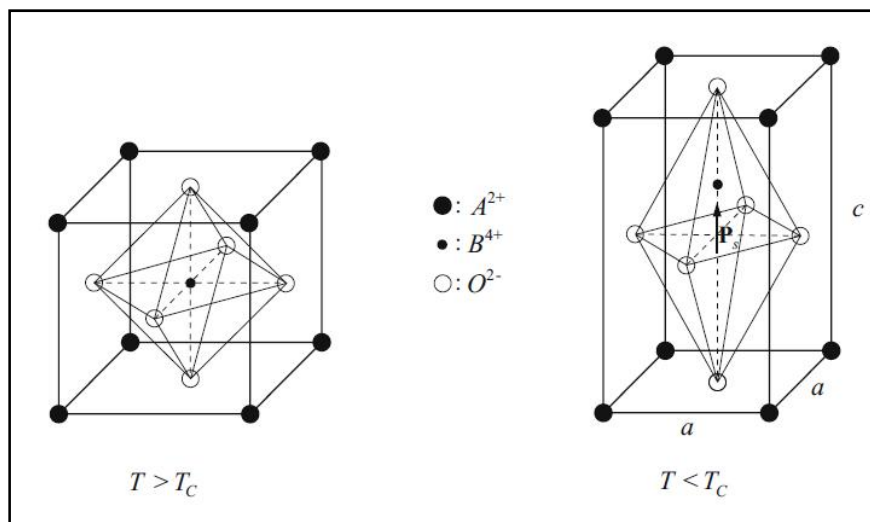
Figure 2.6: Cube and tetragonal structure of a ferroelectric crystal grain [23].

Taking advantage of this characteristic, the piezoceramics are produced in two stages. In the first stage the substrate is prepared at a temperature below T_C to create the tetragonal texture and hence induce the polarization in the grain. However, at this stage the substrate crystal has no piezoelectric characteristics due to the random distribution of the polarized grains thus eliminating the overall (crystal) polarization. In the second stage, sufficient electric field $\mathbb{E}$ in

defined directions is applied on the substrate to align the random grains polarization into the direction of the electric field and hence produce a remnant polarization (piezoelectric behaviour) in the substrate. Figure (2.7) shows the piezoceramic crystal before and after polarization [23].
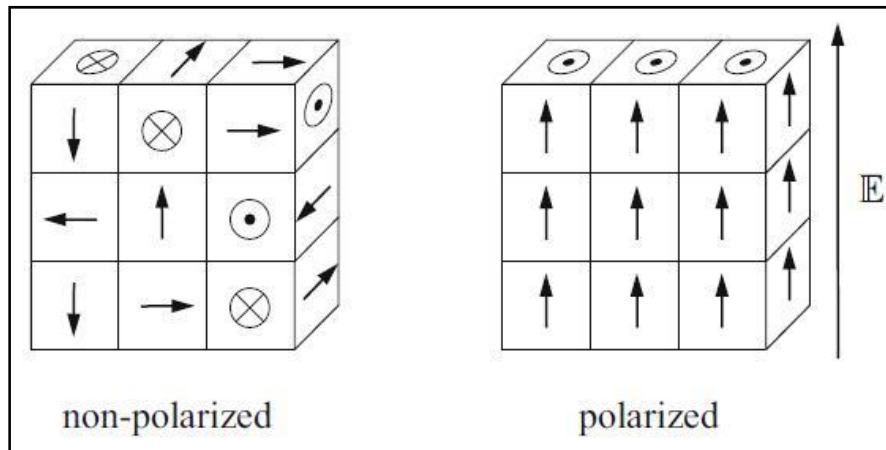
Figure 2.7: Piezoceramic crystal before and after polarization [23].

One of the advantages of the piezoceramics is that they can be prepared in different configurations to meet different requirements. These configurations are based on the polarization direction and the direction of the applied voltage/forces as in Figure (2.8). Also different configurations are based on the number of piezoceramic layers attached to each other; single layer, two layers and multi-layer (stack) motors and generators [25].
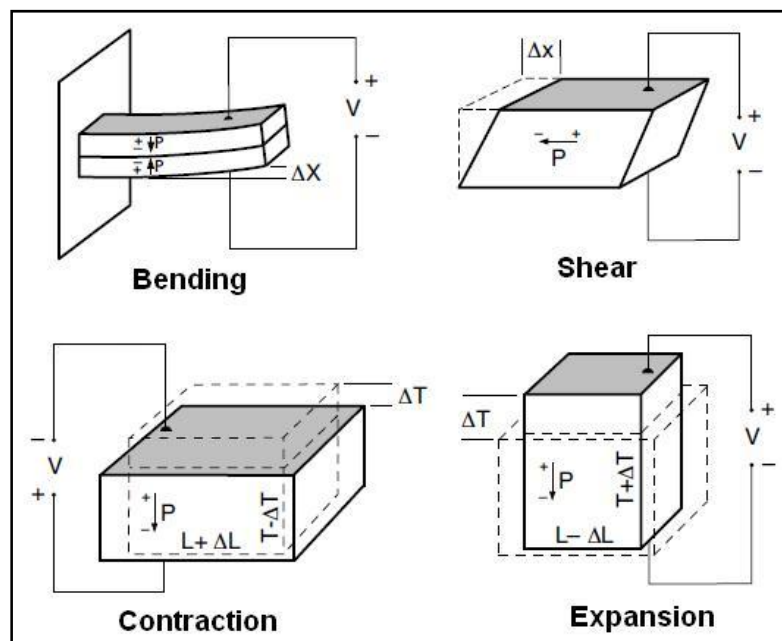
Figure 2.8: Different piezo-effect configurations [25] .

The configuration of more interest in this study is the bimorph (bending) motor/actuator. When bonding a single piezoelectric patch on a beam and clamping it from one side (cantilever) the activation of the patch will produce a bending moment on the beam. This is called *Monomorph* action. If two patches were bonded on the opposite sides of the beam (no clamping) and activated with opposite voltages in such a way that one patch is expanding whilst the other is contracting the patches will produce a bending moment on the beam, this is known as *Bimorph* action as shown in Figure (2.9).
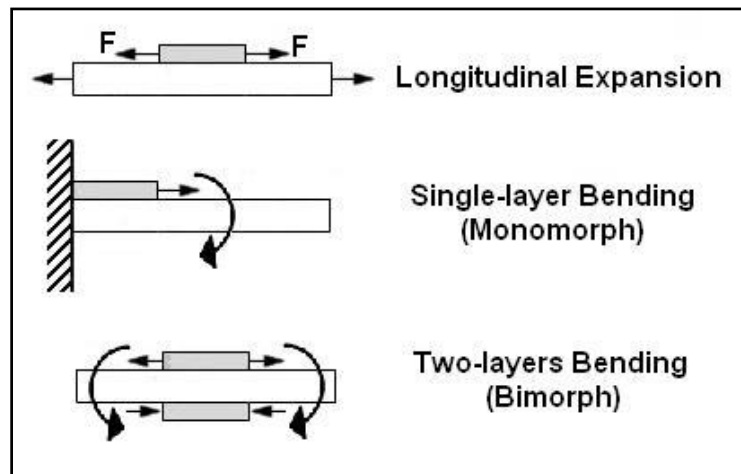
Figure 2.9: Mono & Bi-morph actions.

The easy and low cost manufacturing process in addition to the wide frequency coverage has made the piezoceramics the most popular solid-state generator (sensor; generate electric charge due to strain: direct piezo-effect) and motor (actuator; applying electric field to produce strain: converse piezo-effect). The lead zirconate titanate (PZT) is the most common piezoceramic and it is commercially available and is widely employed in different applications. Several dynamic properties and performances of structures were enhanced by implementing Smart Structures technology employing piezoelectric patches. Faria and Almeida [26] studies proposed a strategy to enhance the non-linear pre-buckling response of slightly crooked composite beams using PZT patches. Low-energy impacts on laminated shells with distributed piezoelectric actuator and sensor layers were investigated by Saravanos and Christoforou [27]. In their study the impact force, displacement and the sensor responses were predicted. They also studied the feasibility active impact control which looked at variation of the natural frequencies of composite laminated beams and plates using the stiffening effect of surface bonded PZT actuators.[28], [29]. Shape control of composite laminated beams using PZT patches were investigated by Sedaghati et al [30].

Suppression of the structures vibrations and acoustic control are the most investigated applications using piezoelectric technology. Vibration and noise suppression is achieved by passive and active techniques. The passive technique basically convert mechanical energy into electrical energy through by connecting the PZT patches with an electrical resistive-inductive shunt circuit [31]. Suleman [32] succeeded in attenuating the noise level in the interior of a closed acoustic cavity using passively actuated PZT patches. In an active technique the system states or the sensors output is fed to a control algorithm and driven the piezoceramic actuators [33]. Moon and Kim [34] presented an active/passive hybrid control design with piezoelectric actuators to suppress nonlinear composite panel flutter.

The major disadvantage of using the piezoceramic actuators in structural dynamics (Smart Structures) is that the higher piezoelectric effect is in the (d_{33} / Z) direction of the polarization and the applied electric field however the action is required in the direction (d_{31} / X) of the hosting structure as shown in Figure (2.10). With unsuccessful efforts of improving the piezoceramic performance (control authority) composition wise, several novel ideas emerged. Raja et al [35] used multilayered (bender) piezoelectric actuators to control the flutter of composite plate.
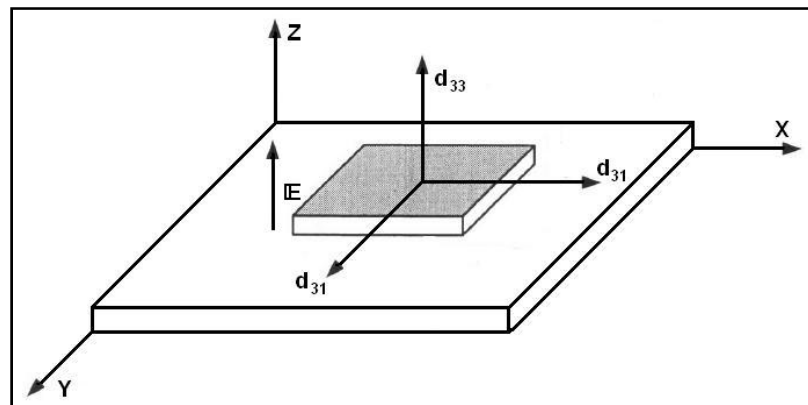
Figure 2.10: Monolithic PZT action directions.

Another method of enhancing the performance of the piezoelectric actuator was achieved by developing the Piezoelectric Fibre Composite (PFC) where composite lamina is constructed using discrete piezoceramic fibres as shown in Figure (2.11) [36], [37], [38]. This method allowed tailoring of the piezoelectric coefficient which enhanced the performance by manipulating the fibre-to-matrix volume ratio and orientation of the fibres. Besides the anisotropic actuation of the PFC, it solved the weak attributes of the monolithic PZT such as low fracture strength, high stiffness and the difficulty in producing complex shapes [37].
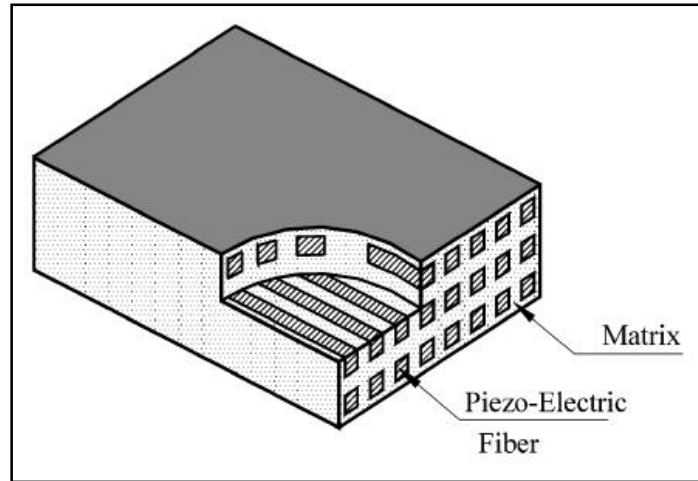
Figure 2.11: PFC structure [38].

However, the multi-layered and the PFC actuators are still utilizing the d_{31} piezoelectric coefficient. The exploitation of the actuation in the d_{33} direction emerged when a novel method of Active Fibre Composites (AFC) actuator was developed by MIT in the early 1990s. The actuator employed the novel Interdigitated Electrodes (IDE) and piezoceramic fibres. As shown in Figure (2.12) the IDE is fabricated in a way that the electric field is in a parallel direction to the longitudinal direction of the piezoelectric fibres which are polarized in the same direction [37], [39].
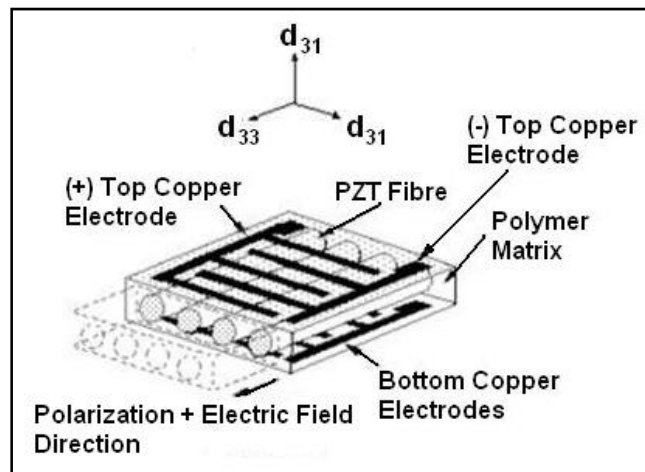
Figure 2.12: Active Fibre Composites (AFC) structure.

The Macro-Fiber Composite™ (LaRC-MFC™) [40] developed by NASA Langley Research Centre is a similar device which retains the AFC features as well as incorporating other new features. The main advantage of this actuator is the low-cost, uniform and repeatable fabrication processes used in making it.

The MFC™/AFC actuators have mostly been employed in vibration and acoustic control. Zhang and Shen [41] developed a three dimensional analytical model of laminated plates

with AFC as damping layers for active control of in-plane axial and transverse vibrations. Azzouz et al [42] studied the effect of the actuation of MFC™ in different locations and at various orientations on the state modal bending and twisting amplitudes of a square and triangular cantilever plates.

The Linear Theory of Piezoelectricity is the famous theory that describes the mathematical relationships between the different piezoelectrics' parameters and effects. The first law of thermodynamics for a piezoelectric medium can be written as [43];

$$\dot{U} = \sigma_{ij}\dot{\mathcal{E}}_{ij} + \mathbb{E}_i\dot{\mathbb{D}}_i \qquad (2.1)$$

Where,

U is the stored energy density for the piezoelectric continuum [44]

σ_{ij} is the stress components

$\mathcal{E}_{ij}$ is the strain components

$\mathbb{E}_i$ is applied electric field

$\mathbb{D}$ is the electric displacement.

Then the linear piezoelectric constitutive equations are derived as [43], [44];

$$\sigma_i = \mathsf{C}_{ij}\mathcal{E}_j - e_{ki}\mathbb{E}_k \qquad (2.2)$$

$$\mathbb{D}_i = e_{ij}\mathcal{E}_j + \epsilon_{ik}\mathbb{E}_k \qquad (2.3)$$

$$\boldsymbol{e} = \boldsymbol{d}\mathsf{C} \qquad (2.4)$$

$$d = \frac{strain\ developed}{applied\ electric\ field} \qquad (2.5)$$

Where,

C_{ij} is the elastic stiffness matrix

ϵ is the permittivity constant.

e is the piezoelectric coupling coefficient for Stress-Charge form, and

d is the piezoelectric strain coefficient for Strain-Charge form.

Eqn. (2.2) is used in actuator mode (Stress-Charge/Voltage form) while Eqn. (2.3) is used in sensor mode (Strain-Charge/Voltafe form).

2.3. Aeroelasticity

Aeroelasticity is a field which looks at the mutual interactions of the three force systems namely; inertial, elastic and aerodynamic forces as depicted in Figure (2.13) [45].
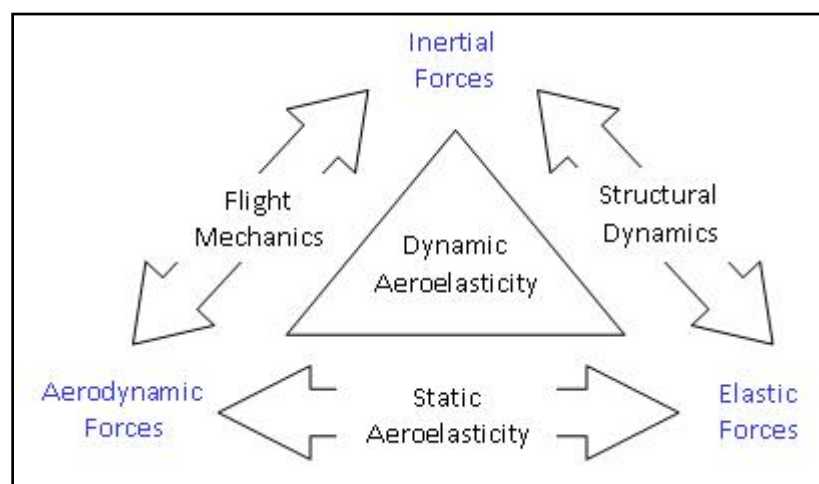
Figure 2.13: Aeroelasticity and the force systems.

Aeroelasticity results from the interaction between the airstream and the structure. By extracting the energy from the airstream, the structure deforms/deflects and hence the air pressure distribution over the structure is changed which in return produces different air-loading and so on and if there is no equilibrium between them the system becomes instable. There are static and dynamic aeroelasticity instabilities. The static instability is due to the interaction between the aerodynamic and the elastic forces such as *Structural divergence*, *Reversal of Control* and *Aerodynamic load distribution* [46]. The dynamic instabilities are due to the interaction of the inertial, aerodynamic and elastic forces. *Flutter*, *Buffeting* and *Gust response* are well known dynamic aeroelasticity instabilities.

Focusing on the flutter, it is an oscillatory motion which occurs due to the interaction of the two modes of wing motion, namely, bending and torsional modes. In stable conditions the plunge/bending and pitch/torsional motions are kept out of phase in a way that the plunge motion is dampened by the pitch motion as shown in Figure (2.14). As the air speed increases the extracted energy increases until a certain point (speed) where the plunge and pitch

motions become in phase and destabilize the system putting it in divergent oscillation (flutter) as shown in Figure (2.15). In other words, the system (lowest) eigenvalues coalesce at this critical speed (flutter speed) as illustrated in Figure (2.16).
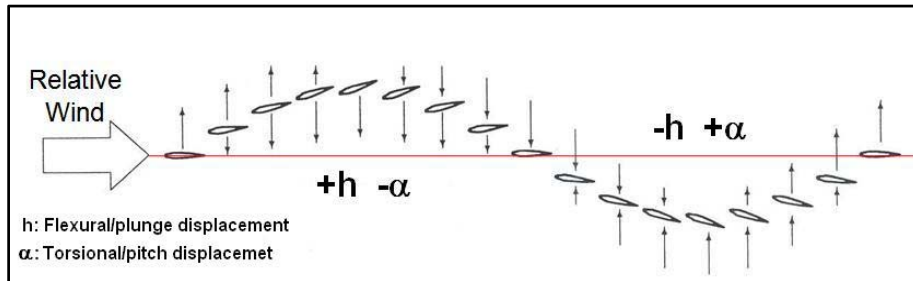
Figure 2.14: Stable wing motion.
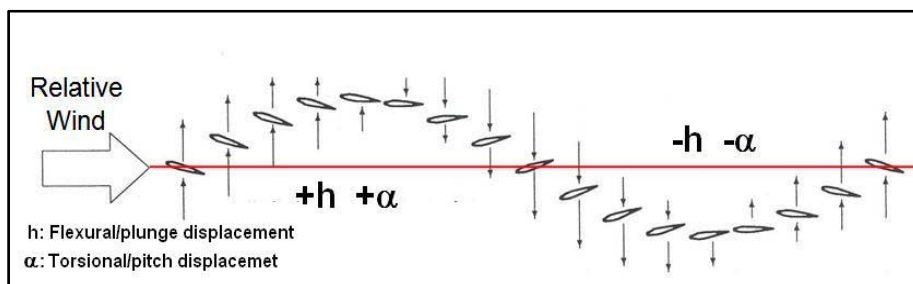
Figure 2.15: Unstable wing motion (flutter).
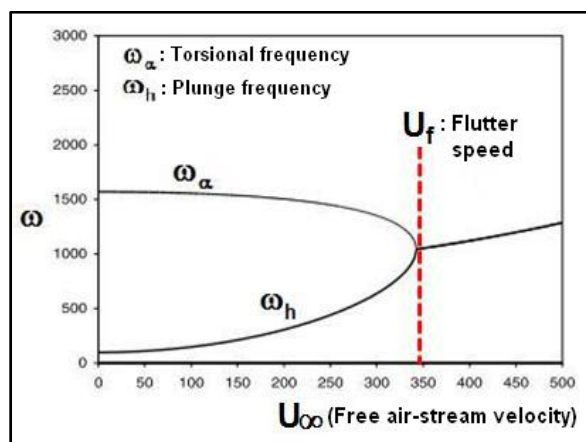
Figure 2.16: Bending and torsional frequencies approaching critical (flutter) speed.

2.3.1. Flutter Analysis

Traditionally, the wing flutter problem (and other Aeroelasticity phenomena) is treated in design stages via altering the stiffness of the structures, the mass distribution and the position of the flexural axes. The process outcome is an operational envelop that limits the boundaries (basically the flutter critical speed) during operation of the aircraft to prevent catastrophic structural failure. So the aim of the flutter analysis is to determine this critical air speed. In general, scientists and design engineers studied and analysed the flutter problem as a dynamic problem. The point-mass model shown in Figure (2.17) consists of wing mass concentrated in

the centre of gravity, the flexural/bending stiffness, torsional stiffness and the control surface stiffness.
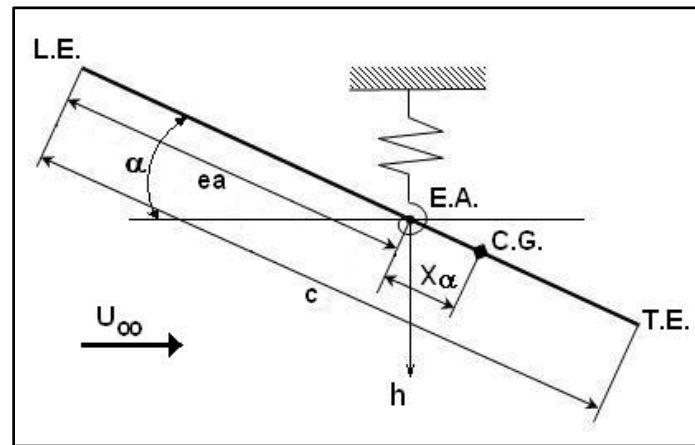
Figure 2.17: Point-mass model used in flutter analysis.

The governing equations of motion derived from this mode are [47];

$$\frac{\partial^2}{\partial y^2}\left(EI\frac{\partial^2 h}{\partial y^2}\right) + m\frac{\partial^2 h}{\partial t^2} + mx_\alpha\frac{\partial^2 \alpha}{\partial t^2} + L = 0 \tag{2.6a}$$

$$\frac{\partial}{\partial y}\left(GJ\frac{\partial \alpha}{\partial y}\right) - I_\alpha\frac{\partial^2 \alpha}{\partial t^2} - mx_\alpha\frac{\partial^2 h}{\partial t^2} + M = 0 \tag{2.6b}$$

Where,

U_∞ is the free stream air speed.

$L = f(\alpha, \ U_\infty)$ and $M = f(\alpha, U_\infty)$ are the lift and the pitching moment respectively.

EI and GJ are the flexural and torsional rigidity respectively.

L.E and T.E. are the leading and trailing edges respectively.

m and I_α are the mass and mass moment of inertia per unit length.

x_α is the distance between the Elastic Axis (E.A.) and the Centre of Gravity (C.G.)

ea is the location of the elastic axis from the leading edge, and

c is the chord.

The lift and pitching moment are traditionally presented in different aerodynamic models such as steady, quasi-steady, unsteady and nonlinear models. The famous more accurate and

complex one is the unsteady model derived by Theodorsen [48]. The other popular model is the quasi-steady model. It is a simplified model and although its validity is questionable in the analysis of the aeroelasticity of subsonic wings [49] it can be used for low-speed applications [47] and for applications requiring a simple aerodynamic model. Several works have used the quasi-steady aerodynamic model [50], [51].

The quasi-steady assumption states that [47];

- o The aerodynamic characteristics of an airfoil whose motion consists of variable linear and angular motions are equal (at any time) to the characteristics of the same airfoil moving with constant linear and angular velocities equal to the actual instantaneous values.
- o The inclination of the flow-velocity vector to the profile is also taken to be constant and equal to the actual instantaneous inclinations.

The quasi-steady lift and pitching moment coefficients are;

$$C_L = Cl_\alpha \left[\alpha + \frac{1}{U_\infty} \dot{h} + \frac{1}{U_\infty} \left(\frac{3}{4} c - ea \right) \dot{\alpha} \right] \qquad (2.7)$$

And,

$$(C_M)_{l.e.} = -\frac{c\pi}{8U_\infty} \dot{\alpha} - \frac{1}{4} C_L \qquad (2.8)$$

where,

Cl_α is the slope of the Lift coefficient vs. Angle of attack curve.

C_L & C_M are the lift and pitching moment coefficients respectively.

2.3.2. Control of Wing Flutter

With the increase in the operation and mission requirements of the aircraft the aeroelastic and vibration control (Aeroservoelasticity) technology has emerged. The flutter and vibration active control is conventionally obtained by using the aerodynamic control surfaces operated by servo-hydraulic actuators [52], [53], [54]. However, this technology suffers several limitations such as; (a) multiple energy conversion (mechanical, hydraulic, electrical); (b)

potential failure sites due to large numbers of parts; (c) high vulnerability of the hydraulic pipes network [3]. Another limitation is the limited actuation bandwidth of the aerodynamic control surfaces. For example, the rudder bandwidth of the F/A-18 aircraft is less than 20 Hz making it ineffective in reducing the buffet responses at the second mode around 45 Hz (first torsion mode) [55], whilst the piezoelectric frequency bandwidth ranges from under 1 Hz to more than 20 KHz [56].

In the last decade, another technique for using distributed piezoelectric patches as actuators for active structural dynamic has emerged. Under the Flutter Research and Experimental device (FRED) project at NASA Langley Research Centre (LaRC), Heeg [57] performed analytical and experimental investigation of flutter suppression by piezoelectric actuation. Two piezoelectric ceramic plates were bonded to opposing sides (poled to form a bimorph-type actuator) and near the root of one of the plunge spring tines of the mount system to actuate the test article. With a Single-Input Single-Output (SISO) gain feedback control law, an increase in flutter speed analytically   of 15.7% (from 560 in/sec to 648 in/sec) and experimentally of 20% (from 58 in/sec to 697 in/sec) was achieved [57]. A joint program between LaRC and Massachusetts Institute of Technology (MIT) named "The Piezoelectric Aeroelastic Response Tailoring Investigation (PARTI)," was the first study using relatively large, multi-degree-of-freedom aeroelastic testbed with cross sectional airfoil of NACA 66-012 aimed to develop detailed analytical and experimental techniques and demonstrate the ability of strain actuated adaptive wings to affect aeroelastic control. Thirty six pairs of piezoelectric wafers were bonded on the top and the bottom surfaces of the model and poled to give bimorph actuation. The piezoelectric wafers were arranged into fifteen groups (Figure 2.18) to perform several control configurations. Control law A of 6 states LQG and SISO configuration actuating all fifteen groups increased the normalized flutter dynamic pressure (speed) by approximately 12.5%, while control law B with gain feedback and SISO configuration actuating groups number 3,4,6,7 & 10 increased it by 8% [58].
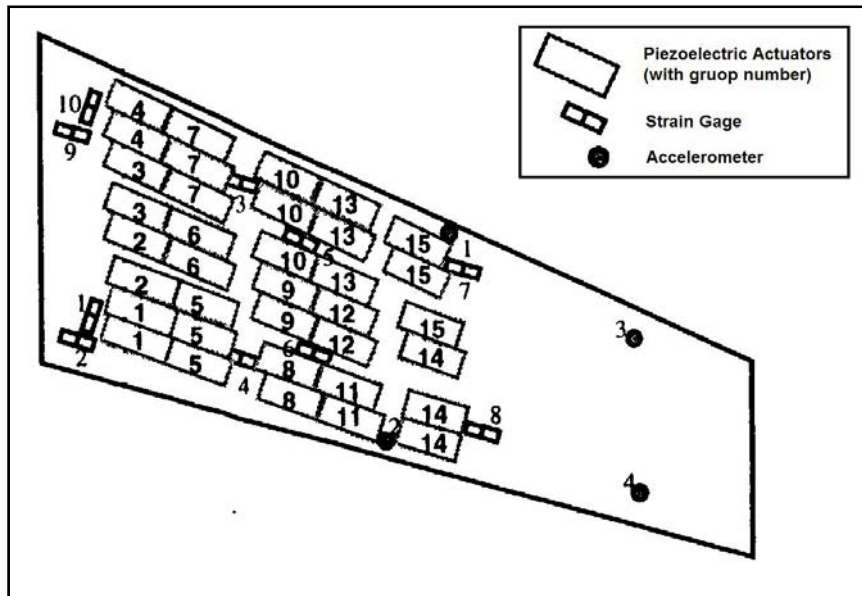
Figure 2.18: Approximate locations of actuators and sensors on the PARTI model [58].

Costa et al [56] investigated the use of piezoelectric actuation technique in controlling flutter and gust response and buffet alleviation of different wing configurations. For a rectangular platform wing consisting of a NACA 0012 airfoil enveloped around a rectangular plate structure a 6% increase in the critical flutter speed was attained. In this configuration, twelve piezoelectric actuator patches were bonded to the top and bottom of the plate near the cantilevered end. In a swept-back aluminium plate wing, an appreciable buffeting reduction from 32% to 47.5% was obtained. Six piezoelectric actuators were bonded on the surfaces at the wing mount root and two shape control actuators near the wing tip were used to control the wing motion. Comparisons between the flutter control using piezoelectric actuators and aerodynamic control surfaces were done on two wing configurations. The 3D piezoelectric and aileron controlled wing has two flat aluminium sheets used as skin for the wing which are activated by pairs of piezoelectric actuators bonded on each sheet surfaces. Two pairs positioned vertically near the leading edge of the wing at the root and mid section and another pair bonded horizontally at the tip of the wing between the outboard most brackets. A maximum reduction in the wing dynamic response of 52% was obtained using the piezoelectric actuators, while a maximum reduction of 15% was obtained by using the aileron control. Also, the piezoelectric activated wing reduced the buffeting vibration amplitude by 41%. In the last configuration of piezoelectric and flaperon controlled CFRP wing, the aluminium sheets were replaced by Carbon Fibre Reinforced Plates (CFRP) with the same actuator positioning. The vibration reduction at 30 m/s of free stream velocity was 72.7% using the piezoelectric control, in comparison to 16.5% using the flaperon control [56].

The shape, location and orientation of the piezoelectric actuators are very important in plate vibration control. Moon and Hwang [59] developed an optimal control strategy to suppress the flutter of a supersonic composite panel using piezoceramic (PZT) actuators. In their study, the PZT patches shape and location are determined using genetic algorithms. Bent, Hagood and Rodgers [36] investigated the twist actuation in isotropic substructures by incorporating several anisotropic plies of different piezoelectric actuators into laminated structures. They showed that the transversely stiff actuators, those with Interdigitated Electrode (AFC), have the high twist actuation capabilities with thin structures and even higher with thicker ones. Cesnik, Ortega-Morales and Patil [60] studied the impact of combined bending and twisting actuation on the aeroelastic performance of highly-flexible active composite wing. They concluded that tailored anisotropic strain actuation improved the performance (controlling aeroelastic instabilities and gust alleviation) of high aspect ratio wings. Azzouz et al [42] compared the actuation effect of MFC™ with PZT actuators at different orientations on the state modal bending and twisting amplitudes of a square and triangular cantilever plates. They showed that in comparison to PZT actuators, the MFC™ provided well actuation of bending amplitudes for a large range of orientations and extremely well actuation of twisting amplitudes for the full range of orientation. Sheta, Moses and Huttsell [55] used skewed pairs of PZT patches over the inboard and outboard surfaces of a full-scale F/A-18 vertical tail to alleviate its buffeting in the first bending and torsion modes.

2.4. Control Protocols

Several control theories and techniques have been used in the controlling task of smart structures. Choi, Park and Fukuda [5] investigated active vibration control of two hybrid smart structures with two different control schemes. One hybrid structure is featured by a piezoceramic (PZT) actuator and a SMA actuator where a sliding mode controller is employed. The other hybrid structure consists of a piezoelectric film (PF) actuator and an electro-rheological fluid (ERF) actuator and controlled by a Neuro-sliding mode controller (NSC). In their study, the goal of the NN learning process is to determine a desired controller rather than a desired response. Since a desired controller cannot be known in advance a real-time learning mechanism based on the idea of sliding mode and Lyapunov stability is employed. Varadarajan, Chandrashekhara and Agrawal [61] designed a robust LQG/LTR-based (Linear Quadratic Gaussian with Loop Transfer Recovery) controller for laminated composite beams with integrated piezoelectric sensors and actuators. The performance of the controller was investigated against the effect of the system parameters variation. In

comparison to the negative velocity (proportional) feedback controller, LQG/LTR- based controller proved to be more robust. Also, it was shown that its performance is better with multimodal vibrations. Valoor, Chandrashekhara and Agrawal [62] developed a neural network based hybrid control system for self-adapting vibration control of laminated plates with piezoelectric sensors and actuators. This control system comprised of a feed-forward Neural Network (NN) identifier and a dynamic diagonal recurrent NN controller. Shen and Homaifar [63] investigated four control methods; rate-feedback control, hybrid fuzzy-PID control, genetic algorithms-designed PID control, and LQG/LTR control and compared their performances in attenuating vibration in structures using piezoelectric actuators. In the hybrid fuzzy-PID controller both fuzzy logic controller and PID controller are combined together to adjust the PID gains online. The same for the genetic algorithms (GA) designed control where a chromosome comprising 15 genes represents a set of PID gains of the system. All four control methods proved to be reliable and efficient in suppression of the steady-state resonance vibrations. Saravanos and Christoforou [27] investigated the feasibility of active control of low-energy impacts on laminated shells of double curvature with distributed piezoelectric sensors and actuators. LQR (Linear Quadratic Regulator) state feedback and output feedback controllers were used in their investigation. Both techniques showed the possibility of reducing the impact force for at least medium mass impactors and for shells of low and intermediate curvatures. Tadi [64] studied the effectiveness of a compensator design for flutter suppression of panel using piezoelectric sensors and actuators. The *compensator* comprises an observer to estimate online the system state from the sensors output and using it in the feedback control law. The results indicated that the compensator is effective in suppressing the amplitude of moderate flutter oscillations. Bhoir and Singh [65] derived a control law based on back-stepping technique for the trajectory control of a linear combination of the plunge displacement and pitch angle as output variable. Also, an observer was designed to estimate the unavailable states using only the plunge displacement, pitch angle and control surface deflection measurements. Han, Tani and Qiu [66] investigated numerically and experimentally the active flutter suppression of a swept-back cantilever lifting surface using piezoelectric actuation. H_2- and μ-synthesized control laws were used in evaluation of the flutter suppression. While both laws showed comparable performance around the flutter point, the μ-synthesized law has improved behaviour over a wide flow speed range. Reddy *et al* [67] designed an adaptive output feedback controller for suppressing aeroelastic vibration on a nonlinear wing section using leading- and trailing-edge control

surface actuation. With the only measurements of plunge and pitch displacements, the algorithm is adaptively compensating for the nonlinearity and uncertainties in all parameters of the model. Kim *et al* [68] constructed an output feedback controller to suppress nonlinear panel flutter. The nonlinearity of the panel motion are compensated by the use of Extended Kalman Filter (EKF).

2.5. Summary

The main historical background and the underlying theories of smart structures technologies and aeroelasticity are presented in this chapter. The review of the past and more recent work showed that most of the SMA smart structure work was based on embedding the SMA materials in the host structures and in addition to that where the SMA materials are used as external control actuators. The first part of this work will investigate the surface mounted SMA materials and its effect on the mechanical behaviour of the host structure. Detailed mathematical modelling and experimental work of this case are presented in Chapter 3. The second part of this work will focus on the control of the flutter speed of aeroelastic structures using patches of piezoelectric materials. The previous works in this field concentrated mainly on the bending effect (morph and bimorph) of the activated patches. The effect of the torsional effect was less investigated. In the second part of this work, deeper investigation of the later effect will be conducted. To achieve this detailed mathematical modelling and control protocol are developed and presented in Chapters 4 and 5 respectively.   The discussion of this chapter justifies the research questions identified in Chapter 1.

Chapter 3.   ALTERATION OF DYNAMIC PROPERTIES OF STRIP STRUCTURE USING SMA WIRES

3.1. Problem Statement

Minimal research has been performed on altering the natural frequency of composite structures using Shape Memory Alloys. In most of the research using SMA's in controlling smart structures, the SMA's were embedded within the structures. In this work, the alteration of the natural frequency of composite plates will be obtained using surface mounted Shape Memory Alloy wires. The SMA wires are used to change the strain energy of the composite plates, this is shown experimentally and the governing strain equations are solved analytically using Rayleigh-Ritz method. The experimental results and the numerical results are compared. Different configurations of SMA placement, namely, straight and zigzag, are studied and compared to computational and experimental findings in order to optimize the control strategy.

3.2. Mathematical Model

The aim of the mathematical model is to construct the equations of motion of the structure under study which relate the stresses/strains with external loadings. These equations are then solved to give the behaviour of the structure under certain loading conditions. To construct the governing equations of motion different relations are used. These relations are:

3.2.1. Kinematic Relations

These are geometrical relations which relate the body strains to its displacements. The rectangular Cartesian form of the Green-Lagrange strain tensor "E" [69]:

$$E_{jk} = \frac{1}{2}\left(\frac{\partial u_j}{\partial X_k} + \frac{\partial u_k}{\partial X_j} + \frac{\partial u_m}{\partial X_j}\frac{\partial u_m}{\partial X_k}\right) \qquad (3.1)$$

Where,

the displacement $\mathcal{U}(X,t) = x(X,t) - X$,

$X = (X_1, X_2, X_3)$ is the particle position before the deformation, and

$x = (x_1, x_2, x_3)$ is the particle position after deformation .

Let $(x_1, x_2, x_3) = (x, y, z)$, also, $(\mathcal{U}_1, \mathcal{U}_2, \mathcal{U}_3) = (u, v, w)$, equation (3.1) can be expanded in explicit form as:

$$E_{xx} = \frac{\partial u}{\partial x} + \frac{1}{2}\left[\left(\frac{\partial u}{\partial x}\right)^2 + \left(\frac{\partial v}{\partial x}\right)^2 + \left(\frac{\partial w}{\partial x}\right)^2\right]$$

$$E_{yy} = \frac{\partial v}{\partial y} + \frac{1}{2}\left[\left(\frac{\partial u}{\partial y}\right)^2 + \left(\frac{\partial v}{\partial y}\right)^2 + \left(\frac{\partial w}{\partial y}\right)^2\right]$$

$$E_{zz} = \frac{\partial w}{\partial z} + \frac{1}{2}\left[\left(\frac{\partial u}{\partial z}\right)^2 + \left(\frac{\partial v}{\partial z}\right)^2 + \left(\frac{\partial w}{\partial z}\right)^2\right]$$

$$E_{xy} = \frac{1}{2}\left(\frac{\partial u}{\partial y} + \frac{\partial v}{\partial x} + \frac{\partial u}{\partial x}\frac{\partial u}{\partial y} + \frac{\partial v}{\partial x}\frac{\partial v}{\partial y} + \frac{\partial w}{\partial x}\frac{\partial w}{\partial y}\right)$$

$$E_{xz} = \frac{1}{2}\left(\frac{\partial u}{\partial z} + \frac{\partial w}{\partial x} + \frac{\partial u}{\partial x}\frac{\partial u}{\partial z} + \frac{\partial v}{\partial x}\frac{\partial v}{\partial z} + \frac{\partial w}{\partial x}\frac{\partial w}{\partial z}\right)$$

$$E_{yz} = \frac{1}{2}\left(\frac{\partial v}{\partial z} + \frac{\partial w}{\partial y} + \frac{\partial u}{\partial y}\frac{\partial u}{\partial z} + \frac{\partial v}{\partial y}\frac{\partial v}{\partial z} + \frac{\partial w}{\partial y}\frac{\partial w}{\partial z}\right) \tag{3.2}$$

3.2.2. Classical Laminated Plate Theory

The formulation of the mathematical model in this work is based on the Classical Laminated Plate Theory (CLPT). The CLPT is an extension of the Classical Plate Theory (CPT) to composite laminates and basically defines the displacements of the structure. The formulation process requires several assumptions of which the fundamental assumptions in the CLPT are that the *Kirchhoff hypothesis* holds [69]:

1) Straight lines perpendicular to the midsurface (i.e., transverse normals) before deformation remain straight after deformation.
2) The transverse normals do not experience elongation (i.e., they are inextensible).
3) The transverse normals rotate such that they remain perpendicular to the midsurface after deformation.

These assumptions lead to the fact that the transverse displacement is independent of the transverse (thickness) coordinate and the transverse normal strain and shear strains are zero;

$$\varepsilon_{zz} = 0, \quad \varepsilon_{xz} = 0, \quad \varepsilon_{yz} = 0 \tag{3.3}$$

And the displacements (u, v, w) are;

$$u(x, y, z, t) = u_0(x, y, t) - z \frac{\partial w}{\partial y}$$

$$v(x, y, z, t) = v_0(x, y, t) - z \frac{\partial w}{\partial y}$$

$$w(x, y, z, t) = w_0(x, y, t) \tag{3.4}$$

For the laminated plate/structure the following assumptions/restrictions are considered:

1) The layers are perfectly bonded together.
2) The material of each layer is linearly elastic and has three planes of material symmetry (orthotropic).
3) Each layer is of uniform thickness.
4) The strains and displacements are small.
5) The transverse shear stresses on the top and bottom surfaces of the laminate are zero.

By assuming that the components of the displacement gradients are of the order ϵ, i.e,

$$\frac{\partial u}{\partial x}, \frac{\partial u}{\partial y}, \frac{\partial w}{\partial x}, \frac{\partial \vartheta}{\partial y}, \frac{\partial w}{\partial z} = O(\epsilon) \tag{3.5}$$

Then the terms of order ϵ^2 are negligible;

$$\left(\frac{\partial u}{\partial x}\right)^2, \left(\frac{\partial \vartheta}{\partial x}\right)^2, \frac{\partial u}{\partial x}\frac{\partial u}{\partial y}, \frac{\partial v}{\partial x}\frac{\partial v}{\partial y} \quad \ldots.. \cong 0 \tag{3.6}$$

And for moderate rotation; $\frac{\partial w_0}{\partial x}, \frac{\partial w_0}{\partial y} \cong (10^\circ\text{-}15^\circ)$,

Then, $\left(\frac{\partial w}{\partial x}\right)^2, \left(\frac{\partial w}{\partial y}\right)^2, \frac{\partial w}{\partial x}\frac{\partial w}{\partial y}$ are small but not negligible compared to ϵ.

Thus (3.2) take the form:

$$\varepsilon_{xx} = \frac{\partial u}{\partial x} + \frac{1}{2}\left(\frac{\partial w}{\partial x}\right)^2, \varepsilon_{yy} = \frac{\partial v}{\partial y} + \frac{1}{2}\left(\frac{\partial w}{\partial y}\right)^2, \varepsilon_{xy} = +\frac{1}{2}\left(\frac{\partial u}{\partial y} + \frac{\partial v}{\partial x} + \frac{\partial w}{\partial x}\frac{\partial w}{\partial y}\right)$$

$$\boldsymbol{\varepsilon_{zz}} = \frac{\partial w}{\partial z}, \ \boldsymbol{\varepsilon_{xz}} = \frac{1}{2}\left(\frac{\partial u}{\partial z} + \frac{\partial w}{\partial x}\right), \ \boldsymbol{\varepsilon_{yz}} = \frac{1}{2}\left(\frac{\partial v}{\partial z} + \frac{\partial w}{\partial y}\right) \tag{3.7}$$

By applying the displacements of Eqn. (3.4) into Eqn. (3.7) the known *Von Kármán strains* are;

$$\varepsilon_{xx} = \frac{\partial u_0}{\partial x} + \frac{1}{2}\left(\frac{\partial w_0}{\partial x}\right)^2 - z\frac{\partial^2 w_0}{\partial x^2}$$

$$\varepsilon_{xy} = \frac{1}{2}\left(\frac{\partial u_0}{\partial y} + \frac{\partial v_0}{\partial x} + \frac{\partial w_0}{\partial x}\frac{\partial w_0}{\partial y}\right) - z\frac{\partial^2 w_0}{\partial x \partial y}$$

$$\varepsilon_{yy} = \frac{\partial v_0}{\partial y} + \frac{1}{2}\left(\frac{\partial w_0}{\partial y}\right)^2 - z\frac{\partial^2 w_0}{\partial x^2}$$

$$\varepsilon_{xz} = \frac{1}{2}\left(-\frac{\partial w_0}{\partial x} + \frac{\partial w_0}{\partial x}\right) = 0$$

$$\varepsilon_{yz} = \frac{1}{2}\left(-\frac{\partial w_0}{\partial y} + \frac{\partial w_0}{\partial y}\right) = 0$$

$$\varepsilon_{zz} = 0 \tag{3.8}$$

The strains in Eqn. (3.8) comprise of the *membrane strains* ($\boldsymbol{\varepsilon^0}$) and the *curvatures* ($\boldsymbol{\varepsilon^1}$) or flexural/bending strains, here ε_{xy} is replaced by the engineering shear strains ($\gamma_{xy} = 2\varepsilon_{xy}$);

$$\boldsymbol{\varepsilon} = \boldsymbol{\varepsilon^0} + z\boldsymbol{\varepsilon^1} \tag{3.9}$$

Or,

$$\begin{Bmatrix} \varepsilon_{xx} \\ \varepsilon_{yy} \\ \gamma_{xy} \end{Bmatrix} = \begin{Bmatrix} \varepsilon_{xx}^0 \\ \varepsilon_{yy}^0 \\ \gamma_{xy}^0 \end{Bmatrix} + z\begin{Bmatrix} \varepsilon_{xx}^1 \\ \varepsilon_{yy}^1 \\ \gamma_{xy}^1 \end{Bmatrix} \tag{3.10}$$

Where,

$$\begin{Bmatrix} \varepsilon_{xx}^0 \\ \varepsilon_{yy}^0 \\ \gamma_{xy}^0 \end{Bmatrix} = \begin{Bmatrix} \frac{\partial u_0}{\partial x} + \frac{1}{2}\left(\frac{\partial w_0}{\partial x}\right)^2 \\ \frac{\partial v_0}{\partial y} + \frac{1}{2}\left(\frac{\partial w_0}{\partial y}\right)^2 \\ \frac{\partial u_0}{\partial y} + \frac{\partial v_0}{\partial x} + \frac{\partial w_0}{\partial x}\frac{\partial w_0}{\partial y} \end{Bmatrix} \quad \& \quad \begin{Bmatrix} \varepsilon_{xx}^1 \\ \varepsilon_{yy}^1 \\ \gamma_{xy}^1 \end{Bmatrix} = \begin{Bmatrix} -\frac{\partial^2 w_0}{\partial x^2} \\ -\frac{\partial^2 w_0}{\partial y^2} \\ -2\frac{\partial^2 w_0}{\partial x \partial y} \end{Bmatrix} \tag{3.11}$$

3.2.3. Lamina Constitutive Equations

These equations relate the material reaction/deformation (strains) to applied forces (stresses) and are known as Hook's Law. The generalised form of Hook's law can be written in the following matrix form [69];

$$\sigma_i = C_{ij}\varepsilon_j$$

or,

$$\begin{Bmatrix} \sigma_1 \\ \sigma_2 \\ \sigma_3 \\ \sigma_4 \\ \sigma_5 \\ \sigma_6 \end{Bmatrix} = \begin{bmatrix} C_{11} & C_{12} & C_{13} & C_{14} & C_{15} & C_{16} \\ C_{21} & C_{22} & C_{23} & C_{24} & C_{25} & C_{26} \\ C_{31} & C_{32} & C_{33} & C_{34} & C_{35} & C_{36} \\ C_{41} & C_{42} & C_{43} & C_{44} & C_{45} & C_{46} \\ C_{51} & C_{52} & C_{53} & C_{54} & C_{55} & C_{56} \\ C_{61} & C_{62} & C_{63} & C_{64} & C_{65} & C_{66} \end{bmatrix} \begin{Bmatrix} \varepsilon_1 \\ \varepsilon_2 \\ \varepsilon_3 \\ \varepsilon_4 \\ \varepsilon_5 \\ \varepsilon_6 \end{Bmatrix} \tag{3.12}$$

where C is known as the *Stiffness tensor*.

For beams and plate strips cases the plane stress state is applied and (3.12) can be written as

$$\begin{Bmatrix} \sigma_1 \\ \sigma_2 \\ \sigma_6 \end{Bmatrix} = \begin{bmatrix} Q_{11} & Q_{12} & 0 \\ Q_{12} & Q_{22} & 0 \\ 0 & 0 & Q_{66} \end{bmatrix} \begin{Bmatrix} \varepsilon_1 \\ \varepsilon_2 \\ \varepsilon_6 \end{Bmatrix} \tag{3.13}$$

Where Q_{ij} is known as *Plane stress-reduced stiffness*, and given by

$$Q_{11} = \frac{E_1}{1 - v_{12}v_{21}}, \qquad Q_{12} = \frac{v_{12}E_2}{1 - v_{12}v_{21}}$$

$$Q_{22} = \frac{E_2}{1 - v_{12}v_{21}}, \quad Q_{66} = G_{12} \quad, \qquad v_{21} = \frac{v_{12}E_2}{E_1} \tag{3.14}$$

For laminated composite structure the stiffness must be transformed from the material coordinate system into problem/structure coordinate system as follow [69];

$$\begin{Bmatrix} \sigma_{xx} \\ \sigma_{yy} \\ \sigma_{xy} \end{Bmatrix} = \begin{bmatrix} \bar{Q}_{11} & \bar{Q}_{12} & \bar{Q}_{16} \\ \bar{Q}_{12} & \bar{Q}_{22} & \bar{Q}_{26} \\ \bar{Q}_{16} & \bar{Q}_{26} & \bar{Q}_{66} \end{bmatrix} \begin{Bmatrix} \varepsilon_{xx} \\ \varepsilon_{yy} \\ \gamma_{xy} \end{Bmatrix} \tag{3.15}$$

where,

$$\begin{Bmatrix} \bar{Q}_{11} \\ \bar{Q}_{12} \\ \bar{Q}_{22} \\ \bar{Q}_{16} \\ \bar{Q}_{26} \\ \bar{Q}_{66} \end{Bmatrix} = \mathbf{L} \cdot \begin{Bmatrix} Q_{11} \\ Q_{12} \\ Q_{22} \\ Q_{66} \end{Bmatrix} \tag{3.16}$$

and,

$$
\mathbf{L} = \begin{bmatrix}
\cos^4\theta & 2\sin^2\theta\cos^2\theta & \sin^4\theta & 4\sin^2\theta\cos^2\theta \\
\sin^2\theta\cos^2\theta & \sin^4\theta + \cos^4\theta & \sin^2\theta\cos^2\theta & -4\sin^2\theta\cos^2\theta \\
\sin^4\theta & 2\sin^2\theta\cos^2\theta & \cos^4\theta & 4\sin^2\theta\cos^2\theta \\
\sin\theta\cos^3\theta & -\sin\theta\cos^3\theta + \sin^3\theta\cos\theta & -\sin^3\theta\cos\theta & -2\sin\theta\cos^3\theta + 2\sin^3\theta\cos\theta \\
\sin^3\theta\cos\theta & -\sin^3\theta\cos\theta + \sin\theta\cos^3\theta & -\sin\theta\cos^3\theta & -2\sin^3\theta\cos\theta + 2\sin\theta\cos^3\theta \\
\sin^2\theta\cos^2\theta & -2\sin^2\theta\cos^2\theta & \sin^2\theta\cos^2\theta & \sin^4\theta + \cos^4\theta - 2\sin^2\theta\cos^2\theta
\end{bmatrix} \tag{3.17}
$$

3.2.4. Laminate Constitutive Equations

For a laminate structure comprising "n" laminas/layers the strains are continuous through the thickness. But due to the change in material coefficients through the thickness (different lamina orientations) the stresses are varied. By lamina-wise integration of the stresses through the thickness the force and moment resultants are [69];

$$
\begin{Bmatrix} N_{xx} \\ N_{yy} \\ N_{xy} \end{Bmatrix} = \sum_{k=1}^{n} \int_{z_k}^{z_{k+1}} \begin{Bmatrix} \sigma_{xx} \\ \sigma_{yy} \\ \sigma_{xy} \end{Bmatrix} dz \tag{3.18}
$$

Substituting Eqn's. (3.15) and (3.10) into Eqn. (3.18);

$$
\begin{Bmatrix} N_{xx} \\ N_{yy} \\ N_{xy} \end{Bmatrix} = \sum_{k=1}^{n} \int_{z_k}^{z_{k+1}} \begin{bmatrix} \bar{Q}_{11} & \bar{Q}_{12} & \bar{Q}_{16} \\ \bar{Q}_{12} & \bar{Q}_{22} & \bar{Q}_{26} \\ \bar{Q}_{16} & \bar{Q}_{26} & \bar{Q}_{66} \end{bmatrix}^{k} \left(\begin{Bmatrix} \varepsilon_{xx}^0 \\ \varepsilon_{yy}^0 \\ \gamma_{xy}^0 \end{Bmatrix} + z \begin{Bmatrix} \varepsilon_{xx}^1 \\ \varepsilon_{yy}^1 \\ \gamma_{xy}^1 \end{Bmatrix} \right) dz
$$

$$
\begin{Bmatrix} N_{xx} \\ N_{yy} \\ N_{xy} \end{Bmatrix} = \begin{bmatrix} A_{11} & A_{12} & A_{16} \\ A_{12} & A_{22} & A_{26} \\ A_{16} & A_{26} & A_{66} \end{bmatrix} \begin{Bmatrix} \varepsilon_{xx}^0 \\ \varepsilon_{yy}^0 \\ \gamma_{xy}^0 \end{Bmatrix} + \begin{bmatrix} B_{11} & B_{12} & B_{16} \\ B_{12} & B_{22} & B_{26} \\ B_{16} & B_{26} & B_{66} \end{bmatrix} \begin{Bmatrix} \varepsilon_{xx}^1 \\ \varepsilon_{yy}^1 \\ \gamma_{xy}^1 \end{Bmatrix} \tag{3.19}
$$

And,

$$
\begin{Bmatrix} M_{xx} \\ M_{yy} \\ M_{xy} \end{Bmatrix} = \sum_{k=1}^{n} \int_{z_k}^{z_{k+1}} \begin{Bmatrix} \sigma_{xx} \\ \sigma_{yy} \\ \sigma_{xy} \end{Bmatrix} z\, dz \tag{3.20}
$$

$$
\begin{Bmatrix} M_{xx} \\ M_{yy} \\ M_{xy} \end{Bmatrix} = \sum_{k=1}^{n} \int_{z_k}^{z_{k+1}} \begin{bmatrix} \bar{Q}_{11} & \bar{Q}_{12} & \bar{Q}_{16} \\ \bar{Q}_{12} & \bar{Q}_{22} & \bar{Q}_{26} \\ \bar{Q}_{16} & \bar{Q}_{26} & \bar{Q}_{66} \end{bmatrix}^{k} \left(\begin{Bmatrix} \varepsilon_{xx}^0 \\ \varepsilon_{yy}^0 \\ \gamma_{xy}^0 \end{Bmatrix} + z \begin{Bmatrix} \varepsilon_{xx}^1 \\ \varepsilon_{yy}^1 \\ \gamma_{xy}^1 \end{Bmatrix} \right) z\, dz
$$

$$
\begin{Bmatrix} M_{xx} \\ M_{yy} \\ M_{xy} \end{Bmatrix} = \begin{bmatrix} B_{11} & B_{12} & B_{16} \\ B_{12} & B_{22} & B_{26} \\ B_{16} & B_{26} & B_{66} \end{bmatrix} \begin{Bmatrix} \varepsilon_{xx}^0 \\ \varepsilon_{yy}^0 \\ \gamma_{xy}^0 \end{Bmatrix} + \begin{bmatrix} D_{11} & D_{12} & D_{16} \\ D_{12} & D_{22} & D_{26} \\ D_{16} & D_{26} & D_{66} \end{bmatrix} \begin{Bmatrix} \varepsilon_{xx}^1 \\ \varepsilon_{yy}^1 \\ \gamma_{xy}^1 \end{Bmatrix} \tag{3.21}
$$

where A_{ij} are called *Extensional stiffnesses*, B_{ij} the *Bending-extensional coupling stiffnesses* and D_{ij} the *Bending stiffnesses* and are defined in terms of the lamina stiffnesses $\bar{Q}_{ij}$ as;

47

$$\left(A_{ij}, B_{ij}, D_{ij}\right) = \int_{-\frac{h}{2}}^{\frac{h}{2}} \bar{Q}_{ij}(1, z, z^2)dz = \sum_{k=1}^{n} \int_{z_k}^{z_{k+1}} \bar{Q}_{ij}^k(1, z, z^2)\, dz \qquad (3.22)$$

or,

$$A_{ij} = \sum_{k=1}^{n} \bar{Q}_{ij}^k (z_{k+1} - z_k)\, dz \ , \ B_{ij} = \frac{1}{2}\sum_{K=1}^{N} \bar{Q}_{ij}^k (z_{k+1}^2 - z_k^2)$$

$$D_{ij} = \frac{1}{3}\sum_{K=1}^{N} \bar{Q}_{ij}^k (z_{k+1}^3 - z_k^3) \qquad (3.23)$$

And in matrix form:

$$\begin{Bmatrix} \{N\} \\ \{M\} \end{Bmatrix} = \begin{bmatrix} [A] & [B] \\ [B] & [D] \end{bmatrix} \begin{Bmatrix} \{\varepsilon^0\} \\ \{\varepsilon^1\} \end{Bmatrix} \qquad (3.24)$$

3.2.5. Equations of Motion

The Hamilton's principle, which is a generalization of the *principle of virtual displacements* [69], is used to derive the equations of motion. The Hamilton's principle states that [70]; "*all of possible paths that a material particle could travel from its position at time t_1 to its position at time t_2, its actual path will be one for which the integral (I) is extremum.*"

Where, $$I = \int_{t_1}^{t_2}(K - W)dt \qquad (3.25)$$

Here, the difference between the kinetic "K" and potential "W" energies is known as the *Lagrangian* function. The potential energy consists of internal which is the strain energy "U" and external which is the work due to the applied forces "V".

For extremum **I**,

$$\delta I = \int_0^T (\delta K - (\delta U + \delta V))dt = 0 \qquad (3.26)$$

or,

$$\int_0^T (\delta U + \delta V - \delta K)dt = 0 \qquad (3.27)$$

The **Strain energy** can be written as;

$$U = \int_{V_0} \sigma_{ij}\, \varepsilon_{ij} dV \qquad (3.28)$$

then,

$$\delta U = \int_{V_0} \left(\sigma_{xx}\delta\varepsilon_{xx} + \sigma_{yy}\delta\varepsilon_{yy} + 2\sigma_{xy}\delta\varepsilon_{xy} \right) dzdxdy \qquad (3.29)$$

Note that from eqn. (3.8); $\varepsilon_{xz} = \varepsilon_{yz} = \varepsilon_{zz} = 0$.

Eqn. (3.29) can be written as;

$$\delta U = \int_{\forall} \int_{-\frac{h}{2}}^{\frac{h}{2}} \left(\sigma_{xx}\delta\varepsilon_{xx} + \sigma_{yy}\delta\varepsilon_{yy} + 2\sigma_{xy}\delta\varepsilon_{xy} \right) dzdxdy \qquad (3.30)$$

from Eqn. (3.10);

$$\delta U = \int_{\forall} \left\{ \int_{-\frac{h}{2}}^{\frac{h}{2}} [\sigma_{xx}(\delta\varepsilon_{xx}^0 + z\delta\varepsilon_{xx}^1) + \sigma_{yy}(\delta\varepsilon_{yy}^0 + z\delta\varepsilon_{yy}^1) + \sigma_{xy}(\delta\gamma_{xy}^0 + z\delta\gamma_{xy}^1)] \, dz \right\} dxdy$$

$$(3.31)$$

For one layer; n=1 Eqn's. (3.18) and (3.20) can be written as;

$$\begin{Bmatrix} N_{xx} \\ N_{yy} \\ N_{xy} \end{Bmatrix} = \int_{-\frac{h}{2}}^{\frac{h}{2}} \begin{Bmatrix} \sigma_{xx} \\ \sigma_{yy} \\ \sigma_{xy} \end{Bmatrix} dz \qquad \& \qquad \begin{Bmatrix} M_{xx} \\ M_{yy} \\ M_{xy} \end{Bmatrix} = \int_{-\frac{h}{2}}^{\frac{h}{2}} \begin{Bmatrix} \sigma_{xx} \\ \sigma_{yy} \\ \sigma_{xy} \end{Bmatrix} z \, dz \qquad (3.32)$$

in Eqn. (3.31);

$$\delta U = \int_{\forall} \left[N_{xx}\delta\varepsilon_{xx}^0 + M_{xx}\delta\varepsilon_{xx}^1 + N_{yy}\delta\varepsilon_{yy}^0 + M_{yy}\delta\varepsilon_{yy}^1 + N_{xy}\delta\gamma_{xy}^0 + M_{xy}\delta\gamma_{xy}^1) \right] dxdy$$

$$(3.33)$$

The **Work done by the applied forces** is:

$$V = - \int_{\forall} q(x,y)w_0 dxdy \qquad (3.34)$$

where, *q(x,y)* is the external force per area. Then,

$$\delta V = - \int_{\forall} q\delta w_0 dxdy \qquad (3.35)$$

Since the **Kinetic energy** is:

$$K = \frac{1}{2}m\mathbb{V}^2 \qquad (3.36)$$

or,

$$K = \int_{\mathcal{V}_0} \frac{1}{2}\rho_0 \left(\frac{\partial \mathcal{U}}{\partial t}\right)^2 dV \tag{3.37}$$

and from Eqn. (3.4) then,

$$K = \int_{\mathcal{V}_0} \frac{1}{2}\rho_0 \left[\left(\dot{u}_0 - z\frac{\partial \dot{w}_0}{\partial x}\right)^2 + \left(\dot{v}_0 - z\frac{\partial \dot{w}_0}{\partial y}\right)^2 + \dot{w}_0^2\right] dV \tag{3.38}$$

Taking "δ" therefore,

$$\delta K = \int_{\forall} \int_{-\frac{h}{2}}^{\frac{h}{2}} \rho_0 \left[\left(\dot{u}_0 - z\frac{\partial \dot{w}_0}{\partial x}\right)\left(\delta \dot{u}_0 - z\frac{\partial \delta \dot{w}_0}{\partial x}\right) + \left(\dot{v}_0 - z\frac{\partial \dot{w}_0}{\partial y}\right)\left(\delta \dot{v}_0 - z\frac{\partial \delta \dot{w}_0}{\partial y}\right) + \right.$$
$$\left. \dot{w}_0 \delta \dot{w}_0\right] dz\,dx\,dy$$

$$\tag{3.39}$$

Let,

$$\begin{Bmatrix} I_0 \\ I_1 \\ I_2 \end{Bmatrix} = \int_{-\frac{h}{2}}^{\frac{h}{2}} \begin{Bmatrix} 1 \\ z \\ z^2 \end{Bmatrix} \rho_0 dz \tag{3.40}$$

in Eqn. (3.39);

$$\delta K = \int_{\forall} \left[I_0(\dot{u}_0 \delta \dot{u}_0 + \dot{v}_0 \delta \dot{v}_0 + \dot{w}_0 \delta \dot{w}_0) + I_1\left(-\frac{\partial \delta \dot{w}_0}{\partial x}\dot{u}_0 - \frac{\partial \dot{w}_0}{\partial x}\delta \dot{u}_0 - \frac{\partial \delta \dot{w}_0}{\partial y}\dot{v}_0 - \frac{\partial \dot{w}_0}{\partial y}\delta \dot{v}_0\right) + \right.$$
$$\left. I_2\left(\frac{\partial \dot{w}_0}{\partial x}\frac{\partial \delta \dot{w}_0}{\partial x} + \frac{\partial \dot{w}_0}{\partial y}\frac{\partial \delta \dot{w}_0}{\partial y}\right)\right] dx\,dy \tag{3.41}$$

Substituting $\delta U, \delta V,$ and δK into Eqn. (3.27),

$$0 = \int_0^T \left\{\int_{\forall} \left[N_{xx}\delta\varepsilon_{xx}^0 + M_{xx}\delta\varepsilon_{xx}^1 + N_{yy}\delta\varepsilon_{yy}^0 + M_{yy}\delta\varepsilon_{yy}^1 + N_{xy}\delta\gamma_{xy}^0 + M_{xy}\delta\gamma_{xy}^1 - q\delta w_0 - \right.\right.$$
$$I_0(\dot{u}_0\delta\dot{u}_0 + \dot{v}_0\delta\dot{v}_0 + \dot{w}_0\delta\dot{w}_0) + I_1\left(\frac{\partial\delta\dot{w}_0}{\partial x}\dot{u}_0 + \frac{\partial\dot{w}_0}{\partial x}\delta\dot{u}_0 + \frac{\partial\delta\dot{w}_0}{\partial y}\dot{v}_0 + \frac{\partial\dot{w}_0}{\partial y}\delta\dot{v}_0\right) -$$
$$\left.\left. I_2\left(\frac{\partial\dot{w}_0}{\partial x}\frac{\partial\delta\dot{w}_0}{\partial x} + \frac{\partial\dot{w}_0}{\partial y}\frac{\partial\delta\dot{w}_0}{\partial y}\right)\right] dx\,dy\right\} dt \tag{3.42}$$

Taking "δ" of Eqn. (3.11);

$$\delta\varepsilon_{xx}^0 = \frac{\partial\delta u_0}{\partial x} + \frac{\partial w_0}{\partial x}\frac{\partial\delta w_0}{\partial x}, \qquad \delta\varepsilon_{xx}^1 = -\frac{\partial^2\delta w_0}{\partial x^2},$$

$$\delta\varepsilon_{yy}^0 = \frac{\partial\delta v_0}{\partial y} + \frac{\partial w_0}{\partial y}\frac{\partial\delta w_0}{\partial y}, \qquad \varepsilon_{yy}^1 = -\frac{\partial^2\delta w_0}{\partial y^2},$$

50

$$\delta\gamma_{xy}^0 = \frac{\partial\delta u_0}{\partial y} + \frac{\partial\delta v_0}{\partial x} + \frac{\partial\delta w_0}{\partial x}\frac{\partial w_0}{\partial y} + \frac{\partial w_0}{\partial x}\frac{\partial\delta w_0}{\partial y}, \qquad \delta\gamma_{xx}^1 = -2\frac{\partial^2\delta w_0}{\partial x\partial y} \qquad (3.43)$$

into Eqn. (3.42);

$$0 = \int_0^T \Big\{ \int_\forall \Big[N_{xx}\Big(\frac{\partial\delta u_0}{\partial x} + \frac{\partial w_0}{\partial x}\frac{\partial\delta w_0}{\partial x}\Big) - M_{xx}\frac{\partial^2\delta w_0}{\partial x^2} + N_{yy}\Big(\frac{\partial\delta v_0}{\partial y} + \frac{\partial w_0}{\partial y}\frac{\partial\delta w_0}{\partial y}\Big) - M_{yy}\frac{\partial^2\delta w_0}{\partial y^2} +$$

$$N_{xy}\Big(\frac{\partial\delta u_0}{\partial y} + \frac{\partial\delta v_0}{\partial x} + \frac{\partial\delta w_0}{\partial x}\frac{\partial\alpha w_0}{\partial y} + \frac{\partial w_0}{\partial x}\frac{\partial\delta w_0}{\partial y}\Big) - 2M_{xy}\frac{\partial^2\delta w_0}{\partial x\partial y} - q\delta w_0 - I_0(\dot u_0\delta\dot u_0 + \dot v_0\delta\dot v_0 +$$

$$\dot w_0\delta\dot w_0) + I_1\Big(\frac{\partial\delta\dot w_0}{\partial x}\dot u_0 + \frac{\partial\dot w_0}{\partial x}\delta\dot u_0 + \frac{\partial\delta\dot w_0}{\partial y}\dot v_0 + \frac{\partial\dot w_0}{\partial y}\delta\dot v_0\Big) - I_2\Big(\frac{\partial\dot w_0}{\partial x}\frac{\partial\delta\dot w_0}{\partial x} + \frac{\partial\dot w_0}{\partial y}\frac{\partial\delta\dot w_0}{\partial y}\Big)\Big] dxdy\Big\} dt$$

(3.44)

Integrating by parts of the terms of Eqn. (3.44) to relieve the virtual displacements (*δu, δv, and δw*) of any differentiation;

$$\int_0^T \Big\{ \int_\forall \Big[N_{xx,x}\delta u_0 - (N_{xx}\frac{\partial w_0}{\partial x})_{,x}\,\delta w_0 - M_{xx,xx}\,\delta w_0 - N_{yy,y}\,\delta v_0 - (N_{yy}\frac{\partial w_0}{\partial y})_{,y}\,\delta w_0 -$$

$$M_{yy,yy}\,\delta w_0 - N_{xy,y}\,\delta u_0 - N_{xy,x}\,\delta v_0 - (N_{xy}\frac{\partial w_0}{\partial y})_{,x}\,\delta w_0 - (N_{xy}\frac{\partial w_0}{\partial x})_{,y}\,\delta w_0 -$$

$$2M_{xy,xy}\,\delta w_0 - q\,\delta w_0 + I_0(\ddot u_0\delta u_0 + \ddot v_0\delta v_0 + \ddot w_0\delta w_0) + I_1\Big(\frac{\partial\ddot u_0}{\partial x}\delta w_0 - \frac{\partial\ddot w_0}{\partial x}\delta u_0 +$$

$$\frac{\partial\delta\ddot v_0}{\partial y}\delta w_0 - \frac{\partial\ddot w_0}{\partial y}\delta v_0\Big) - I_2\Big(\frac{\partial^2\ddot w_0}{\partial x^2} + \frac{\partial^2\ddot w_0}{\partial y^2}\Big)\delta w_0\Big] dxdy + B.C's.\Big\} dt = 0 \qquad (3.45)$$

Collecting the coefficients of each virtual displacement;

$$\delta u_0 \Longrightarrow \qquad \frac{\partial N_{xx}}{\partial x} + \frac{\partial N_{xy}}{\partial y} = I_0\frac{\partial^2 u_0}{\partial t^2} - I_1\frac{\partial^2}{\partial t^2}\Big(\frac{\partial w_0}{\partial x}\Big) \qquad (3.46)$$

$$\delta v_0 \Longrightarrow \qquad \frac{\partial N_{yy}}{\partial y} + \frac{\partial N_{xy}}{\partial x} = I_0\frac{\partial^2 v_0}{\partial t^2} - I_1\frac{\partial^2}{\partial t^2}\Big(\frac{\partial w_0}{\partial y}\Big) \qquad (3.47)$$

$$\delta w_0 \Longrightarrow \qquad \frac{\partial^2 M_{xx}}{\partial x^2} + \frac{\partial^2 M_{xy}}{\partial y\partial x} + \frac{\partial^2 M_{yy}}{\partial y^2} + \mathcal{N}(w_0) + q$$

$$= I_0\frac{\partial^2 w_0}{\partial t^2} + I_1\frac{\partial^2}{\partial t^2}\Big(\frac{\partial u_0}{\partial x} + \frac{\partial v_0}{\partial y}\Big)$$

$$- I_2\frac{\partial^2}{\partial t^2}\Big(\frac{\partial^2 w_0}{\partial x^2} + \frac{\partial^2 w_0}{\partial y^2}\Big) \qquad (3.48)$$

Where,

$$\mathcal{N}(w_0) = \frac{\partial}{\partial x}\Big(N_{xx}\frac{\partial w_0}{\partial x} + N_{xy}\frac{\partial w_0}{\partial y}\Big) + \frac{\partial}{\partial y}\Big(N_{xy}\frac{\partial w_0}{\partial x} + N_{yy}\frac{\partial w_0}{\partial y}\Big)$$

3.3. Analytical Solution Using Rayleigh-Ritz Method

In most practical applications of thin plates the magnitude of the stresses acting on the surface parallel to the middle plane are small compared to the bending and membrane stresses. Since the plate is thin, this implies that the tractions on any surface parallel to the middle plane are small.

A standard coordinate system as shown in Figure (3.1) is considered [17]. The displacements in x, y, z directions are denoted by u, v, w. The following assumptions are made:

1. The plate is thin, i.e., the thickness h is much smaller than the other physical dimensions of the plate.
2. The displacements u, v, w are small compared to the plate thickness.
3. In plane strains $\varepsilon_x, \varepsilon_y$ and ε_{xy} are negligible.
4. In order to include in plane force effects, non linear terms in the equations of motion involving products of stresses and plate slopes are retained. All other nonlinear terms are neglected.
5. The transverse shear stresses σ_{xz}, σ_{yz} vanish on the surfaces $= \mp {}^h/_2$.
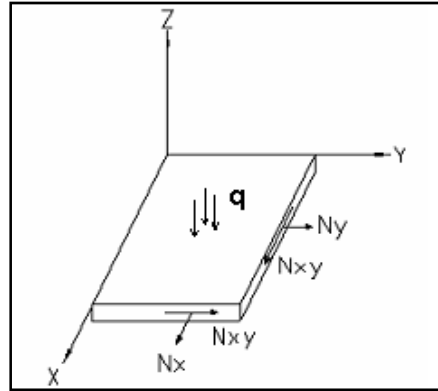
Figure 3.1: Coordinate system of plate [17].

For a symmetric type lay-up of the laminate the $B_{ij} = 0$ as coupling is eliminated and therefore, the third equation of motion can be solved separately [71].

The third equation of motion in terms of displacements takes the following form:

$$D_{11} \frac{\partial^4 w_0}{\partial x^4} + 2(D_{12} + 2D_{66}) \frac{\partial^4 w_0}{\partial x^2 \partial y^2} + D_{22} \frac{\partial^4 w_0}{\partial y^4} - N_x \frac{\partial^2 w_0}{\partial x^2} - 2N_{xy} \frac{\partial^2 w_0}{\partial x \partial y} - N_y \frac{\partial^2 w_0}{\partial y^2}$$

$$= -I_0 \frac{\partial^2 w_0}{\partial t^2} + I_2 \left(\frac{\partial^4 w_0}{\partial x^2 \partial t^2} + \frac{\partial^4 w_0}{\partial y^2 \partial t^2} \right)$$

(3.49)

3.3.1. Mathematical Modelling of Surface Mounted SMAs

The solution for the equation in the case of natural vibration can be assumed as:

$$w_0(x, y, t) = w(x, y)e^{i\omega t} \tag{3.50}$$

Substituting in the governing equation (3.49) the equation takes the form:

$$D_{11}\frac{\partial^4 w_0}{\partial x^4} + 2(D_{12} + 2D_{66})\frac{\partial^4 w_0}{\partial x^2 \partial y^2} + D_{22}\frac{\partial^4 w_0}{\partial y^4} - N_x\frac{\partial^2 w_0}{\partial x^2} - 2N_{xy}\frac{\partial^2 w_0}{\partial x \partial y} - N_y\frac{\partial^2 w_0}{\partial y^2}$$

$$- \omega^2 \left[wI_0 - I_2 \left(\frac{\partial^2 w_0}{\partial x^2} + \frac{\partial^2 w_0}{\partial y^2} \right) \right] e^{i\omega t} = 0$$

$$\tag{3.51}$$

The minimum potential energy form of the above equation is expressed as [70]:

$$0 = \int_0^b \int_0^a \left\{ D_{11}\frac{\partial^2 w}{\partial x^2}\frac{\partial^2 \delta w}{\partial x^2} + D_{12} \left(\frac{\partial^2 w}{\partial y^2}\frac{\partial^2 \delta w}{\partial x^2} + \frac{\partial^2 w}{\partial x^2}\frac{\partial^2 \delta w}{\partial y^2} \right) + 4D_{66}\frac{\partial^2 w}{\partial x \partial y}\frac{\partial^2 \delta w}{\partial x \partial y} \right.$$

$$- N_x\frac{\partial w}{\partial x}\frac{\partial \delta w}{\partial x} - N_y\frac{\partial w}{\partial y}\frac{\partial \delta w}{\partial y} - 2N_{xy}\frac{\partial w}{\partial x}\frac{\partial \delta w}{\partial y} + D_{22}\frac{\partial^2 w}{\partial y^2}\frac{\partial^2 \delta w}{\partial y^2}$$

$$\left. - \omega^2 \left[wI_0\delta w - I_2 \left(\frac{\partial w}{\partial x}\frac{\partial \delta w}{\partial x} + \frac{\partial w}{\partial y}\frac{\partial \delta w}{\partial y} \right) \right] \right\} dxdy$$

$$\tag{3.52}$$

The solution for the above differential equation is obtained by using the **Rayleigh-Ritz** method.

For rectangular plates the Rayleigh-Ritz approximation is [70]:

$$w(x, y) \cong W_{m.n}(x, y) = \sum_{i=1}^{M} \sum_{j=1}^{N} C_{ij}X_i(x)Y_j(y) \tag{3.53}$$

Substituting in equation (3.52) the energy equation takes the form:

$$\{[R] - \omega^2[B]\}\{C\} = 0 \tag{3.54}$$

Where,

$$R_{ijkl} =$$

$$\int_0^b \int_0^a \left\{ D_{11}\frac{d^2 X_i}{dx^2}\frac{d^2 X_k}{dx^2}Y_j Y_l + D_{12} \left(\frac{d^2 Y_j}{dy^2}\frac{d^2 X_k}{dx^2}X_i Y_l + \frac{d^2 X_i}{dx^2}\frac{d^2 Y_l}{dy^2}Y_j X_k \right) + 4D_{66}\frac{dX_i}{dx}\frac{dY_j}{dy}\frac{dX_k}{dx}\frac{dY_l}{dy} + \right.$$

$$\left. D_{22}\frac{d^2 Y_j}{dy^2}\frac{d^2 Y_l}{dy^2}X_i X_k - N_x\frac{dX_i}{dx}\frac{dX_k}{dx}Y_j Y_l - N_y\frac{dY_j}{dy}\frac{dY_l}{dy}X_i X_k - 2N_{xy}\frac{dX_i}{dx}\frac{dY_j}{dy}X_k Y_l \right\} dxdy$$

$$\tag{3.55}$$

$$B_{ijkl} = \int_0^b \int_0^a \left\{ I_0 X_i Y_j X_k Y_l + I_2 \left(\frac{dX_i}{dx} \frac{dX_k}{dx} Y_j Y_l + \frac{d^2 Y_j}{dy^2} \frac{d^2 Y_l}{dy^2} X_i X_k \right) \right\} dx dy$$

(3.56)

3.3.2. Analytical solutions of Surface Mounted SMAs

The composite plate in the experiment is clamped at one end and free at the other three ends (CFFF). The SMA wires are mounted on the plate with the help of bolts of 2mm diameter. The approximation function for CFFF plates will be of the form [70]:

$$X_i = \left(\frac{x}{a} \right)^{i+1} ; \ Y_j = \left(\frac{y}{b} \right)^{j-1}$$

(3.57)

The values of the natural frequencies are obtained by substituting the approximation function into equation (3.54) and then solving it. The values of in plane forces tend to be zero until the SMA wires are actuated. By substituting the values of the in plane forces in the governing equation of motion the changed values of natural frequencies can be determined.

Straight orientation

Figure (3.2) represents the arrangement of the SMA wires on the composite in a straight orientation.
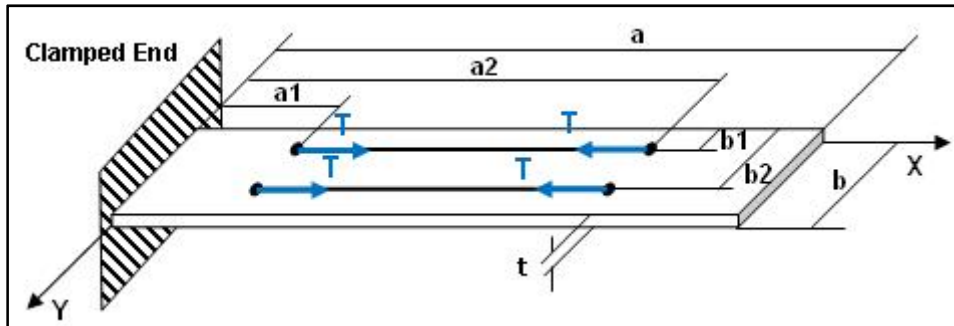
Figure 3.2: SMA wires on the composite in a straight orientation [17].

When the SMA wires are actuated the recovery force T is generated and is represented by N_x.
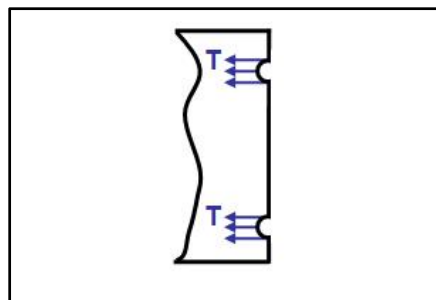
Figure 3.3: SMA recovery forces distribution.

54

This in-plane force will be acting in the x direction only. N_y and N_{xy} tend to be zero. Figure (3.3) shows the T recovery forces acting at the bolt holes, and hence the values of N_x are:

$$N_x = \begin{cases} 0 \ldots\ldots\ldots\ldots\ldots \{0 \leq y < (b_1 - r)\} \\ -T \ldots \ \{(b_1 - r) \leq y \leq (b_1 + r)\} \\ 0 \ldots\ldots\{(b_1 + r) < y < (b_2 - r)\} \\ -T \ldots\{(b_2 - r) \leq y \leq (b_2 + r)\} \\ 0 \ldots\ldots\ldots\ldots\{(b_2 + r) < y \leq b\} \end{cases} \tag{3.58}$$

Zigzag orientation

Figure (3.4) represents the arrangement of the SMA wires on the composite in a Zigzag orientation. The in plane forces acting on the composite plate are N_x, N_y they are determined by resolving the SMA wire force in X, Y directions. The effect of the recovery forces is calculated for one element which is a control volume of each leg of the zigzag and its dimensions are: (b2-b1) × (a2-a1) and is generalised for the entire plate by multiplying the number of the Zigzag legs. The values of N_x, N_y for boundary conditions of the plate are:

$$N_x = \begin{cases} 0 \ldots\ldots\ldots\ldots\ldots\ldots \{0 \leq y < (b_1 - r)\} \\ -T \cos \theta \ldots \ \{(b_1 - r) \leq y \leq (b_1 + r)\} \\ 0 \ldots\ldots\ldots\ldots\ldots\ldots \{(b_1 + r) < y \leq b\} \end{cases} \tag{3.59}$$

$$N_y = \begin{cases} 0 \ldots\ldots\ldots\ldots\ldots^{a3}\{0 \leq x < (a_2 - r)\} \\ -T \sin \theta \ldots \ \{(a_2 - r) \leq x \leq (a_2 + r)\} \\ 0 \ldots\ldots\ldots\ldots\ldots\ldots \{(a_2 + r) < x \leq a\} \end{cases} \tag{3.60}$$
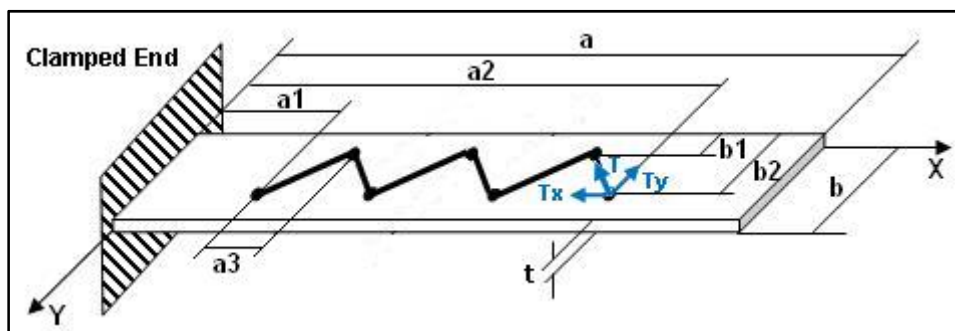
Figure 3.4: Arrangement of the SMA wires on the composite in a Zigzag orientation [17].

3.3.3. Recovery force of the Shape Memory Alloy wires

The recovery force SMA wire is determined by subjecting them to a tensile test on UNITED testing machine. The SMA wires are clamped as shown in Figure (3.5) and voltage is applied. The recovery force generated by the SMA wires is recorded using a computer. The average

force of 6N is observed and the same is used in calculation of natural frequencies of the composite plate when the SMA wires are actuated [17].

Figure 3.5: Tensile test of SMA wires on UNITED testing machine [17].

3.3.4. Experiments

Two SMA wires in straight configuration and one in zigzag configuration are mounted on the composite plates made of carbon fibre as shown in Figures (3.3) and (3.4) respectively. The plate is a 4-Ply plain woven epoxy resin pre-preg and was fabricated using cold vacuum bagging as in Figure (3.6). The experiment setup is shown in Figure (3.7).
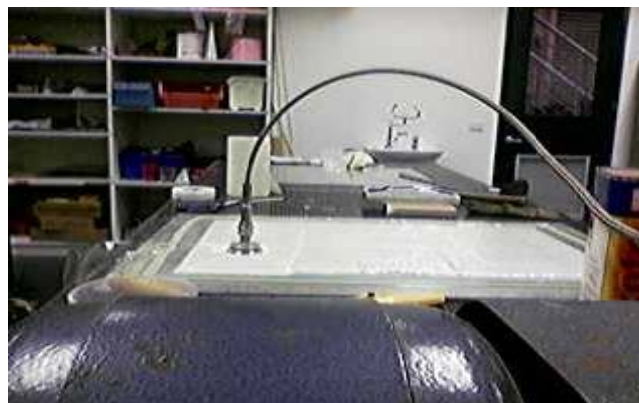
Figure 3.6: Vacuum bagging of the composite plate.
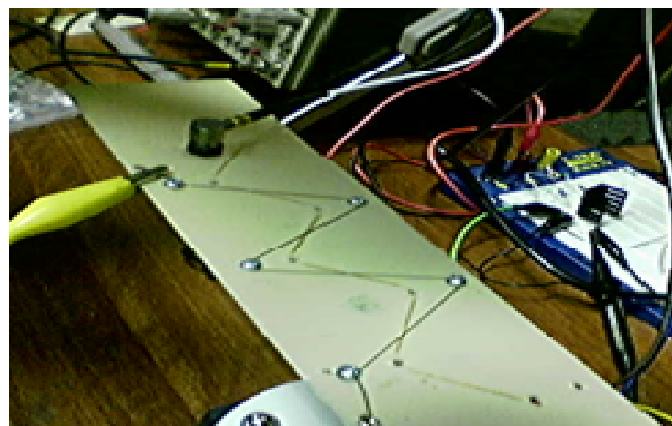
Figure 3.7: Experiment setup of surface mounted SMA wire.

The plate mechanical properties are shown in Table 3.1.

	CFRP [72]	Nitinol-SMA [73]
E(GPa)	42	27-82 (N/A- Activated.)
v_{12}	0.3	/
Diameter (m)	/	0.0001
ρ (kg/m^3)	1702	/
Length (m)	0.185	/
Width (m)	0.04	/
Thickness (m)	0.0005	/
a1 (m)	0.03	/
a2 (m)	0.15	/
a3 (m)	0.02	/
b1 (m)	0.005	/
b2 (m)	0.035	/

Table 3.1: Composite plate and SMA wire properties [72].

The composite plates are then subjected to a white noise forcing function of 1.4 KHz with the help of a mechanical shaker from the bottom. The response of the composite plates, when the SMA wires are not actuated, is recorded by using a Polytech laser vibrometer as shown in Figure (3.8). The SMA wires, as said in the ASET technique, are connected to a DC supply source for actuation.
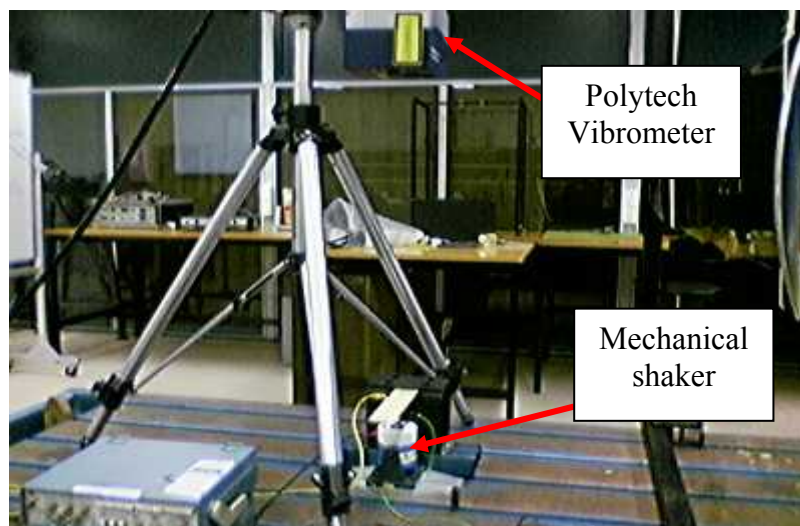
Figure 3.8: Laser vibrometer and the mechanical shaker

The responses of the composite plates after actuation are recorded. The peaks of the plotted graph are identified and recorded as natural frequencies. Figure (3.9) shows the shift of the natural frequencies of the plate when SMA wires are activated. The shift is expected to be

forward where here the shift was backward. This was due to the pre-strain of the plate induced during fabrication.
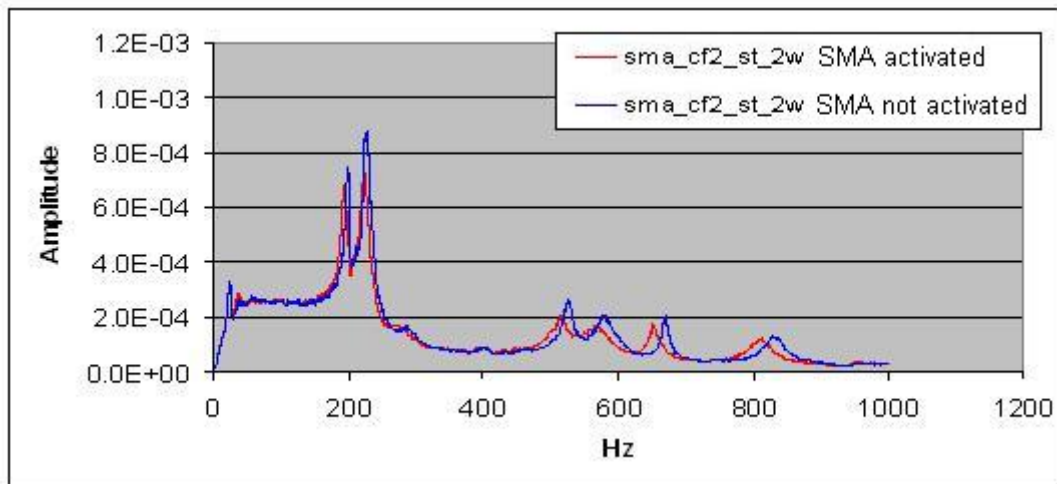
Figure 3.9 : Plots of the response of the carbon fiber plate before and after actuation of SMA wires placed in straight orientation

The experimental and analytical values of natural frequencies for the carbon fibre plate after actuation of the straight oriented SMA wires and the percentage of changes from the natural frequencies with and without activation are described in Table (3.2) and Table (3.3). The comparison between experimental and analytical values is shown in Table (3.4).

S. No	Experimental		
	ω before activation	ω after activation	% Change
1	398.906	398.438	-0.11732
2	579.219	569.688	-1.64549
3	830.938	817.469	-1.620

Table 3.2: Experimental result of Carbon fiber composites with SMA in straight orientation.

S. No	Analytical		
	ω before activation	ω after activation	% Change
1	460.5621	419.963	- 8.8
2	552.9948	563.438	1.8
3	786.0057	860.662	9.49

Table 3.3: Analytical results of Carbon fiber composites with SMA in straight orientation.

S. No	Experimental	Analytical	
	ω	ω	% difference
1	398.438	419.963	5.40
2	569.688	563.438	-1.09
3	817.469	860.662	5.2

Table 3.4: Comparison between Experimental and Analytical results of Carbon fiber composites where, the SMA wires in straight orientation are activated.

Figure (3.10) shows the shift in the natural frequencies of the plate due to the activation of the wire in zigzag configuration. The corresponding values for the zigzag orientation are shown in Tables (3.5) & (3.6) and the comparison between the experimental and analytical values are shown in Table (3.7).
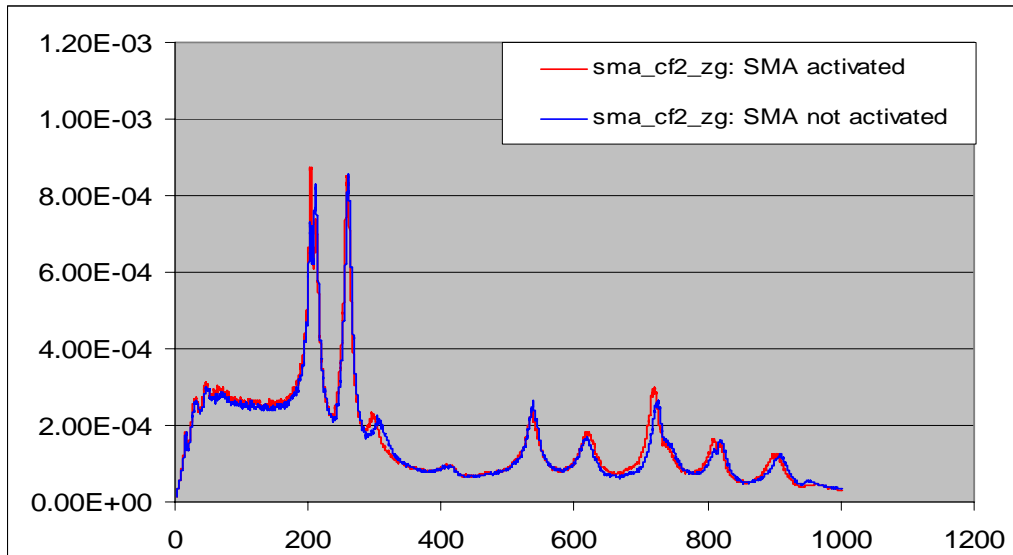
Figure 3.10: Plots of the response of the carbon fiber plate before and after actuation of SMA wires placed in Zigzag orientation.

S. No	Experimental		
	ω before activation	ω after activation	% change
1	303.125	295.938	-2.37097
2	412.969	406.719	-1.51343
3	724.531	717.344	-0.99195

Table 3.5: Experimental results of Carbon fiber composites with SMA in Zigzag orientation.

S. No	Analytical		
	ω before activation	ω after activation	% change
1	354.1872966	360.8557681	1.882753
2	475.1917858	496.8088893	4.549132
3	725.8666473	729.9676982	0.564987

Table 3.6: Analytical results of Carbon fiber composites with SMA in Zigzag orientation.

S. No	Experimental	Analytical	
	ω	ω	% difference
1	303.125	354.187	1.883
2	536.406	475.192	0.252
3	724.531	725.867	0.565

Table 3.7: Comparison between Experimental and Analytical results of Carbon fiber composites where, the SMA wires in Zigzag orientation are not activated.

In comparison to the straight SMA configuration, it was surprising that the natural frequency shift was not more significant for the zigzag configuration. In Tables 3.2–3.7 above, only the first three modes are compared because it was considered that the other modes were not considered significant from energy and prospective applications perspectives. A prospective application area is in the flutter suppression of aerodynamic structures where a shift in the natural frequencies might attenuate the amplitudes of vibration. Other application areas include active vibration of low frequency (<5 Hz) structures such as in slow turning wind turbine blades. However, as seen in Figures (3.9) and (3.10), the most significant shift, relatively, in frequencies for both the configurations in this study, occurred at the 4th mode and higher.

There are a few interesting findings from the experiments. Firstly it is noted that for both the straight and zigzag SMA configurations, the post-activation plate natural frequencies are affected only a little and is reduced slightly. This might be accounted for by the fact that the SMA's contract on activation and when anchored to a plate that might have a slightly fabrication-induced tensile strain, the effective stiffness of the plate will drop as evidenced in these plots. Secondly, it seemed that the straight SMA configuration induced a higher plate stiffness compared to that from the zigzag configuration which is almost contrary to expectations, at least from, strain energy considerations since the zigzag configuration has

more spatial coverage. Also, from Tables 3.4 & 3.7 it is clear that the analytical modelling of this actuation process matches the experimental findings well for both the straight and zigzag SMA configurations [72].

3.4. Summary

The effect of various configurations of surface mounted SMA wires on a composite strip is presented in this chapter. Detailed mathematical modelling based on various theories and relations incorporating motion and strain energy of the materials were used. The effect of tensioning the SMA wires on the natural frequencies of the strip is obtained analytically and experimentally. A good match is observed between the analytical and experimental results.

The same theories and approach will be used in mathematical modelling the beam flutter control using piezoelectric wafers. However, the solution will be obtained numerically by using the Finite Element method.

Chapter 4. AEROELASTIC STRUCTURES INCORPORATING PIEZOELECTRIC WAFERS

4.1. Problem Statement

The aeroelasticity of the structures, such as bridges and aircraft wings, are traditionally treated as dynamic problems rather than structural dynamics where the point-mass modelling method is used for the analysis. In this chapter, a solid mechanic based formulation of a bending-torsion structure problem incorporating piezoelectric patches is derived. The formulation enables the piezoelectric patches to be oriented (skewed) in different angles relative to the host structure.

4.2. Mathematical Model

A simple model is used in aeroelasticity problems analysis. This model is known as *Typical Section*. As in Figure 4.1, the typical section is a system of rigid, flat plate airfoil mounted on a torsional and flexural springs to wind tunnel walls [45].
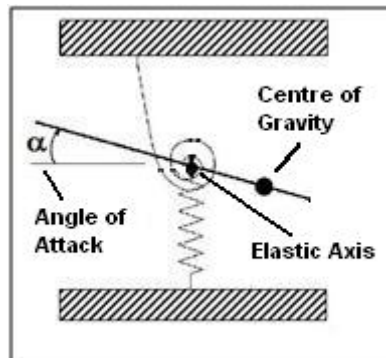
Figure 4.1: Typical section airfoil.

This model helped in determining the basic aeroelasticity design criteria such as wing flutter speed, wing divergence speed, reversal of control surface and gust response. However, since the aeroelasticity is a function of the span-wise aeroloading and mass distribution a 3D model, as shown in Figure 4.2, is used to account for it. For small twist angle ($\alpha \ll 1$) the cantilevered wing displacement "h" in the Z-axis consists of two displacements; translational (also known as plunge and flap) displacement "w" and torsional (also known as pitch) displacement "yα". So Eqn. (3.4) can be written as:

$$u(x, y, z, t) = u_0(x, y, t) - z \frac{\partial w}{\partial y} \qquad (4.1\text{a})$$

$$v(x, y, z, t) = v_0(x, y, t) - z \frac{\partial w}{\partial y} \qquad (4.1\text{b})$$

$$w(x, y, z, t) = h(x, y, t) + y\, \alpha(x, y, t) \qquad (4.1\text{c})$$

Substituting Eqn. (4.1) into *Von Kármán* strains of Eqn. (3.8);
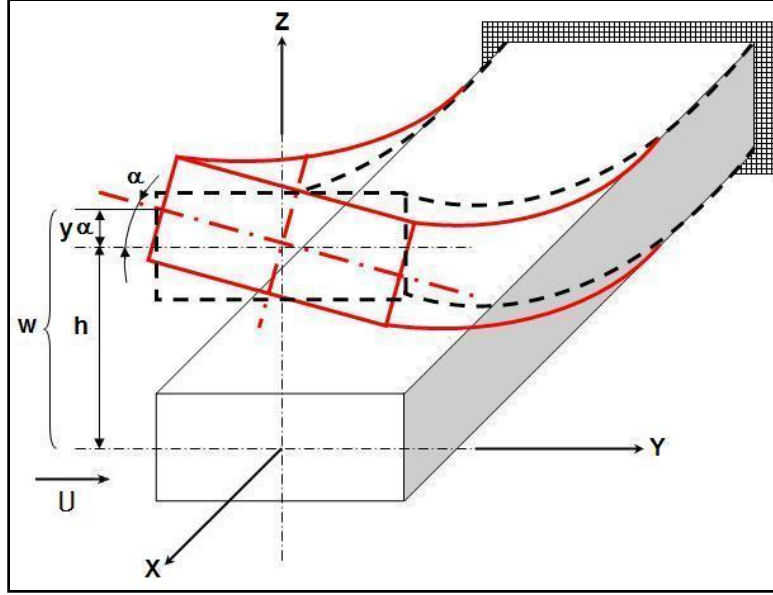
Figure 4.2: 3D Model of cantilevered wing.

$$\varepsilon_{xx} = \frac{\partial u_0}{\partial x} + \frac{1}{2}\left(\frac{\partial h}{\partial x} + y \frac{\partial \alpha}{\partial x}\right)^2 - z\left(\frac{\partial^2 h}{\partial x^2} + y \frac{\partial^2 \alpha}{\partial x^2}\right)$$

$$\varepsilon_{yy} = \frac{\partial \vartheta_0}{\partial y} + \frac{1}{2}\left(\frac{\partial h}{\partial y} + \alpha + y \frac{\partial \alpha}{\partial y}\right)^2 - z\left(\frac{\partial^2 h}{\partial y^2} + 2\frac{\partial \alpha}{\partial y} + y \frac{\partial^2 \alpha}{\partial y^2}\right)$$

$$\varepsilon_{xy} = \frac{1}{2}\left[\frac{\partial u_0}{\partial y} + \frac{\partial \vartheta_0}{\partial x} + \left(\frac{\partial h}{\partial x} + y \frac{\partial \alpha}{\partial y}\right)\left(\frac{\partial h}{\partial y} + \alpha + y \frac{\partial \alpha}{\partial y}\right)\right] - z\left(\frac{\partial^2 h}{\partial x \partial y} + \frac{\partial \alpha}{\partial x} + y \frac{\partial^2 \alpha}{\partial x \partial y}\right)$$

$$(4.2)$$

4.2.1. Equations of Motion

As in chapter 3, the governing equations of motion for the flutter problem is obtained by applying the Hamilton's principle as in Eqn. (3.27);

$$\int_0^{\mathrm{T}} (\delta U + \delta V - \delta K)\, dt = 0 \qquad (4.3)$$

Taking the variation "δ" of the strains in Eqn. (4.2) and putting it in the form of Eqn. (3.9);

$$\delta\varepsilon_{xx}^0 = \frac{\partial \delta u_0}{\partial x} + \frac{1}{2}\delta\left(\frac{\partial h}{\partial x}\right)^2 + \delta\left(y\frac{\partial h}{\partial x}\frac{\partial \alpha}{\partial y}\right) + \frac{1}{2}\delta\left(y^2\left(\frac{\partial \alpha}{\partial x}\right)^2\right)$$

$$\delta\varepsilon_{xx}^0 = \frac{\partial \delta u_0}{\partial x} + \frac{\partial h}{\partial x}\frac{\partial \delta h}{\partial x} + y\frac{\partial \delta h}{\partial x}\frac{\partial \alpha}{\partial x} + y\frac{\partial h}{\partial x}\frac{\partial \delta \alpha}{\partial x} + y^2\frac{\partial \alpha}{\partial x}\frac{\partial \delta \alpha}{\partial x} \qquad (4.4)$$

$$\delta\varepsilon_{xx}^1 = \delta\left(-\frac{\partial^2 h}{\partial x^2} - y\frac{\partial^2 \alpha}{\partial x^2}\right) = -\frac{\partial^2 \delta h}{\partial x^2} - y\frac{\partial^2 \delta \alpha}{\partial x^2} \qquad (4.5)$$

$$\delta\varepsilon_{yy}^0 = \frac{\partial v_0}{\partial y} + \frac{1}{2}\left(\frac{\partial h}{\partial x} + \alpha + y\frac{\partial \alpha}{\partial y}\right)^2$$

$$= \frac{\partial \vartheta_0}{\partial y} + \frac{1}{2}\left[\left(\frac{\partial h}{\partial x} + \alpha\right)^2 + 2y\frac{\partial \alpha}{\partial y}\left(\frac{\partial h}{\partial y} + \alpha\right) + y^2\left(\frac{\partial \alpha}{\partial y}\right)^2\right]$$

$$= \frac{\partial \vartheta_0}{\partial y} + \frac{1}{2}\left[\left(\frac{\partial h}{\partial y}\right)^2 + 2\alpha\frac{\partial h}{\partial y} + \alpha^2\right] + y\frac{\partial \alpha}{\partial y}\frac{\partial h}{\partial y} + y\frac{\partial \alpha}{\partial y}\alpha + \frac{1}{2}y^2\left(\frac{\partial \alpha}{\partial y}\right)^2$$

$$\delta\varepsilon_{yy}^0 = \frac{\partial \delta\vartheta_0}{\partial y} + \frac{\partial h}{\partial y}\frac{\partial \delta h}{\partial y} + \frac{\partial h}{\partial y}\delta\alpha + \alpha\frac{\partial \delta h}{\partial y} + \alpha\delta\alpha + y\frac{\partial h}{\partial y}\frac{\partial \delta\alpha}{\partial y} + y\frac{\partial \alpha}{\partial y}\frac{\partial \delta h}{\partial y} +$$

$$y\alpha\frac{\partial \delta\alpha}{\partial y} + y\frac{\partial \alpha}{\partial y}\,\delta\alpha + y^2\frac{\partial \delta\alpha}{\partial y}\frac{\partial \alpha}{\partial y} \qquad (4.6)$$

$$\delta\varepsilon_{yy}^1 = -\left[\frac{\partial^2 \delta h}{\partial y^2} + 2\frac{\partial \delta\alpha}{\partial y} + y\frac{\partial^2 \delta\alpha}{\partial y^2}\right] \qquad (4.7)$$

$$\varepsilon_{xy}^0 = \frac{1}{2}\left(\frac{\partial u_0}{\partial y} + \frac{\partial \vartheta_0}{\partial x} + \frac{\partial h}{\partial x}\frac{\partial h}{\partial y} + \alpha\frac{\partial h}{\partial x} + y\frac{\partial h}{\partial x}\frac{\partial \alpha}{\partial y} + y\frac{\partial \alpha}{\partial x}\frac{\partial h}{\partial y} + \alpha y\frac{\partial \alpha}{\partial x}\right.$$

$$\left. + y^2\frac{\partial \alpha}{\partial x}\frac{\partial \alpha}{\partial y}\right)$$

$$\delta\varepsilon_{xy}^0 = \frac{1}{2}\left(\frac{\partial \delta u_0}{\partial y} + \frac{\partial \delta\vartheta_0}{\partial x} + \frac{\partial h}{\partial y}\frac{\partial \delta h}{\partial x} + \frac{\partial h}{\partial x}\frac{\partial \delta h}{\partial y} + \frac{\partial h}{\partial x}\delta\alpha + \alpha\frac{\partial \delta h}{\partial x} +\right.$$

$$y\frac{\partial \alpha}{\partial y}\frac{\partial \delta h}{\partial x} + y\frac{\partial h}{\partial x}\frac{\partial \delta\alpha}{\partial y}\right) + y\frac{\partial h}{\partial y}\frac{\partial \delta\alpha}{\partial x} + y\frac{\partial \alpha}{\partial x}\frac{\partial \delta h}{\partial y} + y\frac{\partial \alpha}{\partial x}\,\delta\alpha + y\alpha\frac{\partial \delta\alpha}{\partial x} +$$

$$y^2\frac{\partial \alpha}{\partial x}\frac{\partial \delta\alpha}{\partial y} + y^2\frac{\partial \alpha}{\partial y}\,\frac{\partial \delta\alpha}{\partial x} \qquad (4.8)$$

$$\delta\varepsilon_{xy}^1 = -\left(\frac{\partial^2 \delta h}{\partial x\partial y} + \frac{\partial \delta\alpha}{\partial x} + y\frac{\partial^2 \delta\alpha}{\partial x\partial y}\right) \qquad (4.9)$$

Since ($\gamma_{xy} = 2\varepsilon_{xy}$), substituting Eqn's (4.4) to (4.9) in Eqn. (3.33) the **Strain Energy** is:

$$\delta U = \int_\forall \left[N_{xx} \left(\frac{\partial \delta u_0}{\partial x} + \frac{\partial h}{\partial x}\frac{\partial \delta h}{\partial x} + y\frac{\partial \delta h}{\partial x}\frac{\partial \alpha}{\partial x} + y\frac{\partial h}{\partial x}\frac{\partial \delta \alpha}{\partial x} + y^2\frac{\partial \alpha}{\partial x}\frac{\partial \delta x}{\partial x} \right) + \right.$$

$$M_{xx}\left(-\frac{\partial^2 \delta h}{\partial x^2} - y\frac{\partial^2 \delta \alpha}{\partial x^2} \right) + N_{yy}\left(\frac{\partial \delta \vartheta_0}{\partial y} + \frac{\partial h}{\partial y}\frac{\partial \delta h}{\partial y} + \frac{\partial h}{\partial y}\delta \alpha + \alpha\frac{\partial \delta h}{\partial y} + \alpha\delta \alpha + \right.$$

$$y\frac{\partial h}{\partial y}\frac{\partial \delta \alpha}{\partial y} + y\frac{\partial \alpha}{\partial y}\frac{\partial \delta h}{\partial y} + y\alpha\frac{\partial \delta \alpha}{\partial y} + y\frac{\partial \alpha}{\partial y}\delta \alpha + y^2\frac{\partial \delta \alpha}{\partial y}\frac{\partial \alpha}{\partial y} \right) + M_{yy}\left(-\frac{\partial^2 \delta h}{\partial y^2} - 2\frac{\partial \delta \alpha}{\partial y} - \right.$$

$$\left. y\frac{\partial^2 \delta \alpha}{\partial y^2} \right) + N_{xy}\left(\frac{\partial \delta u_0}{\partial y} + \frac{\partial \delta \vartheta_0}{\partial x} + \frac{\partial h}{\partial y}\frac{\partial \delta h}{\partial x} + \frac{\partial h}{\partial x}\frac{\partial \delta h}{\partial y} + \frac{\partial h}{\partial x}\delta \alpha + \alpha\frac{\partial \delta h}{\partial y} + y\frac{\partial \alpha}{\partial y}\frac{\partial \delta h}{\partial x} + \right.$$

$$y\frac{\partial h}{\partial x}\frac{\partial \delta \alpha}{\partial y} + y\frac{\partial h}{\partial y}\frac{\partial \delta \alpha}{\partial x} + y\frac{\partial \alpha}{\partial x}\frac{\partial \delta h}{\partial y} + y\frac{\partial \alpha}{\partial x}\delta \alpha + y\alpha\frac{\partial \delta \alpha}{\partial y} + y^2\frac{\partial \alpha}{\partial x}\frac{\partial \delta \alpha}{\partial y} + y^2\frac{\partial \alpha}{\partial y}\frac{\partial \delta \alpha}{\partial x} \right) -$$

$$\left. 2M_{xy}\left(\frac{\partial^2 \delta h}{\partial x\partial y} + \frac{\partial \delta \alpha}{\partial x} + y\frac{\partial^2 \delta \alpha}{\partial x\partial y} \right) \right] dxdy \tag{4.10}$$

Let;

$$Y_0, Y_1, \ Y_0 = \int_{chord}(1, y, y^2)dy \tag{4.11}$$

Eqn. (4.10) can be rewritten as;

$$\delta U =$$

$$\int_0^l \left\{ N_{xx}\left[Y_0\left(\frac{\partial \delta u_0}{\partial x} + \frac{\partial h}{\partial x}\frac{\partial \delta h}{\partial x} \right) + Y_1\left(\frac{\partial \delta h}{\partial x}\frac{\partial \alpha}{\partial x} + \frac{\partial h}{\partial x}\frac{\partial \delta \alpha}{\partial x} \right) + Y_2\frac{\partial \alpha}{\partial x}\frac{\partial \delta x}{\partial x} \right] - M_{xx}\left(Y_0\frac{\partial^2 \delta h}{\partial x^2} + \right. \right.$$

$$Y_1\frac{\partial^2 \delta \alpha}{\partial x^2} \right) - M_{yy}\left[Y_0\left(\frac{\partial^2 \delta h}{\partial y^2} + 2\frac{\partial \delta \alpha}{\partial y} \right) + Y_1\frac{\partial^2 \delta \alpha}{\partial y^2} \right] - 2M_{xy}\left[Y_0\left(\frac{\partial^2 \delta h}{\partial x\partial y} + \frac{\partial \delta \alpha}{\partial x} \right) + \right.$$

$$\left. Y_1\frac{\partial^2 \delta \alpha}{\partial x\partial y} \right] + N_{yy}\left[Y_0\left(\frac{\partial \delta \vartheta_0}{\partial y} + \frac{\partial h}{\partial y}\frac{\partial \delta h}{\partial y} + \frac{\partial h}{\partial y}\delta \alpha + \alpha\frac{\partial \delta h}{\partial y} + \alpha\delta \alpha \right) + Y_1\left(\frac{\partial h}{\partial y}\frac{\partial \delta \alpha}{\partial y} + \right. \right.$$

$$\left. \frac{\partial \alpha}{\partial y}\frac{\partial \delta h}{\partial y} + \alpha\frac{\partial \delta \alpha}{\partial y} + \frac{\partial \alpha}{\partial y}\delta \alpha \right) + Y_2\frac{\partial \delta \alpha}{\partial y}\frac{\partial \alpha}{\partial y} \right] + N_{xy}\left[Y_0\left(\frac{\partial \delta u_0}{\partial y} + \frac{\partial \delta \vartheta_0}{\partial x} + \frac{\partial h}{\partial y}\frac{\partial \delta h}{\partial x} + \right. \right.$$

$$\frac{\partial h}{\partial x}\frac{\partial \delta h}{\partial y} + \frac{\partial h}{\partial x}\delta \alpha + \alpha\frac{\partial \delta h}{\partial y} \right) + Y_1\left(\frac{\partial \alpha}{\partial y}\frac{\partial \delta h}{\partial x} + \frac{\partial h}{\partial x}\frac{\partial \delta \alpha}{\partial y} + \frac{\partial h}{\partial y}\frac{\partial \delta \alpha}{\partial x} + \frac{\partial \alpha}{\partial x}\frac{\partial \delta h}{\partial y} + \frac{\partial \alpha}{\partial x}\delta \alpha + \right.$$

$$\left. \left. \left. \alpha\frac{\partial \delta \alpha}{\partial y} \right) + Y_2\left(\frac{\partial \alpha}{\partial x}\frac{\partial \delta \alpha}{\partial y} + \frac{\partial \alpha}{\partial y}\frac{\partial \delta \alpha}{\partial x} \right) \right] \right\} dx \tag{4.12}$$

For the **Kinetic Energy** Eqn. (3.37) can be written as;

$$K = \int_{v_0} \frac{1}{2}\rho_0\left(\dot{u}^2 + \dot{\vartheta}^2 + \dot{w}^2 \right)dzdxdy \tag{4.13}$$

Taking the variation of Eqn. (4.13);

$$\delta K = \int_{v_0} \frac{1}{2}\rho_0\left(\delta\dot{u}^2 + \delta\dot{\vartheta}^2 + \delta\dot{w}^2\right)dzdxdy \tag{4.14}$$

By substituting Eqn. (4.1c) in Eqns. (4.1a & 4.1b);

$$u = u_0 - z\left(\frac{\partial h}{\partial x} + y\frac{\partial \alpha}{\partial x}\right)$$

$$\vartheta = \vartheta_0 - z\left(\frac{\partial h}{\partial y} + \alpha + y\frac{\partial \alpha}{\partial y}\right)$$

$$w = h + y\alpha \tag{4.15}$$

By differentiating Eqn. (4.15) the displacement velocities are;

$$\dot{u} = \dot{u}_0 - z\left(\frac{\partial \dot{h}}{\partial x} + y\frac{\partial \dot{\alpha}}{\partial x}\right)$$

$$\dot{\vartheta} = \dot{\vartheta}_0 - z\left(\frac{\partial \dot{h}}{\partial x} + \dot{\alpha} + y\frac{\partial \dot{\alpha}}{\partial y}\right)$$

$$\dot{w} = \dot{h} + y\dot{\alpha} \tag{4.16}$$

Taking the variation "δ" of the square velocities in Eqn. (4.16);

$$\delta\dot{u}^2 = \delta\left[\dot{u}_0 - z\left(\frac{\partial \dot{h}}{\partial x} + y\frac{\partial \dot{\alpha}}{\partial x}\right)\right]^2$$

$$\delta\dot{u}^2 = 2\left(\dot{u}_0 - z\frac{\partial \dot{h}}{\partial x} - zy\frac{\partial \dot{\alpha}}{\partial x}\right)\left(\delta\dot{u}_0 - z\frac{\partial \delta\dot{h}}{\partial x} - zy\frac{\partial \delta\dot{\alpha}}{\partial x}\right) \tag{4.17a}$$

$$\delta\dot{\vartheta}^2 = \delta\left[\dot{\vartheta}_0 - Z\left(\frac{\partial \dot{h}}{\partial x} + \dot{\alpha} + y\frac{\partial \dot{\alpha}}{\partial y}\right)\right]^2$$

$$\delta\dot{\vartheta}^2 = 2\left(\dot{\vartheta}_0 - z\frac{\partial \dot{h}}{\partial y} - z\dot{\alpha} - zy\frac{\partial \dot{\alpha}}{\partial y}\right)\left(\delta\dot{\vartheta}_0 - z\frac{\partial \dot{h}}{\partial y} - z\dot{\alpha} - zy\frac{\partial \dot{\alpha}}{\partial y}\right) \tag{4.17b}$$

$$\delta\dot{w}^2 = \delta\left(\dot{h} + y\dot{\alpha}\right)^2$$

$$\delta\dot{w}^2 = 2\left(\dot{h} + y\dot{\alpha}\right)\left(\delta\dot{h} + y\delta\dot{\alpha}\right) \tag{4.17c}$$

Substituting Eqn. (4.17 in Eqn. (4.14);

$$\delta K = \int_{v_0} \frac{1}{2}\rho_0 \left[2\left(\dot{u}_0 - z\frac{\partial \dot{h}}{\partial x} - zy\frac{\partial \dot{\alpha}}{\partial x}\right)\left(\delta\dot{u}_0 - z\frac{\partial \delta\dot{h}}{\partial x} - zy\frac{\partial \delta\dot{\alpha}}{\partial x}\right) + 2\left(\dot{\vartheta}_0 - z\frac{\partial \dot{h}}{\partial y} - \right.\right.$$

$$\left.\left. z\dot{\alpha} - zy\frac{\partial \dot{\alpha}}{\partial y}\right)\left(\delta\dot{\vartheta}_0 - z\frac{\partial \delta\dot{h}}{\partial y} - zy\frac{\partial \delta\dot{\alpha}}{\partial y}\right) + 2\left(\dot{h} + y\dot{\alpha}\right)\left(\delta\dot{h} + y\delta\dot{\alpha}\right) \right] dxdydz$$

(4.18)

$$\delta K = \int_{\forall} \rho_0 \left[\dot{u}_0\delta\dot{u}_0 - \dot{u}_0 Z\frac{\partial \delta\dot{h}}{\partial x} - \dot{u}_0 zy\frac{\partial \delta\dot{\alpha}}{\partial x} - z\frac{\partial \dot{h}}{\partial x}\delta\dot{u}_0 + z^2\frac{\partial \dot{h}}{\partial x}\frac{\partial \delta\dot{h}}{\partial x} + \right.$$

$$z^2 y\frac{\partial \dot{h}}{\partial x}\frac{\partial \delta\dot{\alpha}}{\partial x} - zy\frac{\partial \dot{\alpha}}{\partial x}\delta\dot{u}_0 + z^2 y\frac{\partial \dot{\alpha}}{\partial x}\frac{\partial \delta\dot{h}}{\partial x} + z^2 y^2\frac{\partial \dot{\alpha}}{\partial x}\frac{\partial \delta\dot{\alpha}}{\partial x} - \dot{\vartheta}\,\delta\dot{\vartheta}_0 - \dot{\vartheta}_0 z\frac{\partial \delta\dot{h}}{\partial y} - $$

$$\dot{\vartheta}_0 z\delta\dot{\alpha} - \dot{\vartheta}_0 zy\frac{\partial \delta\dot{\alpha}}{\partial y} - z\frac{\partial \dot{h}}{\partial x}\delta\dot{\vartheta}_0 + z^2\frac{\partial \dot{h}}{\partial y}\frac{\partial \delta\dot{h}}{\partial y} + z^2\frac{\partial \dot{h}}{\partial y}\delta\dot{\alpha} + z^2 y\frac{\partial \dot{h}}{\partial y}\frac{\partial \delta\dot{\alpha}}{\partial y} - z\dot{\alpha}\delta\dot{\vartheta}_0 + $$

$$z^2\dot{\alpha}\frac{\partial \delta\dot{h}}{\partial y} + z^2\dot{\alpha}\delta\dot{\alpha} + z^2 y\dot{\alpha}\frac{\partial \delta\dot{\alpha}}{\partial y} - zy\frac{\partial \dot{\alpha}}{\partial y}\delta\dot{\vartheta}_0 + z^2 y\frac{\partial \dot{\alpha}}{\partial y}\frac{\partial \delta\dot{h}}{\partial y} + z^2 y\frac{\partial \dot{\alpha}}{\partial y}\delta\dot{\alpha} + $$

$$z^2 y^2\frac{\partial \dot{\alpha}}{\partial y}\frac{\partial \delta\dot{\alpha}}{\partial y} + \dot{h}\,\delta\dot{h} + y\dot{h}\delta\dot{\alpha} + y\dot{\alpha}\delta\dot{h} + y^2\dot{\alpha}\delta\dot{\alpha} \right] dxdydz$$

(4.19)

Let;

$$I_{00}, I_{01}, I_{02} = \int_{\forall} \rho_0(1, y, y^2)dydz$$

$$I_{10}, I_{11}, I_{12} = \int_{\forall} \rho_0(1, y, y^2)zdydz$$

$$I_{20}, I_{21}, I_{22} = \int_{\forall} \rho_0(1, y, y^2)z^2dydz$$

(4.20)

Using Eqn. (4.20) in Eqn. (4.19);

$$\delta K =$$

$$\int_0^\ell \left[I_{00}\left(\dot{u}_0\delta\dot{u}_0 + \dot{\vartheta}\delta\dot{\vartheta}_0 + \dot{h}\delta\dot{h}\right) + I_{01}\left(\dot{h}\delta\dot{\alpha} + \dot{\alpha}\delta\dot{h}\right) + I_{02}\dot{\alpha}\delta\dot{\alpha} - I_{10}\left(\dot{u}_0\frac{\partial \delta\dot{h}}{\partial x} + \right.\right.$$

$$\frac{\partial \dot{h}}{\partial x} \delta \dot{u}_0 + \dot{\vartheta}_0 \frac{\partial \delta h}{\partial y} + \dot{\vartheta}_0 \delta \dot{\alpha} + \frac{\partial \dot{h}}{\partial y} \delta \dot{\vartheta} + \dot{\alpha} \delta \dot{\vartheta} \Big) - I_{11} \Big(\dot{u}_0 \frac{\partial \delta \dot{\alpha}}{\partial x} + \frac{\partial \dot{\alpha}}{\partial x} \delta \dot{u}_0 + \dot{\vartheta}_0 \frac{\partial \delta \dot{\alpha}}{\partial y} +$$

$$\frac{\partial \dot{\alpha}}{\partial y} \delta \dot{\vartheta} \Big) + I_{20} \Big(\frac{\partial \dot{h}}{\partial x} \frac{\partial \delta \dot{h}}{\partial x} + \frac{\partial \dot{h}}{\partial y} \frac{\partial \delta \dot{h}}{\partial y} + \frac{\partial \dot{h}}{\partial y} \delta \dot{\alpha} + \dot{\alpha} \frac{\partial \delta \dot{h}}{\partial y} + \dot{\alpha} \delta \dot{\alpha} \Big) + I_{21} \Big(\frac{\partial \dot{h}}{\partial x} \frac{\partial \delta \dot{\alpha}}{\partial x} + \frac{\partial \dot{\alpha}}{\partial x} \frac{\partial \delta \dot{h}}{\partial x} +$$

$$\frac{\partial \dot{h}}{\partial y} \frac{\partial \delta \dot{\alpha}}{\partial y} + \dot{\alpha} \frac{\partial \delta \dot{\alpha}}{\partial y} + \frac{\partial \dot{\alpha}}{\partial y} \frac{\partial \delta \dot{h}}{\partial y} + \frac{\partial \dot{\alpha}}{\partial y} \delta \dot{\alpha} \Big) + I_{22} \Big(\frac{\partial \dot{\alpha}}{\partial x} \frac{\partial \delta \dot{\alpha}}{\partial x} + \frac{\partial \dot{\alpha}}{\partial y} \frac{\partial \delta \dot{\alpha}}{\partial y} \Big) \Big] dx$$

<div align="right">(4.21)</div>

For the work done by external applied forces and moments (lift and pitching moment) as shown in Figure (4.3) can be written as;
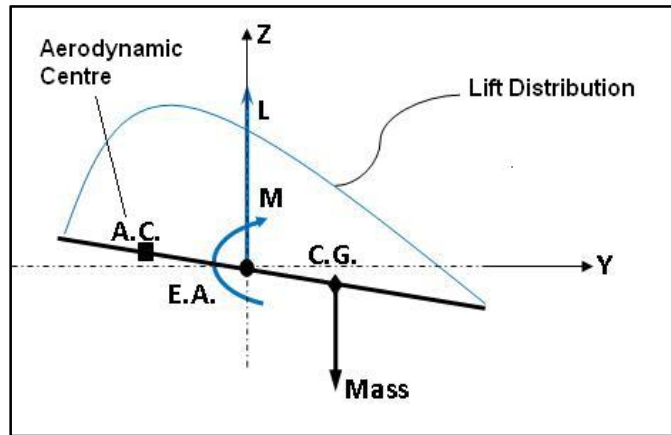
Figure 4.3: External applied (Lift) forces.

$$V = - \int_{\forall} p \ dx dy \ w \tag{4.22}$$

$$V = - \int_0^\ell \int_0^c p \ (h + y\alpha) dy dx$$

$$V = - \int_0^\ell \int_0^c (ph + py \ \alpha) dy dx$$

$$V = - \int_0^\ell \left(\int_0^c p \ h \ dy + \int_0^c p \ y \ dy \ \alpha \right) dx$$

$$V = - \int_0^\ell (Lh + M_y \alpha) \ dx \tag{4.23}$$

Taking the variation;

$$\delta V = - \int_0^\ell (L\delta h + M_y \delta \alpha) \ dx \tag{4.24}$$

Substituting Eqns. (4.12), (4.21) & (4.24) in Eqn. (4.3), integrating by parts and setting the coefficients of $\delta u_0, \delta \vartheta_0, \delta h \,\&\, \delta \alpha$ separately to zero, the Equations of Motion (Euler-Lagrange) are:

$$\delta u_0 \Longrightarrow \quad -Y_0\left(\frac{\partial N_{xx}}{\partial x} + \frac{\partial N_{xy}}{\partial y}\right) + I_{00}\,\ddot{u}_0 - I_{10}\,\frac{\partial \ddot{h}}{\partial x} - I_{11}\,\frac{\partial \ddot{\alpha}}{\partial x} = 0$$

(4.25)

$$\delta \vartheta_0 \Longrightarrow \quad -Y_0\left(\frac{\partial N_{yy}}{\partial y} + \frac{\partial N_{xy}}{\partial x}\right) + I_{00}\,\ddot{\vartheta}_0 - I_{10}\left(\frac{\partial \ddot{h}}{\partial y} + \ddot{\alpha}\right) - I_{11}\,\frac{\partial \ddot{\alpha}}{\partial x} = 0$$

(4.26)

$$\delta h \Longrightarrow \quad -Y_0\left(\frac{\partial^2 M_{xx}}{\partial x^2} + \frac{\partial^2 M_{yy}}{\partial y^2} + 2\frac{\partial^2 M_{xy}}{\partial x \partial y}\right) - \frac{\partial}{\partial x}\left[Y_0\left(N_{xx}\frac{\partial h}{\partial x} + N_{xy}\frac{\partial h}{\partial y} + \right.\right.$$
$$\left.\left. N_{xy}\alpha\right) + Y_1\left(N_{xx}\frac{\partial \alpha}{\partial x} + N_{xy}\frac{\partial \alpha}{\partial y}\right)\right] - \frac{\partial}{\partial y}\left[Y_0\left(N_{yy}\frac{\partial h}{\partial y} + \alpha N_{yy} + N_{xy}\frac{\partial h}{\partial x}\right) + \right.$$
$$\left. Y_1\left(N_{yy}\frac{\partial \alpha}{\partial y} + N_{xy}\frac{\partial \alpha}{\partial x}\right)\right] + I_{00}\,\ddot{h} - I_{01}\ddot{\alpha} + I_{10}\left(\frac{\partial \ddot{u}_0}{\partial x} + \frac{\partial \ddot{\vartheta}_0}{\partial y}\right) - I_{20}\left(\frac{\partial^2 \ddot{h}}{\partial x^2} + \frac{\partial^2 \ddot{h}}{\partial y^2} + \right.$$
$$\left. \frac{\partial \ddot{\alpha}}{\partial y}\right) - I_{21}\left(\frac{\partial^2 \ddot{\alpha}}{\partial x^2} + \frac{\partial^2 \ddot{\alpha}}{\partial y^2}\right) - L = 0$$

(4.27)

$$\delta \alpha \Longrightarrow \quad Y_0\left(2\frac{M_{yy}}{\partial y} + N_{yy}\frac{\partial h}{\partial y} + N_{yy}\alpha + N_{xy}\frac{\partial h}{\partial x} + 2\frac{\partial M_{xy}}{\partial x}\right) + Y_1\left(N_{yy}\frac{\partial \alpha}{\partial y} - \right.$$
$$\frac{\partial^2 M_{xx}}{\partial x^2} - \frac{\partial^2 M_{yy}}{\partial y^2} + N_{xy}\frac{\partial \alpha}{\partial x} - 2\frac{\partial^2 M_{xy}}{\partial x \partial y}\right) - \frac{\partial}{\partial x}\left[Y_1\left(N_{xx}\frac{\partial h}{\partial x} + N_{xy}\frac{\partial h}{\partial y} + \right.\right.$$
$$\left.\left. \alpha N_{xy}\right) + Y_2\left(N_{xx}\frac{\partial \alpha}{\partial x} + N_{xy}\frac{\partial \alpha}{\partial y}\right)\right] - \frac{\partial}{\partial y}\left[Y_1\left(N_{yy}\frac{\partial h}{\partial y} + \alpha N_{yy} + N_{xy}\frac{\partial h}{\partial x}\right) + \right.$$
$$\left. Y_2\left(N_{yy}\frac{\partial \alpha}{\partial y} + N_{xy}\frac{\partial \alpha}{\partial x}\right)\right] + I_{01}\,\ddot{h} - I_{02}\ddot{\alpha} + I_{10}\left[\frac{\partial \ddot{u}_0}{\partial x} - \ddot{\vartheta}_0\right] + $$
$$I_{11}\frac{\partial \ddot{\vartheta}_0}{\partial y} + I_{20}\left(\ddot{\alpha} + \frac{\partial \ddot{h}}{\partial y}\right) - I_{21}\left(\frac{\partial^2 \ddot{h}}{\partial x^2} + \frac{\partial^2 \ddot{h}}{\partial y^2}\right) - I_{22}\frac{\partial^2 \ddot{\alpha}}{\partial x^2} - M = 0 \qquad (4.28)$$

4.3. Uniform Beam Wing Model

To model the bending-torsion motion of a uniform cantilever beam wing the following assumptions are considered:

- Bending and twisting displacements are only functions of span-wise distance and time; $h(x,t)$ & $\alpha(x,t)$, therefore,

$$\frac{\partial h}{\partial y} = \frac{\partial^2 h}{\partial y^2} = \frac{\partial \alpha}{\partial y} = \frac{\partial^2 \alpha}{\partial y^2} = 0$$

- To account for the actions of the piezoelectric actuators in both X and Y directions the following forces and moments (as shown in Figure 4.4) are considered:

$$N_{xx}, N_{yy}, N_{xy}, M_{xx}, M_{yy} \ \& \ M_{xy}$$

- The in-plan displacements are neglected; $u_0 = \vartheta_0 \cong 0$, therefore, only Eqns. (4.27) and (4.28) are used.
- For linear analysis Eqns. (4.27) and (4.28) are solved separately.
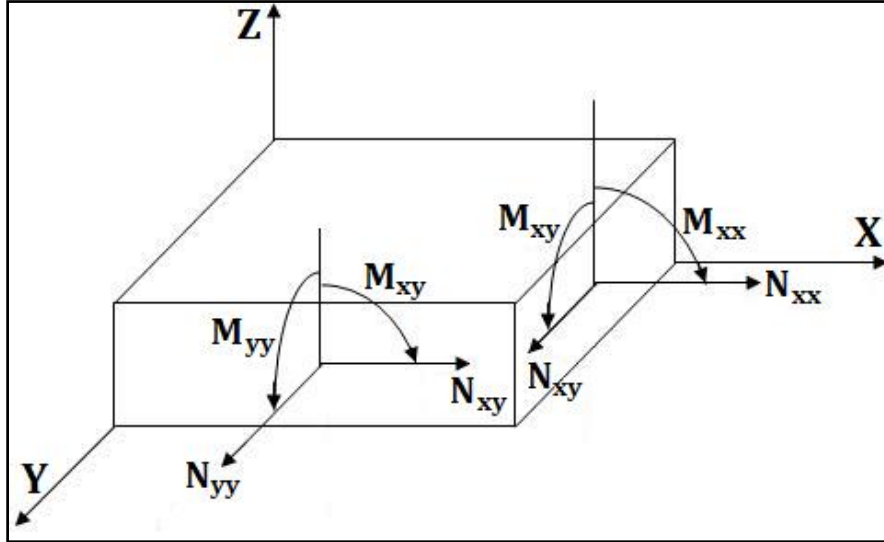
Figure 4.4: Forces and Moments on a beam element.

Using these assumptions, Eqns. (4.27) and (4.28) can be reduced to:

$$-Y_0 \left(\frac{\partial^2 M_{xx}}{\partial x^2} + \frac{\partial^2 M_{yy}}{\partial y^2} + 2 \frac{\partial^2 M_{xy}}{\partial x \partial y} \right) - N_{xx} \left(Y_0 \frac{\partial^2 h}{\partial x^2} + Y_1 \frac{\partial^2 \alpha}{\partial x^2} \right) - Y_0 N_{xy} \frac{\partial \alpha}{\partial x} + I_{00} \ddot{h} -$$

$$I_{01} \ddot{\alpha} - I_{20} \frac{\partial^2 \ddot{h}}{\partial x^2} - I_{21} \frac{\partial^2 \ddot{\alpha}}{\partial x^2} - L = 0$$

$$(4.29)$$

$$2Y_0 \left(\frac{\partial M_{yy}}{\partial y} + \frac{\partial M_{xy}}{\partial x} \right) - Y_1 \left(\frac{\partial^2 M_{xx}}{\partial x^2} + \frac{\partial^2 M_{yy}}{\partial y^2} + 2 \frac{\partial^2 M_{xy}}{\partial x \partial y} \right) - N_{xx} \left(Y_1 \frac{\partial^2 h}{\partial x^2} + Y_2 \frac{\partial^2 \alpha}{\partial x^2} \right) +$$

$$Y_0 \alpha N_{yy} - Y_0 N_{xy} \frac{\partial h}{\partial x} + I_{01} \ddot{h} + (I_{02} + I_{20}) \ddot{\alpha} - I_{21} \frac{\partial^2 \ddot{h}}{\partial x^2} - I_{22} \frac{\partial^2 \ddot{\alpha}}{\partial x^2} - M = 0$$

For piezoelectric layers, as in Eqn. (2.2), the piezoelectric effects are added to Eqns. (3.19) and (3.21) [69];

$$\begin{Bmatrix} N_{xx} \\ N_{yy} \\ N_{xy} \end{Bmatrix} = \begin{bmatrix} A_{11} & A_{12} & A_{16} \\ A_{12} & A_{22} & A_{26} \\ A_{16} & A_{26} & A_{66} \end{bmatrix} \begin{Bmatrix} \varepsilon_{xx}^0 \\ \varepsilon_{yy}^0 \\ \gamma_{xy}^0 \end{Bmatrix} + \begin{bmatrix} B_{11} & B_{12} & B_{16} \\ B_{12} & B_{22} & B_{26} \\ B_{16} & B_{26} & B_{66} \end{bmatrix} \begin{Bmatrix} \varepsilon_{xx}^1 \\ \varepsilon_{yy}^1 \\ \gamma_{xy}^1 \end{Bmatrix} - \{N^P\} \quad (4.31)$$

$$\begin{Bmatrix} M_{xx} \\ M_{yy} \\ M_{xy} \end{Bmatrix} = \begin{bmatrix} B_{11} & B_{12} & B_{16} \\ B_{12} & B_{22} & B_{26} \\ B_{16} & B_{26} & B_{66} \end{bmatrix} \begin{Bmatrix} \varepsilon_{xx}^0 \\ \varepsilon_{yy}^0 \\ \gamma_{xy}^0 \end{Bmatrix} + \begin{bmatrix} D_{11} & D_{12} & D_{16} \\ D_{12} & D_{22} & D_{26} \\ D_{16} & D_{26} & D_{66} \end{bmatrix} \begin{Bmatrix} \varepsilon_{xx}^1 \\ \varepsilon_{yy}^1 \\ \gamma_{xy}^1 \end{Bmatrix} - \{M^P\} \quad (4.32)$$

And in a combined matrix form:

$$\begin{Bmatrix} \{N\} \\ \{M\} \end{Bmatrix} = \begin{bmatrix} [A] & [B] \\ [B] & [D] \end{bmatrix} \begin{Bmatrix} \{\varepsilon^0\} \\ \{\varepsilon^1\} \end{Bmatrix} - \begin{Bmatrix} \{N^P\} \\ \{M^P\} \end{Bmatrix} \quad (4.33)$$

Where,

$$\{N^P\} = \begin{bmatrix} N_x^P \\ N_y^P \\ N_{xy}^P \end{bmatrix} = \sum_{k=1}^n \int_{z_k}^{z_{k+1}} \begin{bmatrix} \bar{e}_{31} \\ \bar{e}_{32} \\ \bar{e}_{36} \end{bmatrix}^k \mathbb{E}_3 \, dz \quad (4.34)$$

$$\{M^P\} = \begin{bmatrix} M_x^P \\ M_y^P \\ M_{xy}^P \end{bmatrix} = \sum_{k=1}^n \int_{z_k}^{z_{k+1}} \begin{bmatrix} \bar{e}_{31} \\ \bar{e}_{32} \\ \bar{e}_{36} \end{bmatrix}^k \mathbb{E}_3 \, z \, dz \quad (4.35)$$

Here the piezoelectric stress coefficient e is related to the strain coefficient d as follows [74], [75];

$$\begin{bmatrix} \bar{e}_{31} \\ \bar{e}_{32} \\ \bar{e}_{36} \end{bmatrix}^k = \begin{bmatrix} \bar{Q}_{11} & \bar{Q}_{12} & \bar{Q}_{16} \\ \bar{Q}_{12} & \bar{Q}_{22} & \bar{Q}_{26} \\ \bar{Q}_{16} & \bar{Q}_{26} & \bar{Q}_{66} \end{bmatrix}^k \begin{bmatrix} \bar{d}_{31} \\ \bar{d}_{32} \\ \bar{d}_{36} \end{bmatrix}^k \quad (4.36)$$

and,

$$\begin{bmatrix} \bar{d}_{31} \\ \bar{d}_{32} \\ \bar{d}_{36} \end{bmatrix}^k = \begin{bmatrix} d_{31}cos^2\theta + d_{32}sin^2\theta \\ d_{31}sin^2\theta + d_{32}cos^2\theta \\ (d_{31} - d_{32})cos\theta sin\theta \end{bmatrix} \tag{4.37}$$

And writing the *membrane strains* ($\boldsymbol{\varepsilon}^0$) and the *curvatures* flexural/bending strains ($\boldsymbol{\varepsilon}^1$) in Eqn. (4.2) in matrix form as in Eqn. (3.11);

$$\begin{Bmatrix} \varepsilon_{xx}^0 \\ \varepsilon_{yy}^0 \\ \gamma_{xy}^0 \end{Bmatrix} = \begin{Bmatrix} \frac{1}{2}\left(\frac{\partial h}{\partial x} + y\frac{\partial \alpha}{\partial x}\right)^2 \\ \frac{1}{2}\left(\frac{\partial h}{\partial y} + \alpha + y\frac{\partial \alpha}{\partial y}\right)^2 \\ \left(\frac{\partial h}{\partial x} + y\frac{\partial \alpha}{\partial y}\right)\left(\frac{\partial h}{\partial y} + \alpha + y\frac{\partial \alpha}{\partial y}\right) \end{Bmatrix} \tag{4.38a}$$

$$\begin{Bmatrix} \varepsilon_{xx}^1 \\ \varepsilon_{yy}^1 \\ \gamma_{xy}^1 \end{Bmatrix} = \begin{Bmatrix} -\left(\frac{\partial^2 h}{\partial x^2} + y\frac{\partial^2 \alpha}{\partial x^2}\right) \\ -\left(\frac{\partial^2 h}{\partial y^2} + 2\frac{\partial \alpha}{\partial y} + y\frac{\partial^2 \alpha}{\partial y^2}\right) \\ -2\left(\frac{\partial^2 h}{\partial x\partial y} + \frac{\partial \alpha}{\partial x} + y\frac{\partial^2 \alpha}{\partial x\partial y}\right) \end{Bmatrix} = \begin{Bmatrix} -\left(\frac{\partial^2 h}{\partial x^2} + y\frac{\partial^2 \alpha}{\partial x^2}\right) \\ 0 \\ -2\left(\frac{\partial^2 h}{\partial x\partial y} + \frac{\partial \alpha}{\partial x} + y\frac{\partial^2 \alpha}{\partial x\partial y}\right) \end{Bmatrix} \tag{4.38b}$$

With the assumption of $\frac{\partial h}{\partial x}, \frac{\partial \alpha}{\partial x} = O(\epsilon)$, this means that the terms of order ϵ^2 are negligible;

$$\left(\frac{\partial h}{\partial x}\right)^2, \left(\frac{\partial \alpha}{\partial x}\right)^2, \frac{\partial h}{\partial x}\frac{\partial \alpha}{\partial x} \quad \ldots\ldots \cong 0 \tag{4.39}$$

Therefore, Eqns. (4.38) can be rewritten as;

$$\begin{Bmatrix} \varepsilon_{xx}^0 \\ \varepsilon_{yy}^0 \\ \gamma_{xy}^0 \end{Bmatrix} = \begin{Bmatrix} 0 \\ \frac{1}{2}\alpha^2 \\ -2\frac{\partial \alpha}{\partial x} \end{Bmatrix}, \text{ and } \begin{Bmatrix} \varepsilon_{xx}^1 \\ \varepsilon_{yy}^1 \\ \gamma_{xy}^1 \end{Bmatrix} = \begin{Bmatrix} -\left(\frac{\partial^2 h}{\partial x^2} + y\frac{\partial^2 \alpha}{\partial x^2}\right) \\ 0 \\ -2\frac{\partial \alpha}{\partial x} \end{Bmatrix} \tag{4.40}$$

The $\{N\}$ and $\{M\}$ for symmetrical laminated ($B_{ij} = 0$) cantilever beam wing are:

$$N_{xx} = A_{12}\left(\frac{1}{2}\alpha^2\right) + A_{16}\left(\alpha\frac{\partial h}{\partial x} + \alpha y\frac{\partial \alpha}{\partial x}\right) - N_x^P \tag{4.41a}$$

$$N_{yy} = A_{22}\left(\frac{1}{2}\alpha^2\right) + A_{26}\left(\alpha\frac{\partial h}{\partial x} + \alpha y\frac{\partial \alpha}{\partial x}\right) - N_y^P \tag{4.41a}$$

$$N_{xy} = A_{26}\left(\frac{1}{2}\alpha^2\right) + A_{66}\left(\alpha\frac{\partial h}{\partial x} + \alpha y\frac{\partial \alpha}{\partial x}\right) - N_{xy}^P \tag{4.41a}$$

And,

$$M_{xx} = -D_{11}\left(\frac{\partial^2 h}{\partial x^2} + y\frac{\partial^2 \alpha}{\partial x^2}\right) - 2D_{16}\frac{\partial \alpha}{\partial x} - M_x^P \tag{4.42a}$$

$$M_{yy} = -D_{12}\left(\frac{\partial^2 h}{\partial x^2} + y\frac{\partial^2 \alpha}{\partial x^2}\right) - 2D_{26}\frac{\partial \alpha}{\partial x} - M_y^P \tag{4.42a}$$

$$M_{xy} = -D_{16}\left(\frac{\partial^2 h}{\partial x^2} + y\frac{\partial^2 \alpha}{\partial x^2}\right) - 2D_{66}\frac{\partial \alpha}{\partial x} - M_{xy}^P \tag{4.42a}$$

For $(\alpha \ll 1)$;

$$\alpha^2, \alpha\frac{\partial \alpha}{\partial x}, \alpha\frac{\partial h}{\partial x} \quad \ldots.. \cong 0 \tag{4.43}$$

Eqns. (4.41) are reduced to:

$$\begin{bmatrix} N_{xx} \\ N_{yy} \\ N_{xy} \end{bmatrix} = \begin{bmatrix} -N_x^P \\ -N_y^P \\ -N_{xy}^P \end{bmatrix} \tag{4.44}$$

Substituting Eqns. (4.42) and (4.44) in Eqn. (4.29);

$$-Y_0\left[\frac{\partial^2}{\partial x^2}\left(-D_{11}\frac{\partial^2 h}{\partial x^2} - D_{11}y\frac{\partial^2 \alpha}{\partial x^2} - 2D_{16}\frac{\partial \alpha}{\partial x} - M_x^P\right) + \frac{\partial^2}{\partial y^2}\left(-D_{12}\frac{\partial^2 h}{\partial x^2} - D_{12}y\frac{\partial^2 \alpha}{\partial x^2} - \right.\right.$$

$$\left.\left. 2D_{26}\frac{\partial \alpha}{\partial x} - M_y^P\right) + 2\frac{\partial^2}{\partial x\partial y}\left(-D_{16}\frac{\partial^2 h}{\partial x^2} - D_{16}y\frac{\partial^2 \alpha}{\partial x^2} - 2D_{66}\frac{\partial \alpha}{\partial x} - M_{xy}^P\right)\right] +$$

$$N_x^P\left(Y_0\frac{\partial^2 h}{\partial x^2} + Y_1\frac{\partial^2 \alpha}{\partial x^2}\right) + Y_0 N_{xy}^P\frac{\partial \alpha}{\partial x} + I_{00}\ddot{h} + I_{01}\ddot{\alpha} - I_{20}\frac{\partial^2 \ddot{h}}{\partial x^2} - L = 0$$

$$\tag{4.45}$$

Differentiating and letting $[\frac{\partial}{\partial y}(N, M) = 0]$, the equation of the bending motion "h" is:

$$Y_0 D_{11} \frac{\partial^4 h}{\partial x^4} + Y_1 D_{11} \frac{\partial^4 \alpha}{\partial x^4} + 4 Y_0 D_{16} \frac{\partial^3 \alpha}{\partial x^3} + Y_0 \frac{\partial^2 M_x^P}{\partial x^2} + N_x^P \left(Y_0 \frac{\partial^2 h}{\partial x^2} + Y_1 \frac{\partial^2 \alpha}{\partial x^2} \right)$$

$$+ Y_0 N_{xy}^P \frac{\partial \alpha}{\partial x} + I_{00} \ddot{h} + I_{01} \ddot{\alpha} - I_{20} \frac{\partial^2 \ddot{h}}{\partial x^2} - I_{21} \frac{\partial^2 \ddot{\alpha}}{\partial x^2} - L = 0$$

(4.46)

The same procedure for Eqn. (4.30);

$$-Y_1 \left[\frac{\partial^2}{\partial x^2} \left(-D_{11} \frac{\partial^2 h}{\partial x^2} - D_{11} y \frac{\partial^2 \alpha}{\partial x^2} - 2D_{16} \frac{\partial \alpha}{\partial x} - M_x^P \right) - \frac{\partial^2}{\partial y^2} \left(-D_{12} \frac{\partial^2 h}{\partial x^2} - D_{12} y \frac{\partial^2 \alpha}{\partial x^2} - \right.$$

$$\left. 2D_{26} \frac{\partial \alpha}{\partial x} - M_y^P \right) + 2 \frac{\partial^2}{\partial x \partial y} \left(-D_{16} \frac{\partial^2 h}{\partial x^2} - D_{16} y \frac{\partial^2 \alpha}{\partial x^2} - 2D_{66} \frac{\partial \alpha}{\partial x} - M_{xy}^P \right) \right] +$$

$$2Y_0 \left[\frac{\partial}{\partial y} \left(-D_{12} \frac{\partial^2 h}{\partial x^2} - D_{12} y \frac{\partial^2 \alpha}{\partial x^2} - 2D_{26} \frac{\partial \alpha}{\partial x} - M_y^P \right) + \frac{\partial}{\partial x} \left(-D_{16} \frac{\partial^2 h}{\partial x^2} - D_{16} y \frac{\partial^2 \alpha}{\partial x^2} - \right. \right.$$

$$\left. \left. 2D_{66} \frac{\partial \alpha}{\partial x} - M_{xy}^P \right) \right] + N_x^P \left(Y_1 \frac{\partial^2 h}{\partial x^2} + Y_2 \frac{\partial^2 \alpha}{\partial x^2} \right) - Y_0 \alpha N_y^P + Y_0 N_{xy}^P \frac{\partial h}{\partial x} + I_{01} \ddot{h} +$$

$$(I_{02} + I_{20}) \ddot{\alpha} - I_{21} \frac{\partial^2 \ddot{h}}{\partial x^2} - I_{22} \frac{\partial^2 \ddot{\alpha}}{\partial x^2} - M = 0$$

(4.47)

And therefore, the equation of the torsional motion "α" is:

$$Y_1 D_{11} \frac{\partial^4 h}{\partial x^4} + Y_2 D_{11} \frac{\partial^4 \alpha}{\partial x^4} + Y_1 \frac{\partial^2 M_x^P}{\partial x^2} - 2 Y_0 D_{12} \frac{\partial^2 \alpha}{\partial x^2} - 2 Y_0 D_{16} \frac{\partial^3 h}{\partial x^3}$$

$$+ 2 Y_1 D_{16} \frac{\partial^3 \alpha}{\partial x^3} - 4 Y_0 D_{66} \frac{\partial^2 \alpha}{\partial x^2} - 2 Y_0 \frac{\partial M_{xy}^P}{\partial x} + N_x^P \left(Y_1 \frac{\partial^2 h}{\partial x^2} + Y_2 \frac{\partial^2 \alpha}{\partial x^2} \right)$$

$$- Y_0 N_y^P \alpha + Y_0 N_{xy}^P \frac{\partial h}{\partial x} + I_{01} \ddot{h}$$

$$+ (I_{02} + I_{20}) \ddot{\alpha} - I_{21} \frac{\partial^2 \ddot{h}}{\partial x^2} - I_{22} \frac{\partial^2 \ddot{\alpha}}{\partial x^2} - M = 0$$

(4.48)

4.4. Finite Element Model

The derivation of finite element equations of a differential equation $f(x, t)$ is done in three steps [76];

1. Development of the weighted-residual or weak form of the differential equation; which involves:

    a. Constructing the Weighted-integral statement by multiplying the entire differential equation by weighted function $v(x)$ and integrate it over the element length; $\int_0^l f(x,t).v(x)dx = 0$,

    b. Shifting half of the derivatives from f to v by integrating by parts,

    c. Imposing the problem actual boundary conditions.

2. Assumption of the approximate solution, using the separation of variables technique, the differential equation is approximately equal to the summation of the multiplication of time dependent function $f(t)$ by shape function $v(x)$;

$$f(x,t) = \sum_{j=1}^n f_j^e(t).v_j^e(x) \tag{4.49}$$

3. Substitution of the approximate solution to derive the finite element equations.

Applying the previous steps on Eqn. (4.46);

$$\int_0^l \left(Y_0 D_{11} \frac{\partial^4 h}{\partial x^4} v + Y_1 D_{11} \frac{\partial^4 \alpha}{\partial x^4} v + Y_0 \frac{\partial^2 M_x^P}{\partial x^2} v + Y_0 N_x^P \frac{\partial^2 h}{\partial x^2} v + + Y_1 N_x^P \frac{\partial^2 \alpha}{\partial x^2} v \right.$$

$$+ 4Y_0 D_{16} \frac{\partial^3 \alpha}{\partial x^3} v + Y_0 N_{xy}^P \frac{\partial \alpha}{\partial x} v + I_{00} \ddot{h} v$$

$$\left. + I_{01} \ddot{\alpha} v - I_{20} \frac{\partial^2 \ddot{h}}{\partial x^2} v - I_{21} \frac{\partial^2 \ddot{\alpha}}{\partial x^2} v - L v \right) dx = 0$$

$$\tag{4.50}$$

Integrating by parts;

$$\int_0^l \left(Y_0 D_{11} \frac{\partial^2 h}{\partial x^2} \frac{\partial^2 v}{\partial x^2} + Y_1 D_{11} \frac{\partial^2 \alpha}{\partial x^2} \frac{\partial^2 v}{\partial x^2} + Y_0 \frac{\partial^2 v}{\partial x^2} M_x^P - 2\, Y_0 \frac{\partial v}{\partial x} \frac{\partial h}{\partial x} N_x^P \right.$$

$$+ 4Y_0 D_{16} \frac{\partial^2 v}{\partial x^2} \frac{\partial \alpha}{\partial x} - Y_0 \alpha \frac{\partial v}{\partial x} N_{xy}^P + I_{00}\, \ddot{h} v$$

$$\left. + I_{01} \ddot{\alpha}\, v + I_{20} \frac{\partial \ddot{h}}{\partial x} \frac{\partial v}{\partial x} + I_{21} \frac{\partial \ddot{\alpha}}{\partial x} \frac{\partial v}{\partial x} - L\, v \right) dx = 0$$

<div align="right">(4.51)</div>

The same for Eqn. (4.48);

$$\int_0^l \left(Y_1 D_{11} \frac{\partial^4 h}{\partial x^4}\, v + Y_2 D_{11} \frac{\partial^4 \alpha}{\partial x^4}\, v + Y_1 \frac{\partial^2 M_x^P}{\partial x^2}\, v - 2Y_0 D_{12} \frac{\partial^2 \alpha}{\partial x^2}\, v - 2Y_0 D_{16} \frac{\partial^3 h}{\partial x^3}\, v - \right.$$

$$2Y_1 D_{16} \frac{\partial^3 \alpha}{\partial x^3}\, v - 4Y_0 D_{66} \frac{\partial^2 \alpha}{\partial x^2}\, v - 2Y_0 \frac{\partial M_{xy}^P}{\partial x}\, v + Y_1 N_x^P \frac{\partial^2 h}{\partial x^2}\, v + Y_2 N_x^P \frac{\partial^2 \alpha}{\partial x^2}\, v -$$

$$Y_0 N_y^P \alpha\, v + Y_0 N_{xy}^P \frac{\partial h}{\partial x} + I_{01} \ddot{h}\, v +$$

$$(I_{02} + I_{20}) \ddot{\alpha}\, v - I_{21} \frac{\partial^2 \ddot{h}}{\partial x^2}\, v - I_{22} \frac{\partial^2 \ddot{\alpha}}{\partial x^2}\, v - M\, v \right) dx = 0 \qquad \text{(4.52)}$$

Integrating by parts;

$$\int_0^l \left(Y_1 D_{11} \frac{\partial^2 h}{\partial x^2} \frac{\partial^2 v}{\partial x^2} + Y_2 D_{11} \frac{\partial^2 \alpha}{\partial x^2} \frac{\partial^2 v}{\partial x^2} + Y_1 \frac{\partial^2 v}{\partial x^2} M_x^P + 2Y_0 D_{12} \frac{\partial \alpha}{\partial x} \frac{\partial v}{\partial x}\, h + \right.$$

$$2Y_0 D_{16} \frac{\partial^2 h}{\partial x^2} \frac{\partial v}{\partial x} + 2Y_1 D_{16} \frac{\partial^2 \alpha}{\partial x^2} \frac{\partial v}{\partial x} + 4Y_0 D_{66} \frac{\partial \alpha}{\partial x} \frac{\partial v}{\partial x} + 2Y_0 \frac{\partial v}{\partial x} M_{xy}^P - Y_1 \frac{\partial v}{\partial x} \frac{\partial h}{\partial x} N_x^P -$$

$$Y_2 N_x^P \frac{\partial \alpha}{\partial x} \frac{\partial v}{\partial x} - Y_0\, N_y^P \alpha\, v - Y_0 h N_{xy}^P \frac{\partial v}{\partial x} + I_{01} \ddot{h}\, v + (I_{02} + I_{20}) \ddot{\alpha}\, v +$$

$$I_{21} \frac{\partial \ddot{h}}{\partial x} \frac{\partial v}{\partial x} + I_{22} \frac{\partial \ddot{\alpha}}{\partial x} \frac{\partial v}{\partial x} - M\, v \right) dx = 0 \qquad \text{(4.53)}$$

Assume the approximate solutions as:

$$h(x,t) \cong \sum_{j=1}^n h_j^e(t) \psi_j^e(x) \qquad \text{(4.54)}$$

$$\alpha(x,t) \cong \sum_{k=1}^m \alpha_k^e(t) \phi_k^e(x) \qquad \text{(4.55)}$$

And,
$$v(x) = \psi_i^e(x), \phi_l^e(x) \qquad \text{(4.56)}$$

Substituting (4.54), (4.55) and (4.56) in Eqn. (4.51);

$$\int_0^l \left(\sum_{j=1}^n Y_0 D_{11} \frac{d^2\psi_i^e}{dx^2} \frac{d^2\psi_j^e}{dx^2} h_j^e(t) + \sum_{k=1}^m Y_1 D_{11} \frac{d^2\phi_k^e}{dx^2} \frac{d^2\psi_i^e}{dx^2} \alpha_k^e(t) + \right.$$

$$\sum_{k=1}^m 4Y_0 D_{16} \frac{d^2\psi_i^e}{dx^2} \frac{d\phi_k^e}{dx} \alpha_k^e(t) + Y_0 \frac{d^2\psi_i^e}{dx^2} M_x^P - \sum_{j=1}^n 2 Y_0 \frac{d\psi_i^e}{dx} \frac{d\psi_j^e}{dx} h_j^e(t) N_x^P -$$

$$\sum_{k=1}^m 2Y_0 N_{xy}^P \frac{d\psi_i^e}{dx} \phi_k^e \alpha_k^e(t) - \sum_{k=1}^m 2Y_1 N_x^P \frac{d\psi_i^e}{dx} \frac{d\phi_k^e}{dx} \alpha_k^e(t) +$$

$$\sum_{j=1}^n I_{00} \psi_i^e \psi_j^e \ddot{h}_j^e(t) + \sum_{k=1}^m I_{01} \psi_i^e \phi_k^e \ddot{\alpha}_k^e(t) + \sum_{j=1}^n I_{20} \frac{d\psi_i^e}{dx} \frac{d\psi_j^e}{dx} \ddot{h}_j^e(t) +$$

$$\left. \sum_{k=1}^m I_{21} \frac{d\psi_i^e}{dx} \frac{d\phi_k^e}{dx} \ddot{\alpha}_k^e(t) - L\,\psi_i^e \right) dx = 0 \qquad\qquad (4.57)$$

Rewrite Eqn. (4.57);

$$0 =$$

$$\sum_{j=1}^n \left(KH_{ij} - GH_{ij}\right) h_j^e(t) + \sum_{k=1}^m (Ka_{ik} + Ga_{ik})\, \alpha_k^e(t) + \sum_{j=1}^n Mhh_{ij}\, \ddot{h}_j^e(t) +$$

$$\sum_{k=1}^m Mha_{ik}\, \ddot{\alpha}_k^e(t) + F_i^e + Fhp_i^e$$

$$(4.58)$$

Where,

$$KH_{ij} = \int_0^l Y_0 D_{11} \frac{d^2\psi_i^e}{dx^2} \frac{d^2\psi_j^e}{dx^2}\, dx$$

$$GH_{ij} = \int_0^l Y_0 N_x^P \frac{d\psi_i^e}{dx} \frac{d\psi_j^e}{dx}\, dx$$

$$Ka_{ik} = \int_0^l \left(Y_1 D_{11} \frac{d^2\phi_k^e}{dx^2} \frac{d^2\psi_i^e}{dx^2} + 4Y_0 D_{16} \frac{d^2\psi_i^e}{dx^2} \frac{d\phi_k^e}{dx} \right) dx$$

$$Ga_{ik} = \int_0^l \left(Y_0 N_{xy}^P \frac{d\psi_i^e}{dx} \phi_k^e + Y_1 N_x^P \frac{d\psi_i^e}{dx} \frac{d\phi_k^e}{dx} \right) dx$$

$$Mhh_{ij} = \int_0^l \left(I_{00}\, \psi_i^e \psi_j^e + I_{20} \frac{d\psi_i^e}{dx} \frac{d\psi_j^e}{dx} \right) dx$$

$$Mha_{ik} = \int_0^l \left(I_{01}\psi_i^e \phi_k^e + I_{21} \frac{d\psi_i^e}{dx} \frac{d\phi_k^e}{dx} \right) dx$$

$$F_i^e = \int_0^l -L\, \psi_i^e\, dx \qquad \text{and,} \qquad Fhp_i^e = \int_0^l Y_0 \frac{d^2\psi_i^e}{dx^2} M_x^P\, dx \qquad (4.59)$$

Substituting (4.54), (4.55) and (4.56) in Eqn. (4.53);

$$\int_0^l \left(\sum_{j=1}^n Y_1 D_{11} \frac{d^2\psi_j^e}{dx^2} \frac{d^2\phi_l^e}{dx^2} h_j^e(t) + \sum_{k=1}^m Y_2 D_{11} \frac{d^2\phi_k^e}{dx^2} \frac{d^2\phi_l^e}{dx^2} \alpha_k^e(t) + Y_1 \frac{d^2\phi_l^e}{dx^2} M_x^P + \right.$$

$$\sum_{k=1}^m 2Y_0 D_{12} \frac{d\phi_l^e}{dx} \frac{d\phi_k^e}{dx} \alpha_k^e(t) + \sum_{j=1}^n 2Y_0 D_{16} \frac{d^2\psi_j^e}{dx^2} \frac{d\phi_k^e}{dx} h_j^e(t) +$$

$$\sum_{k=1}^m 2Y_1 D_{16} \frac{d^2\phi_k^e}{dx^2} \frac{d\phi_l^e}{dx} \alpha_k^e(t) + \sum_{k=1}^m 4Y_0 D_{66} \frac{d\phi_k^e}{dx} \frac{d\phi_l^e}{dx} \alpha_k^e(t) + 2Y_0 M_{xy}^P \frac{d\phi_l^e}{dx} -$$

$$\sum_{j=1}^n Y_1 N_x^P \frac{d\phi_l^e}{dx} \frac{d\psi_j^e}{dx} h_j^e(t) - \sum_{k=1}^m Y_2 N_x^P \frac{d\phi_k^e}{dx} \frac{d\phi_l^e}{dx} \alpha_k^e(t) -$$

$$\sum_{k=1}^m Y_0 N_y^P \phi_l^e \phi_k^e \alpha_k^e(t) - \sum_{j=1}^n Y_0 N_{xy}^P \frac{d\phi_l^e}{dx} \psi_i^e h_j^e(t) + \sum_{j=1}^n I_{01} \phi_l^e \psi_j^e \ddot{h}_j^e(t) +$$

$$\sum_{k=1}^m (I_{02} + I_{20}) \phi_l^e \phi_k^e \ddot{\alpha}_k^e(t) + \sum_{j=1}^n I_{21} \frac{d\phi_l^e}{dx} \frac{d\psi_j^e}{dx} \ddot{h}_j^e(t) +$$

$$\left. \sum_{k=1}^m I_{22} \frac{d\phi_l^e}{dx} \frac{d\phi_k^e}{dx} \ddot{\alpha}_k^e(t) - M \phi_l^e \right) dx = 0$$

(4.60)

Rewrite Eqn. (4.60);

$$0 = \sum_{k=1}^m (JA_{lk} + KA_{lk} - GA_{lk}) \alpha_k^e(t) + \sum_{j=1}^n (Kh_{lj} - Gh_{lj}) h_j^e(t) +$$

$$\sum_{j=1}^n Mah_{lj} \ddot{h}_j^e(t) + \sum_{k=1}^m Maa_{lk} \ddot{\alpha}_k^e(t) + Fa_k^e + Fap_k^e$$

(4.61)

Where,

$$JA_{lk} = \int_0^l 4Y_0 D_{66} \frac{d\phi_k^e}{dx} \frac{d\phi_l^e}{dx} dx$$

$$KA_{lk} = \int_0^l \left(2Y_0 D_{12} \frac{d\phi_l^e}{dx} \frac{d\phi_k^e}{dx} + 2Y_1 D_{16} \frac{d^2\phi_k^e}{dx^2} \frac{d\phi_l^e}{dx} + Y_2 D_{11} \frac{d^2\phi_k^e}{dx^2} \frac{d^2\phi_l^e}{dx^2}_1 \right) dx$$

$$GA_{lk} = \int_0^l \left(Y_2 N_x^P \frac{d\phi_k^e}{dx} \frac{d\phi_l^e}{dx} + Y_0 N_y^P \phi_l^e \phi_k^e \right) dx$$

$$Kh_{lj} = \int_0^l \left(2Y_0 D_{16} \frac{d^2\psi_j^e}{dx^2} \frac{d\phi_l^e}{dx} + Y_1 D_{11} \frac{d^2\psi_j^e}{dx^2} \frac{d^2\phi_l^e}{dx^2} \right) dx$$

$$Gh_{lj} = \int_0^l \left(Y_0 N_{xy}^P \frac{d\phi_l^e}{dx} \psi_i^e + Y_1 N_x^P \frac{d\phi_l^e}{dx} \frac{d\psi_j^e}{dx} \right) dx$$

$$Mah_{lj} = \int_0^l \left(I_{01} \, \phi_i^e \psi_j^e + I_{21} \frac{d\phi_i^e}{dx} \frac{d\psi_j^e}{dx} \right) dx$$

$$Maa_{lk} = \int_0^l \left((I_{02} + I_{20}) \phi_i^e \phi_k^e + I_{22} \frac{d\phi_i^e}{dx} \frac{d\phi_k^e}{dx} \right) dx$$

$$Fa_k^e = \int_0^l - M \, \phi_i^e \, dx$$

$$Fap_k^e = \int_0^l \left(2Y_0 M_{xy}^P \frac{d\phi_i^e}{dx} + Y_1 \frac{d^2\phi_i^e}{dx^2} M_x^P \right) dx \qquad (4.62)$$

4.4.1. Beam Element Characteristic Matrices and Vectors

The wing element is shown in Figure 4.5. The element has two nodes and six degrees of freedom (three per node). The three nodal degrees of freedom are; translational (x_1, x_4), rotational/angular (x_2, x_5) and torsional (x_3, x_6) displacements.
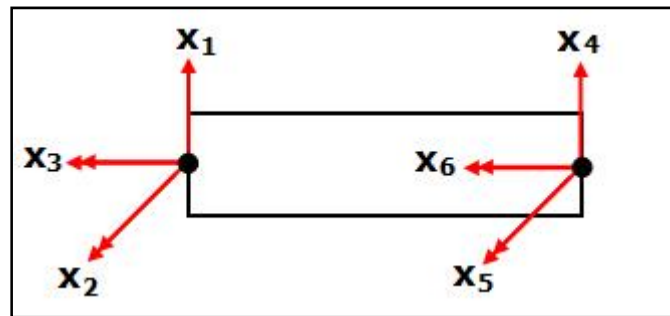
Figure 4.5: Nodal degrees of freedom.

The characteristic matrices and vectors listed in Eqn's (4.59 & 4.62) are evaluated by considering the Hermite Interpolation Functions [77, 78] as the shape functions of the translational and angular displacements;

$$\psi_i^e(x) = H_i^e(x) = \begin{cases} 1 - 3\frac{x^2}{l^2} + 2\frac{x^3}{l^3} \\ x - 2\frac{x^2}{l} + \frac{x^3}{l^2} \\ 3\frac{x^2}{l^2} - 2\frac{x^3}{l^3} \\ -\frac{x^2}{l} + \frac{x^3}{l^2} \end{cases} \qquad (4.63)$$

and the interpolation function for the torsional displacement is given by [78];

$$\phi_i^e(x) = \begin{cases} 1 - \frac{x}{l} \\ \frac{x}{l} \end{cases} \qquad (4.64)$$

Where, i, j = 1, 2, 4 & 5, and k, l = 3 & 6.

Applying Eqn's (4.63 & 4.64) into Eqn's (4.59 & 4.62) the characteristic matrices and vectors are;

$$KH_{ij} = \frac{Y_0 D_{11}}{l^3}\begin{bmatrix} 12 & 6l & -12 & 6l \\ 6l & 4l^2 & -6l & 2l^2 \\ -12 & -6l & 12 & -6l \\ 6l & 2l^2 & -6l & 4l^2 \end{bmatrix}$$

$$GH_{ij} = \frac{Y_0 N_x^p}{30l}\begin{bmatrix} 36 & 3l & -36 & 3l \\ 3l & 4l^2 & -3l & -l^2 \\ -36 & -3l & 36 & -3l \\ 3l & -l^2 & -3l & 4l^2 \end{bmatrix}$$

$$Ka_{ik} = \frac{4Y_0 D_{16}}{l}\begin{bmatrix} 0 & 0 \\ 1 & -1 \\ 0 & 0 \\ -1 & 1 \end{bmatrix}$$

$$Ga_{ik} = \frac{Y_1 N_x^p}{l}\begin{bmatrix} 1 & -1 \\ 0 & 0 \\ -1 & 1 \\ 0 & 0 \end{bmatrix} + \frac{Y_0 N_{xy}^p}{12}\begin{bmatrix} -6 & -6 \\ l & -l \\ 6 & 6 \\ -l & l \end{bmatrix}$$

$$Mhh_{ij} = \frac{I_{00}l}{420}\begin{bmatrix} 156 & 22l & 54 & -13l \\ 22l & 4l^2 & 13l & -3l^2 \\ 54 & 13l & 156 & -22l \\ -13l & -3l^2 & -22l & 4l^2 \end{bmatrix} + \frac{I_{20}}{30l}\begin{bmatrix} 36 & 3l & -36 & 3l \\ 3l & 4l^2 & -3l & -l^2 \\ -36 & -3l & 36 & -3l \\ 3l & -l^2 & -3l & 4l^2 \end{bmatrix}$$

$$Mha_{ik} = \frac{I_{01}l}{60}\begin{bmatrix} 21 & 9 \\ 3l & 2l \\ 9 & 21 \\ -2l & -3l \end{bmatrix} + \frac{I_{21}}{l}\begin{bmatrix} 1 & -1 \\ 0 & 0 \\ -1 & 1 \\ 0 & 0 \end{bmatrix}$$

$$F_i^e = \frac{-Ll}{12}\begin{bmatrix} 6 \\ l \\ 6 \\ -l \end{bmatrix}$$, for uniform lift distribution over the element. And,

$$Fhp_i^e = Y_0 M_x^p \begin{bmatrix} 0 \\ -1 \\ 0 \\ 1 \end{bmatrix} \tag{4.65}$$

And,

$$JA_{lk} = 4Y_0 D_{66}\begin{bmatrix} 1 & -1 \\ -1 & 1 \end{bmatrix}$$

$$KA_{lk} = \frac{2Y_0 D_{12}}{l}\begin{bmatrix} 1 & -1 \\ -1 & 1 \end{bmatrix}$$

$$GA_{lk} = \frac{Y_2 N_x^P}{l}\begin{bmatrix} 1 & -1 \\ -1 & 1 \end{bmatrix} + \frac{Y_0 l N_y^P}{6}\begin{bmatrix} 2 & 1 \\ 1 & 2 \end{bmatrix}$$

$$Kh_{lj} = \frac{2Y_0 D_{16}}{l}\begin{bmatrix} 0 & 1 & 0 & -1 \\ 0 & -1 & 0 & 1 \end{bmatrix}$$

$$Gh_{lj} = \frac{Y_1 N_x^P}{l}\begin{bmatrix} 1 & 0 & -1 & 0 \\ -1 & 0 & 1 & 0 \end{bmatrix} + \frac{Y_0 N_{xy}^P}{12}\begin{bmatrix} -6 & -l & -6 & l \\ 6 & l & 6 & -l \end{bmatrix}$$

$$Mah_{lj} = \frac{I_{01} l}{60}\begin{bmatrix} 21 & 3l & 9 & -2l \\ 9 & 2l & 21 & -3l \end{bmatrix} + \frac{I_{21}}{l}\begin{bmatrix} 1 & 0 & -1 & 0 \\ -1 & 0 & 1 & 0 \end{bmatrix}$$

$$Maa_{lk} = \frac{(I_{02}+I_{20})l}{6}\begin{bmatrix} 2 & 1 \\ 1 & 2 \end{bmatrix} + \frac{I_{22}}{l}\begin{bmatrix} 1 & -1 \\ -1 & 1 \end{bmatrix}$$

$$Fa_k^e = \frac{-Ml}{2}\begin{bmatrix} 1 \\ 1 \end{bmatrix}$$, for pitching moment due to uniform lift distribution over the element.

$$Fap_k^e = 2Y_0 M_{xy}^P\begin{bmatrix} -1 \\ 1 \end{bmatrix} \tag{4.66}$$

Letting;

$$KHH_{ij} = KH_{ij} - GH_{ij}$$

$$KHa_{jk} = Ka_{jk} + Ga_{jk}$$

$$KAA_{lk} = JA_{lk} + KA_{lk} - GA_{lk}$$

$$KAh_{kj} = Kh_{kj} - Gh_{kj} \tag{4.67}$$

The global stiffness matrix (for m, n = 1, 2 ...6) can be written as;

$$K_{mn} = \begin{bmatrix} KHH_{11} & KHH_{12} & KHa_{13} & KHH_{14} & KHH_{15} & KHa_{16} \\ KHH_{21} & KHH_{22} & KHa_{23} & KHH_{24} & KHH_{25} & KHa_{26} \\ KAh_{31} & KAh_{32} & KAA_{33} & KAh_{34} & KAh_{35} & KAA_{36} \\ KHH_{41} & KHH_{42} & KHa_{43} & KHH_{44} & KHH_{45} & KHa_{46} \\ KHH_{51} & KHH_{52} & KHa_{53} & KHH_{54} & KHH_{55} & KHa_{56} \\ KAh_{61} & KAh_{62} & KAA_{63} & KAh_{64} & KAh_{65} & KAA_{66} \end{bmatrix} \tag{4.68}$$

In the same manner, the global mass matrix can be written as;

$$M_{mn} = \begin{bmatrix} Mhh_{11} & Mhh_{12} & Mha_{13} & Mhh_{14} & Mhh_{15} & Mha_{16} \\ Mhh_{21} & Mhh_{22} & Mha_{23} & Mhh_{24} & Mhh_{25} & Mha_{26} \\ Mah_{31} & Mah_{32} & Maa_{33} & Mah_{34} & Mah_{35} & Maa_{36} \\ Mhh_{41} & Mhh_{42} & Mha_{43} & Mhh_{44} & Mhh_{45} & Mha_{46} \\ Mhh_{51} & Mhh_{52} & Mha_{53} & Mhh_{54} & Mhh_{55} & Mha_{56} \\ Mah_{61} & Mah_{62} & Maa_{63} & Mah_{64} & Mah_{65} & Maa_{66} \end{bmatrix} \tag{4.69}$$

The global external (Aerodynamic) forces (AF_m^e) and the piezoelectric control forces (PF_m^e) vectors are;

$$AF_m^e = \begin{bmatrix} F_1^e \\ F_2^e \\ Fa_3^e \\ F_4^e \\ F_5^e \\ Fa_6^e \end{bmatrix}, \text{ and } \quad PF_m^e = \begin{bmatrix} Fhp_1^e \\ Fhp_2^e \\ Fap_3^e \\ Fhp_4^e \\ Fhp_5^e \\ Fap_6^e \end{bmatrix} \tag{4.70}$$

Therefore, Eqns. (4.58 & 4.61) can be written in global form as;

$$[K_{mn}][x] + [M_{mn}][\ddot{x}] - [AF_m^e] - [PF_m^e] = 0 \tag{4.71}$$

4.4.2. Aerodynamic Forces Model

The lift forces (F_i^e) in Eqn. (4.65) and the corresponding pitching moments (Fa_k^e) in Eqn. (4.66) which construct the elemental aerodynamic forces (AF_m^e) are evaluated based on a uniform aerodynamic distribution over the element as shown in Figure (4.6) [79].
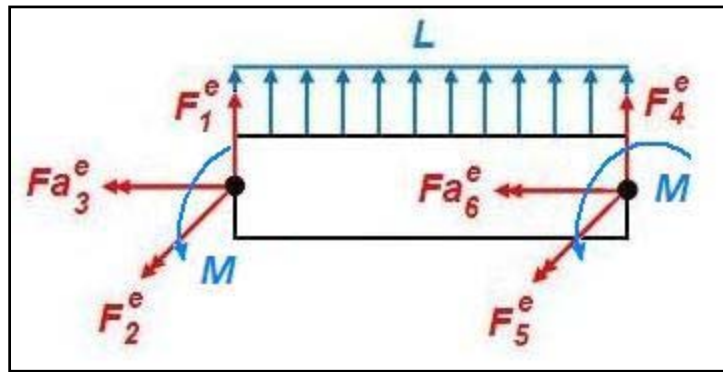
Figure 4.6: Nodal forces due to uniform aerodynamic loading.

However, since the element is under twisting motion (in addition to the bending motion) this means that each node has a different twist angle (Angle of Attack). Therefore, the aerodynamic loading with linear varying distribution can be considered as shown in Figure (4.7).
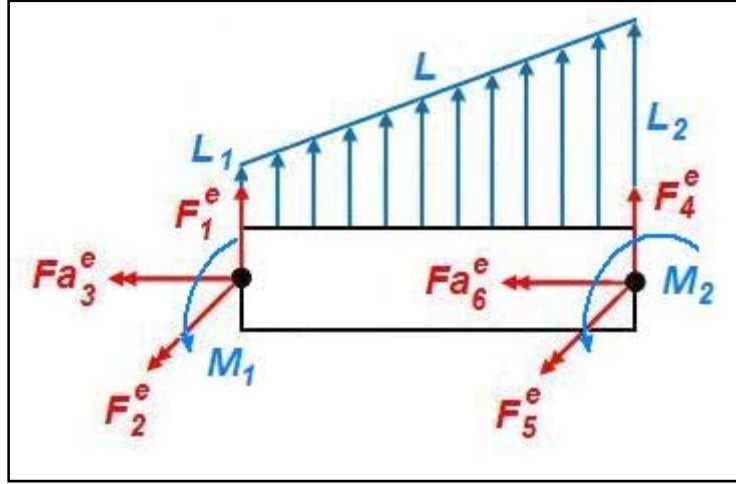
Figure 4.7: Nodal forces due to linear varying aerodynamic loading.

And hence, the elemental aerodynamic forces (AF_m^e) can be rewritten as a function of L_1, L_2, M_1 and M_2 (see A.1);

$$AF_m^e = \begin{bmatrix} F_1^e \\ F_2^e \\ Fa_3^e \\ F_4^e \\ F_5^e \\ Fa_6^e \end{bmatrix} = -\frac{l}{60} \begin{bmatrix} 3(7L_1 + 3L_2) \\ l(3L_1 + 2L_2) \\ 10(2M_1 + M_2) \\ 3(3L_1 + 7L_2) \\ -l(2L_1 + 3L_2) \\ 10(M_1 + 2M_2) \end{bmatrix} \tag{4.72}$$

Using the *quasi-steady* aerodynamic model in Eqns. (2.7 & 2.8) the aerodynamic forces and moments are calculated as;

$$L_1 = qcCl_\alpha(\alpha^1 + \frac{\dot{h}^1}{U_\infty} + \frac{c\,ea_2\dot{\alpha}^1}{U_\infty}) \tag{4.73}$$

$$L_2 = qcCl_\alpha(\alpha^2 + \frac{\dot{h}^2}{U_\infty} + \frac{c\,ea_2\dot{\alpha}^2}{U_\infty}) \tag{4.74}$$

And,

$$M_1 = qc^2[\frac{-a\dot{\alpha}^1}{U_\infty} + ea_1Cl_\alpha(\alpha^1 + \frac{\dot{h}^1}{U_\infty} + \frac{c\,ea_2\dot{\alpha}^1}{U_\infty})] \tag{4.75}$$

$$M_2 = qc^2[\frac{-a\dot{\alpha}^2}{U_\infty} + ea_1Cl_\alpha(\alpha^2 + \frac{\dot{h}^2}{U_\infty} + \frac{c\,ea_2\dot{\alpha}^2}{U_\infty})] \tag{4.76}$$

where,

$$ea_1 = ea - 0.25 \quad \text{and} \quad ea_2 = 0.75 - ea \tag{4.77}$$

h^1, h^2 and α^1, α^2 are the flexural (plunge) and torsional (pitch) displacements at element nodes 1 and 2 respectively.

4.5. Summary

Detailed mathematical model of the bending-torsion behaviour of the cantilever beam (wing) incorporating piezoelectric patches with varying orientations. The model was then derived in a Finite Element form to find the effect of the activation of the piezoelectric patches on the onset of the flutter and the corresponding critical speeds. The model incorporates the aerodynamic loading - based on the quasi-steady theory and control forces. The control law modelling will be presented in the following chapter as well as the numerical results and discussion.

Chapter 5. CONTROL OF BEAM FLUTTER

This chapter is about the investigation of the controllability range of the beam using the attached piezoelectric patches.

The well known Multi-Input Multi-Output (MIMO) *Full State Feedback* control law in particular, the Linear Quadratic Regulator (LQR) theory has been employed to realize the objective of flutter suppression of an Aeroelastic beam.

5.1. LQR Control Law

The LQR method is basically finding the optimal state feedback control gain matrix G which minimizes a performance function J of the problem [80]. The process of finding G can be summarized as following [79];

For a dynamic system represented in a state-space form;

$$\{\dot{x}\} = [A]\{x\} + [B]\{C\} \tag{5.1}$$

Where,

$\{x, \dot{x}\}$: are the state variables, and $\{x\} = \begin{bmatrix} x_i \\ \dot{x}_i \end{bmatrix}$, $\{\dot{x}\} = \begin{bmatrix} \dot{x}_i \\ \ddot{x}_i \end{bmatrix}$

$[A]$: is the system matrix generated from the stiffness and mass matrices $[K]$ & $[M]$,

$[B]$: is the control/actuator matrix generated from control forces matrix $[F]$, and

$\{C\}$: is the control input calculated by LQR method.

The control input is resulted from multiplying the gain matrix by the state vector;

$$\{C\} = -[G]\{x\} \tag{5.2}$$

For the performance function of;

$$J = \frac{1}{2}\int_0^\infty (\{x\}^T[Q]\{x\} + \{C\}^T[R]\{C\})dt \tag{5.3}$$

The Hamiltonian of the system is;

$$H = \frac{1}{2}(\{x\}^T[Q]\{x\} + \{C\}^T[R]\{C\}) + \{\lambda\}^T([A]\{x\} + [B]\{C\}) \tag{5.4}$$

Applying the optimality conditions of;

$$\{\dot{\lambda}\} = -\frac{\partial H}{\partial \{x\}} = -[Q]\{x\} - [A]^T\{\lambda\}, \qquad \{\lambda(\infty)\} = 0 \tag{5.5}$$

$$\frac{\partial H}{\partial \{\mathcal{C}\}} = -[R]\{\mathcal{C}\} + [B]^T\{\lambda\} \tag{5.6}$$

Thus, the optimal control input is;

$$\{\mathcal{C}\} = -[R]^{-1}[B]^T\{\lambda\} \tag{5.7}$$

Using the *Riccati* matrix $\boldsymbol{S}$, the *Lagrange multiplier* $\boldsymbol{\lambda}$ can be written as;

$$\{\lambda\} = [S]\{x\} \tag{5.8}$$

Substituting Eqn. (5.8) into Eqn. (5.5) and for the steady state of the system where the *Riccati* matrix satisfies $[\dot{S}] = 0$, the so-called *Algebraic Ricatti Equation (ARE)* is obtained;

$$[0] = [S][A] + [A]^T[S] - [S][B][R]^{-1}[B]^T[S] + [Q] \tag{5.9}$$

Solving Eqn. (5.6) to find the *Riccati* matrix $\boldsymbol{S}$, then the control input $\boldsymbol{\mathcal{C}}$ in Eqn. (5.7) is written as;

$$\{\mathcal{C}\} = -[R]^{-1}[B]^T[S]\{x\} \tag{5.10}$$

Therefore, the gain matrix is;

$$[G] = -[R]^{-1}[B]^T[S] \tag{5.11}$$

5.2. Aerodynamic Forces in State-Space Form

Revisiting the quasi-steady aerodynamic forces in Eqns. (4.73 – 4.76) it can be seen that these forces are function in the system states, namely, $\dot{h}, \alpha$ & $\dot{\alpha}$. In other words, the aerodynamic forces have components that depend on the system state velocities which are considered as aerodynamic damping components. Therefore, it is obvious to rewrite these forces in state-space form to be added to its mechanical counterparts in the system Equations of Motion (Eqn. 4.71) [81, 82].

The state-space form of the element states of Figure (4.5) is;

$$\{\mathbb{x}\} = \begin{bmatrix} x_1 \\ x_2 \\ x_3 \\ x_4 \\ x_5 \\ x_6 \\ \dot{x}_1 \\ \dot{x}_2 \\ \dot{x}_3 \\ \dot{x}_4 \\ \dot{x}_5 \\ \dot{x}_6 \end{bmatrix} \text{ or in physical variables; } \{\mathbb{x}\} = \begin{bmatrix} h^1 \\ r^1 \\ \alpha^1 \\ h^2 \\ r^2 \\ \alpha^2 \\ \dot{h}^1 \\ \dot{r}^1 \\ \dot{\alpha}^1 \\ \dot{h}^2 \\ \dot{r}^2 \\ \dot{\alpha}^2 \end{bmatrix} \tag{5.12}$$

Where,

r: is the rotational (bending) displacement of the element nodes.

For numerical simulation purposes, initial condition of lift coefficient (Cl_0) is added to the aerodynamic forces equations (4.73 – 4.76);

$$L_1 = qcCl_\alpha \left(\alpha^1 + \frac{\dot{h}^1}{U_\infty} + \frac{c\, ea_2 \dot{\alpha}^1}{U_\infty} \right) + qcCl_0 \tag{5.13}$$

$$L_2 = qcCl_\alpha \left(\alpha^2 + \frac{\dot{h}^2}{U_\infty} + \frac{c\, ea_2 \dot{\alpha}^2}{U_\infty} \right) + qcCl_0 \tag{5.14}$$

And,

$$M_1 = qc^2 [\frac{-a\dot{\alpha}^1}{U_\infty} + ea_1 Cl_\alpha (\alpha^1 + \frac{\dot{h}^1}{U_\infty} + \frac{c\, ea_2 \dot{\alpha}^1}{U_\infty})\,] + qea_1 c^2 Cl_0 \tag{5.15}$$

$$M_2 = qc^2 [\frac{-a\dot{\alpha}^2}{U_\infty} + ea_1 Cl_\alpha (\alpha^2 + \frac{\dot{h}^2}{U_\infty} + \frac{c\, ea_2 \dot{\alpha}^2}{U_\infty})] + qea_1 c^2 Cl_0 \tag{5.16}$$

Applying Eqns. (5.13 – 5.16) into Eqn. (4.72) the aerodynamic forces in can be written as;

$$AF_m^e = \begin{bmatrix} F_1^e \\ F_2^e \\ Fa_3^e \\ F_4^e \\ F_5^e \\ Fa_6^e \end{bmatrix} = [K_a]\{x_i\} + [C_a]\{\dot{x}_i\} + \{Cl_{0_i}\} \tag{5.17}$$

Where,

$$[K_a] = -\frac{lqcCl_\alpha}{60}\begin{bmatrix} 0 & 0 & 21 & 0 & 0 & 9 \\ 0 & 0 & 3l & 0 & 0 & 2l \\ 0 & 0 & 20cea_1 & 0 & 0 & 10cea_1 \\ 0 & 0 & 9 & 0 & 0 & 21 \\ 0 & 0 & -2l & 0 & 0 & -3l \\ 0 & 0 & 10cea_1 & 0 & 0 & 20cea_1 \end{bmatrix} \quad (5.18)$$

$$[C_a] = -\frac{lqcCl_\alpha}{60U_\infty}\begin{bmatrix} 21 & 0 & 21cea_2 & 9 & 0 & 9cea_2 \\ 3l & 0 & 3lcea_2 & 2l & 0 & 2lcea_2 \\ 20cea_1 & 0 & 20c(cea_2ea_1 - \frac{a}{Cl_\alpha}) & 10cea_1 & 0 & 10c(cea_2ea_1 - \frac{a}{Cl_\alpha}) \\ 9 & 0 & 9cea_2 & 21 & 0 & 21cea_2 \\ -21 & 0 & -2lcea_2 & -3l & 0 & -3lcea_2 \\ 10cea_1 & 0 & 10c(cea_2ea_1 - \frac{a}{Cl_\alpha}) & 20cea_1 & 0 & 20c(cea_2ea_1 - \frac{a}{Cl_\alpha}) \end{bmatrix} \quad (5.19)$$

$$\{Cl_{0i}\} = -\frac{lqcCl_\alpha}{60}\begin{bmatrix} 30\alpha_0 \\ 5l\alpha_0 \\ 30cea_1\alpha_0 \\ 30\alpha_0 \\ -5l\alpha_0 \\ 30cea_1\alpha_0 \end{bmatrix} \quad (5.20)$$

$$\{x_i\} = \begin{bmatrix} h^1 \\ r^1 \\ \alpha^1 \\ h^2 \\ r^2 \\ \alpha^2 \end{bmatrix}, \text{ and } \{\dot{x}_i\} = \begin{bmatrix} \dot{h}^1 \\ \dot{r}^1 \\ \dot{\alpha}^1 \\ \dot{h}^2 \\ \dot{r}^2 \\ \dot{\alpha}^2 \end{bmatrix} \quad (5.21)$$

Eqn. (4.71) can then be written as;

$$[K_m - K_a][x] + [C_m - C_a][\dot{x}] + [M_m][\ddot{x}] - [Cl_{0i}] - [PF_m^e] = 0 \quad (5.22)$$

Where the mechanical proportional damping component is [83, 84], [84];

$$[C_m] = \zeta[K_m] + \beta[M_m] \quad (5.23)$$

Where,

ζ , and β: are the frictional and the structural damping constants respectively.

5.3. Piezoelectric Actuator/Control Matrix

Considering the mechanical and aerodynamic damping and initial lift condition components in Eqn. (5.22), Eqn. (5.1) can be rewritten as;

$$[\dot{x}] = [A][x] + [Cl_{0_i}] + [M_m]^{-1}[PF_m^e] \tag{5.24}$$

By comparing Eqn. (5.24) with Eqn. (5.1);

$$[B]\{C\} = +[M_m]^{-1}[PF_m^e] \tag{5.24}$$

Or from Eqn. (5.2),

$$-[B][G]\{x\} = [M_m]^{-1}[PF_m^e] \tag{5.26}$$

From Eqns. (4.65, 4.66 & 4.70) the actuator force matrix in element domain is;

$$PF_m^e = \begin{bmatrix} Fhp_1^e \\ Fhp_2^e \\ Fap_3^e \\ Fhp_4^e \\ Fhp_5^e \\ Fap_6^e \end{bmatrix} = Y_0 \begin{bmatrix} 0 \\ -M_x^p \\ -2M_{xy}^p \\ 0 \\ M_x^p \\ 2M_{xy}^p \end{bmatrix} \tag{5.27}$$

Since the actuator forces are a function of the applied electric field $\mathbb{E}_3$ ($\mathbb{E}_1$ in Micro Fibre Composite MFC actuator case) Eqn. (5.27) can be rewritten as;

$$PF_m^e = Y_0 \int_{t_p} \begin{bmatrix} 0 \\ -\bar{e}_{31} \\ -2\bar{e}_{36} \\ 0 \\ \bar{e}_{31} \\ 2\bar{e}_{36} \end{bmatrix} z \, dz \,.\, \mathbb{E}_3 \tag{5.28}$$

Substitute Eqn. (5.28) into Eqn. (5.26);

$$[B] = -Y_0 [M_m]^{-1} \int_{t_p} \begin{bmatrix} 0 \\ -\bar{e}_{31} \\ -2\bar{e}_{36} \\ 0 \\ \bar{e}_{31} \\ 2\bar{e}_{36} \end{bmatrix} z \, dz \tag{5.29}$$

And the input control (electric field) is,

$$\mathbb{E}_3 = [G]\{x\} \tag{5.30}$$

For the purpose of multi-control of each elemental actuator, the global control matrix PF is modified by assembling each element control matrix PF^e;
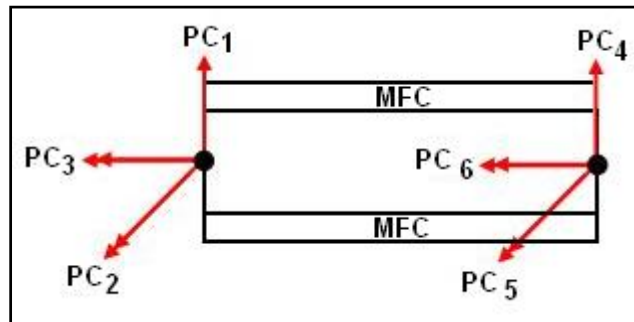
Figure 5.1: Basic control effects due to MFC actuation.

Figure (5.1) shows the general notation of the control forces and moments generated from the actuation of the MFC layers. Similar to Eqn. (4.70) element control matrix PF^e can be written in the form of;

$$PF^e = \begin{bmatrix} PC_1 \\ PC_2 \\ PC_3 \\ PC_4 \\ PC_5 \\ PC_6 \end{bmatrix}^e \tag{5.31}$$

For example, the global control matrix of the multi-control input of two MFC-elements as in Figure (5.2) is;
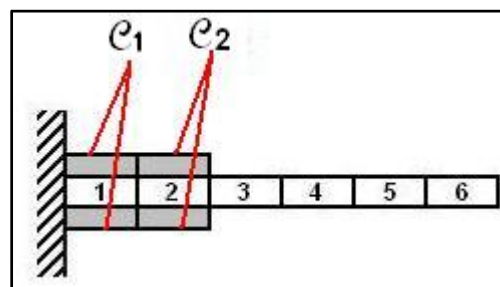
Figure 5.2: Multi-control inputs.

$$PF = \begin{bmatrix} PC_1^1 & 0 \\ PC_2^1 & 0 \\ PC_3^1 & 0 \\ PC_4^1 & PC_1^2 \\ PC_5^1 & PC_2^2 \\ PC_6^1 & PC_3^2 \\ 0 & PC_4^2 \\ 0 & PC_5^2 \\ 0 & PC_6^2 \end{bmatrix} \tag{5.32}$$

And consequently, the control matrix B will be;

$$[B] = [M_m]^{-1}[PF] \tag{5.33}$$

This leads to a modified control input vector;

$$\{\mathcal{C}\} = \begin{bmatrix} \mathcal{C}_1 \\ \mathcal{C}_2 \end{bmatrix} = \begin{bmatrix} \mathbb{E}_3^1 \\ \mathbb{E}_3^2 \end{bmatrix} = [G]_{j \times 2}\{\mathbb{x}\}_{1 \times j} \tag{5.34}$$

5.4. Numerical Simulation

A six-element beam is used to simulate the flutter case and its control. The control effect is generated from a pair of piezoelectric MFC wafers bonded on top and bottom surfaces of the beam which are polarized in the same manner to produce a bi-morphing action at each element under actuation. The flutter control was investigated in six MFC placements configurations. In each configuration the orientation (skew) angle of the MFC was varied. Table 5.1 shows the free six-elements beam, the MFC skew angle variation and the six actuation configurations.

The simulation configurations are;

a. Three configurations; each is for individual actuation of elements 1, 2 and 3 with MFC skew angle variation ranges from -90º to 90º,

b. Three configurations; each is a combination of two actuated elements (1+2, 1+3 and 2+3) with MFC skew angle variation ranges from -60º to 60º.
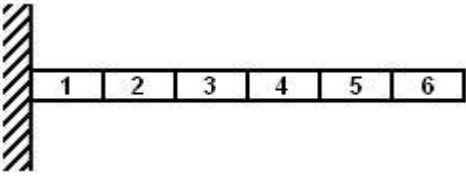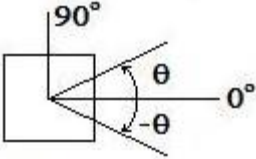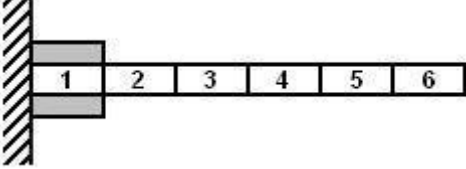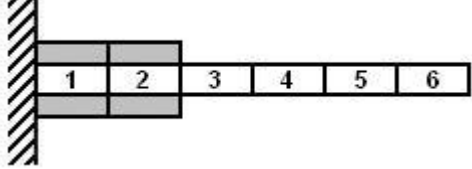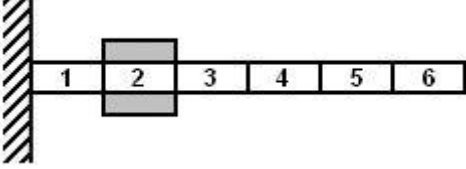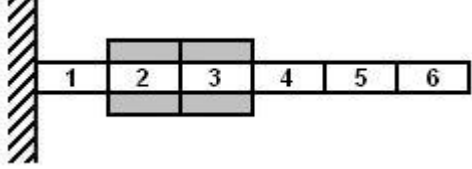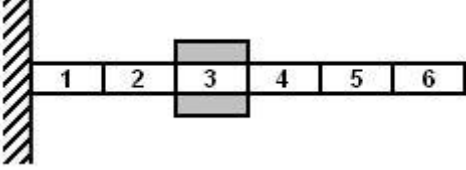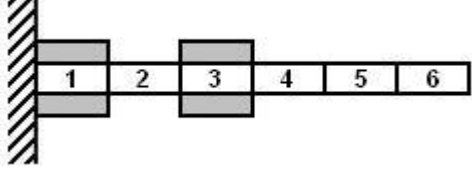
Table 5.1: Simulation configurations and MFC skew angle variation.

A MATLAB program was constructed to conduct these simulations. The flow chart and the listing of the simulation program are shown in appendix A.3.

5.4.1. Program Validation

The MATLAB© program constructed in this study was validated based on previous numerical work. The program algorithm must obtain the effect of the piezoelectric actuators on a bending-torsion (aeroelastic) beam model. Most of the work done in the control of smart structures using piezoelectric actuators was conducted on bending beam models and on the other hand, most of the aeroelastic problems incorporating piezoelectric actuators were numerical and/or experimental customized treatments. Because of these reasons, the validation process was conducted in two parts; validation of the piezoelectric effect and validation of the bending-torsion beam model.

Piezoelectric Effect Validation

The validation of the program code for the piezoelectric effect is conducted on a [0°/90°/90°/0°] cross-ply symmetric laminated (AS/3501) beam with one layer of

piezoceramic material (G-1195) bonded on the top and the bottom of the beam. The tip deflections of the beam due to applied voltages are shown in Figure (5.3). It shows good agreement between the current model and the work done by Donthireddy and Chandrashekhara [85].
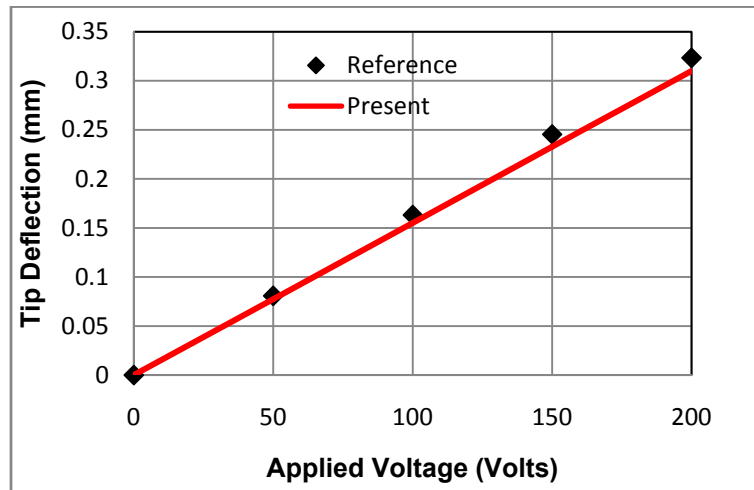
Figure 5.3: Effect of actuator on tip deflection.

Aeroelastic Model Validation

The majority of the work conducted in wing flutter control is validated and compared with the well-known work (Goland's wing) by Martin Goland [86]. The exact Goland's solution for flutter speed of a uniform cantilever wing employs the aerodynamic forces derived by Theodorsen [48]. This is not the case for the present work where the aerodynamic forces are based on the quasi-steady aerodynamic theory. Moosavi *et al.* [51] developed a procedure to predict the flutter speed and frequency based on Galerkin's method and quasi-steady aerodynamic theory and used Goland's wing to validate the proposed model.

The validation of the present aeroelastic FE model is done in two steps. In the first step the Galerkin's method presented in Fung [47] is constructed using Mathcad© software (see Appendix A2.1) to solve the Goland's wing and then it is compared the work by Moosavi *et al.* [51] . Table 5.2 shows good correlation between the two models.

Model	Flutter Speed (Mach#)	Flutter Frequency (Hz)
Moosavi et al. [51]	0.554	11.15
Galerkin [47]	0.543	13.796

Table 5.2: Comparison of the calculated flutter results.

Then in the second step, the Galerkin's method is used to validate the FE model as shown in Appendix A2.2. Table 5.3 shows also a good correlation between the two models.

Model	Flutter Speed (m/s)	Flutter Frequency (rad/s)
Galerkin [47]	33.51	27.12
FE Model	34	29.361

Table 5.3: Galerkin vs. FE model comparison.

5.4.2. Materials' Properties

To obtain the objectives of the present investigation the substrate and actuator materials are adopted from different sources. The substrate material is decided to be regular Aluminium. The piezoelectric actuator material is chose to be MFC™ with the assumption that its properties do not affected by varying its skew (orientation) angle. The mechanical and electromechanical properties are listed in Table 5.4.

	MFC™ [42]	Aluminium [73]
E_{11}(GPa)	36.5	69.0
E_{22}(GPa)	7.60	69.0
G_{12}(GPa)	14.6	27.0
ν_{12}	0.25	0.32
d_{31}(m/V)	$530E^{-12}$	/
d_{32}(m/V)	$-210E^{-12}$	/
ρ (kg/m^3)	7552.0	2700.0
Length (m)	0.10	0.60
Width (m)	0.10	0.10
Thickness (m)	0.001	0.002

Table 5.4: Substrate and actuator materials' properties.

5.4.3. Simulation Results and Discussion

Cases I, II & III

The effects of the three individual actuation configurations on the beam aeroelastic behaviour are depicted in Figure (5.4). The dotted lines represent the increase in the flutter speed due to the (static) stiffness added to the beam by attaching the MFC actuators. As expected, the maximum effect happens at the root of the cantilever beam and it decreases away from it. Also, the increased profile is symmetrical around the 0˚ skew angle. The aim of showing the lines of the static stiffness effect in the figure is to differentiate between the effects of the deactivated and activated actuator on the flutter speed. The effect of the (controlled) activation of the actuator is very clear as depicted with the solid line(s).
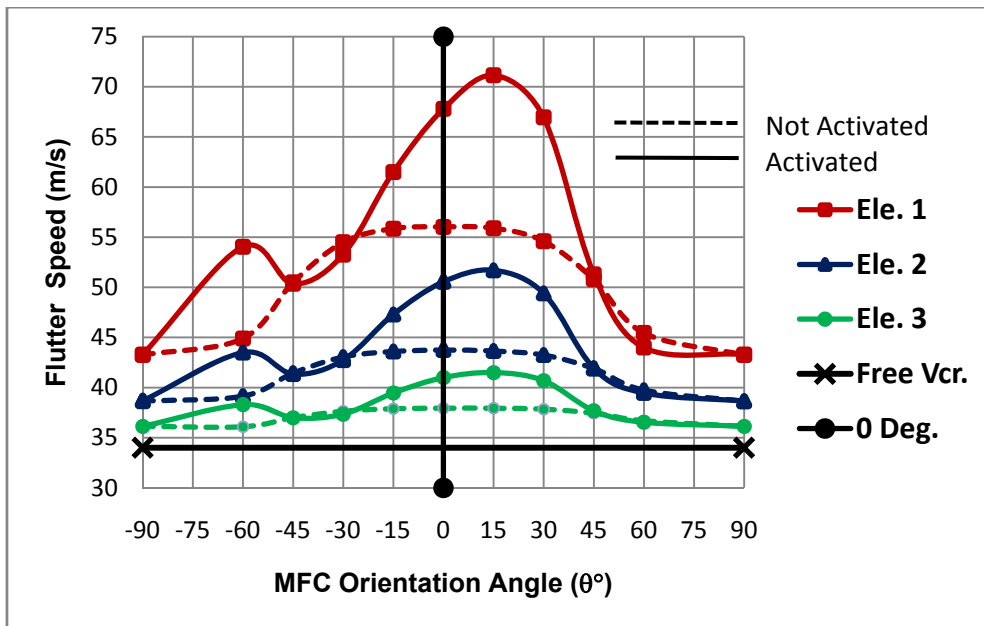
Figure 5.4: The effect of actuator skew angles on the flutter speed.

The first point to notice is that the profile of the effect is asymmetrical around 0° which highlights the importance of the MFC orientation angle. The second important observation is the angle where the highest increase in the flutter speed occurs. As shown in the figure this angle is 15°. This can be contributed to the resultant actuator moments applied to the system. As seen in Figure (5.5) the maximum resultant actuator moment occurs at within the 15°- 30° region.
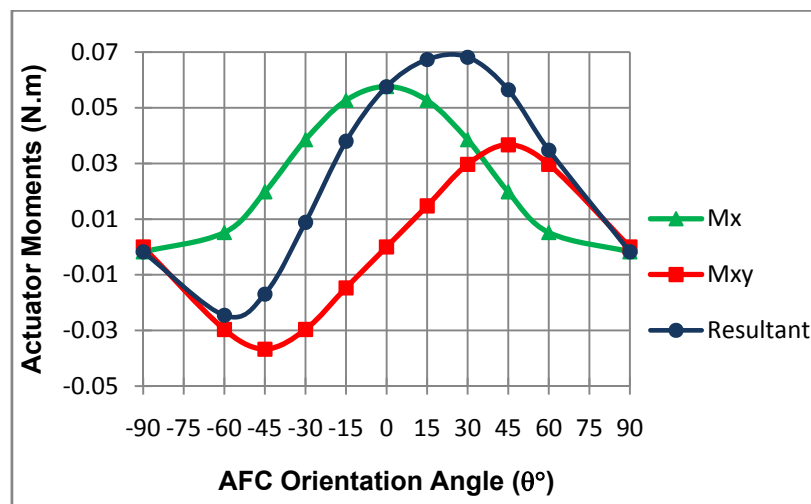
Figure 5.5: Actuator resultant moment due to activated actuator of different orientations.

Another interesting point is the -60° orientation angle. At this angle, the flutter speed increased opposing the decreasing trend. On the other side, the 60° orientation reduced the flutter speed below the deactivated line. Relating this to the resultant actuator moment

(Figure 5.5) it can be seen that the maximum negative moment occurs in between -60˚ and -45˚. The +45˚ and -45˚ produce the same flutter speed. By comparing the deactivated and activated lines the flutter speed curve can be divided into four regions;

- − -90˚ < θ < -45˚ flutter speed increases,
- − -45˚ < θ < -30˚ flutter speed decreases,
- − -30˚ < θ < 45˚ flutter speed increases,
- −   45˚ < θ < 90˚   flutter speed decreases.

Figures (5.6) and (5.7) show the plunge (flexural) and pitch damping ratios respectively. Both behave in the same manner to that for flutter speed. However, the activation of a 60˚ MFC on the first element produces the highest divergent (negative damping ratio) pitch behaviour which led to flutter speed lower than the base line for the static stiffness.
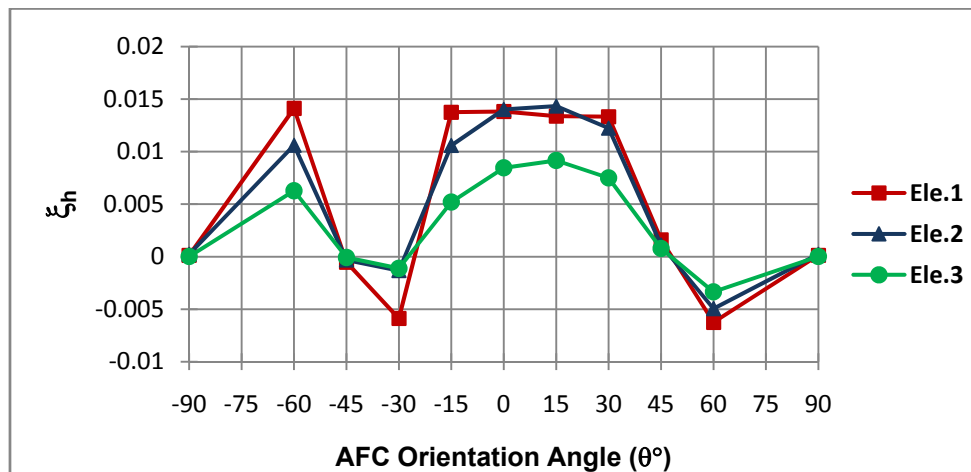
Figure 5.6: Plunge/Flexural damping ratio.
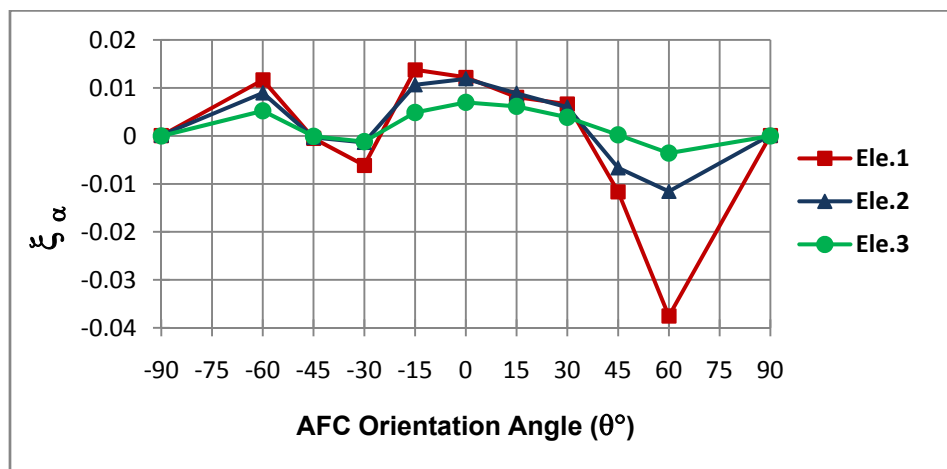
Figure 5.7: Pitch damping ratio.

Case IV

The plunge and pitch damping ratios are shown in Figures (5.8 & 5.9) respectively. The figures show the damping ratio of each element one orientation with varying the orientation of element two. From the figures, the damping ratio profiles can be divided into three regions:
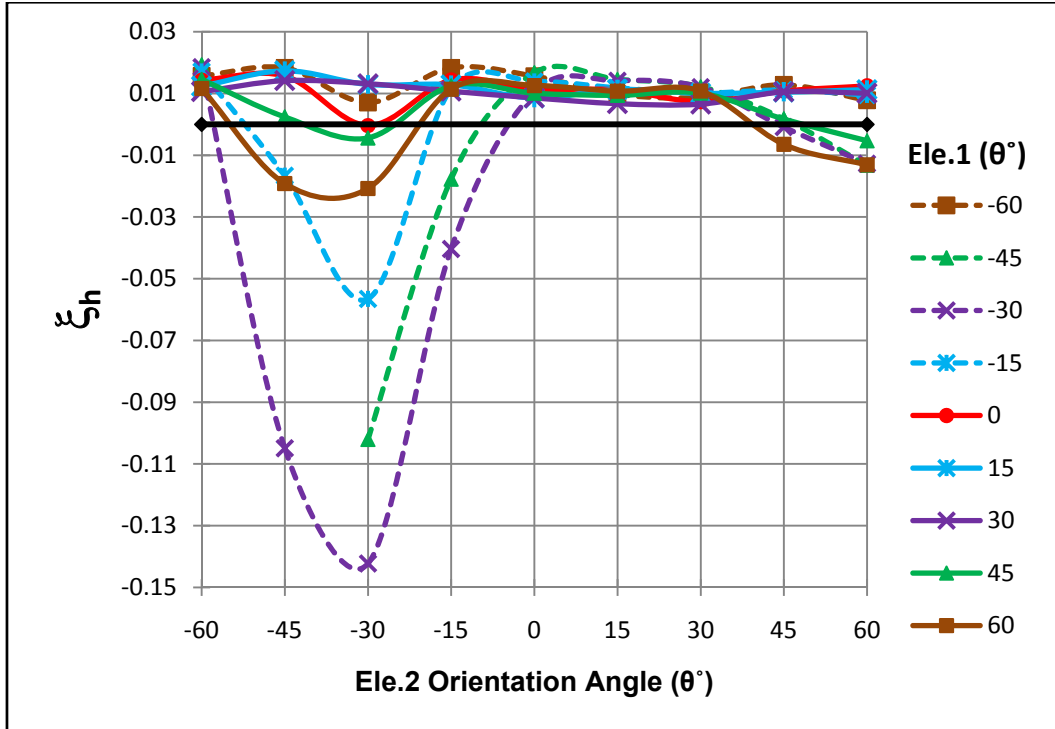
Figure 5.8: Plunge damping ratio; Elements 1&2 combinations.

1. Negative element two (θ_2) orientations; $\theta_2 < 0°$; this region shows variable trends for different element one (θ_1) orientations. The asymmetric behaviour of element one (θ_1) orientations is clear in this region; the -15°, -30°, -45° and 60° orientations produce unstable (negative damping ratios) behaviours while the 0°, 15°, 30°, 45° and -60° produce stable (positive damping ratios) behaviours.

2. The second region lies between $0° < \theta_2 < 30°$; at this region all element one (θ_1) orientations are bundled together and produce stable behaviours.

3. The third region is where $\theta_2 > 30°$; at this region the behaviours are again divided into two groups. The -60°, -45°, -30° and 45° orientations group have stable behaviours in between $30° < \theta_2 < 45°$ and unstable ones over 45°.

The -60°, 0°, 15° and 30° orientations of element one (θ_1) produce positive plunge damping ratios (stable behaviours) all over the range of element two (θ_2) orientations.
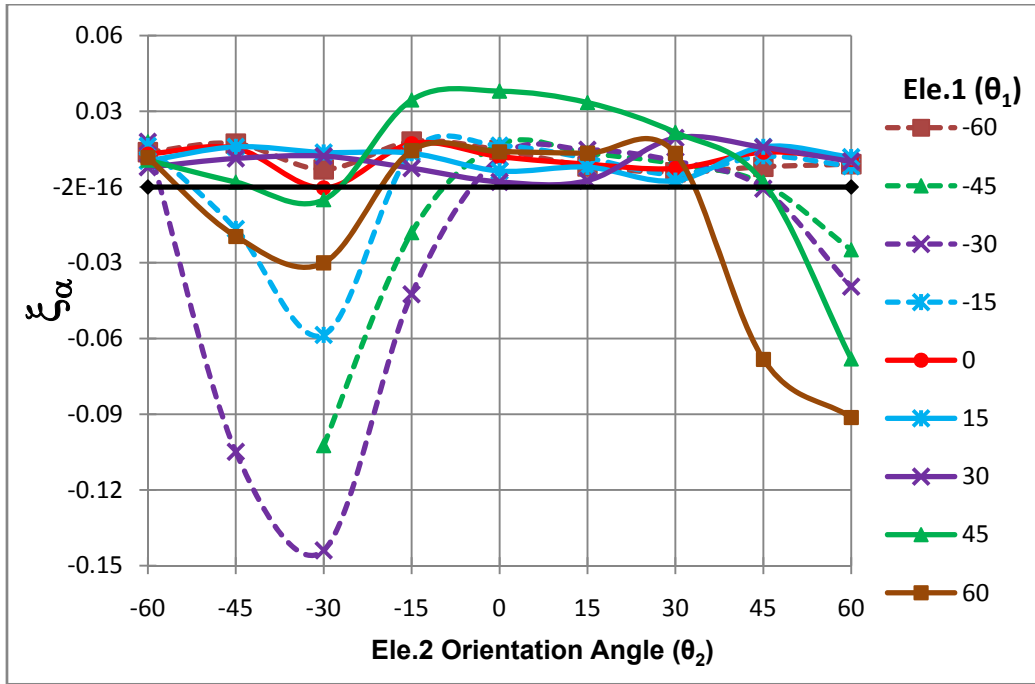
Figure 5.9: Pitch damping ratio; Elements 1&2 combinations.

The pitch damping ratio curves of the elements one and two combinations behave in the same manner as the plunge damping ratios with more dispersed tendencies. This demonstrates the sensitivity of the pitch/torsional motion in comparison to the flexural one. The 45° and 60° orientations of element one (θ_1) show a distinguishable trend. The 45° orientation produces positive damping ratios all over the θ_2 range except for the regions of -45° < θ_2 < -30° and 45° < θ_2 < 60°. The highest pitch damping ratio occurs at the combination of (45°, 0°). The 60° orientation of element one (θ_1) is stable only over the range of -15° < θ_2 < 30°.

Case V

The plunge and pitch damping ratios due to elements two and three combinations are shown in Figures (5.10 and 5.11) respectively. The plunge damping ratio behaviours of this case illustrate clear and uniform clustering and asymmetry. Two groups of trend lines are formed; the first group consists of the -60°, -15°, 0°, 15° and 30° of element two (θ_2) orientations. This group has a narrow band variation (0.008 to 0.015). The other group contains the -45°, -30°, 45° and 60° has a wider band variation (-0.01 to 0.01). Both groups follow the same profile where the damping ratios start negative at the 60° orientation of element three (θ_3) and rise to the maximum at 15° then drops to reach a bottom at -30° to rise back to positive values at the -60° orientation of element three (θ_3).
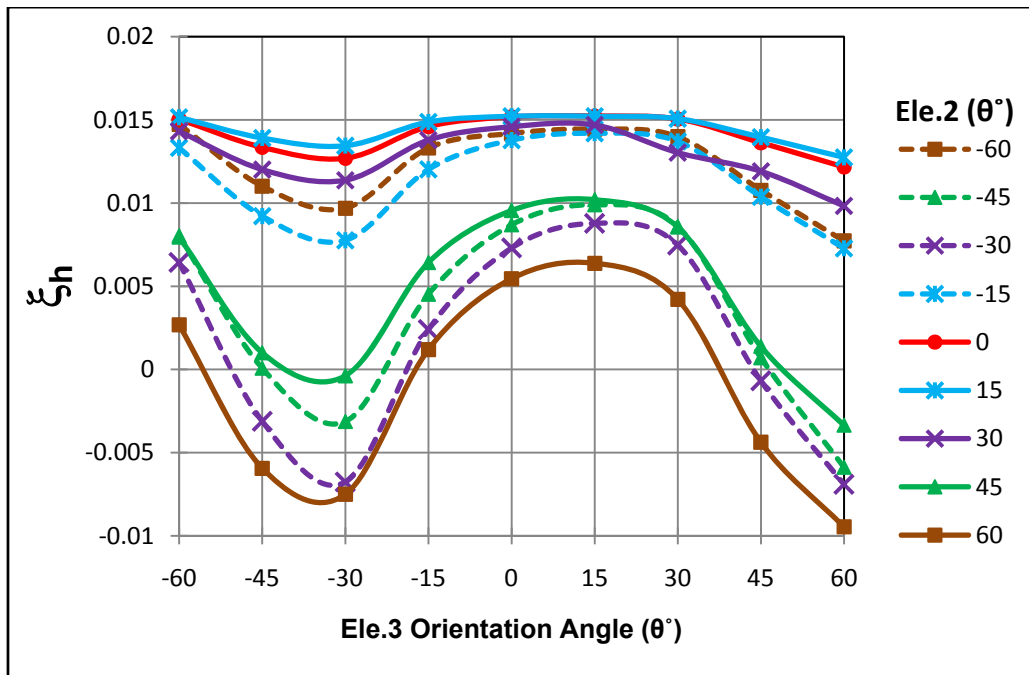
Figure 5.10: Plunge damping ratio; Elements 2&3 combinations.

The pitch damping ratio behaviour can be divided into two regions. The first region lies between $-60° < \theta_3 < -30°$. This experiences a similar clustering as of the plunge damping ratio behaviours. In the second region (between $-30° < \theta_3 < 60°$), the pitch damping ratio behaviours are grouped together and then re-divided into two groups at $\theta_3 > 30°$. This is true except for the 30°, 45° and 60° element two (θ_2) orientations where they have different and wide variations.
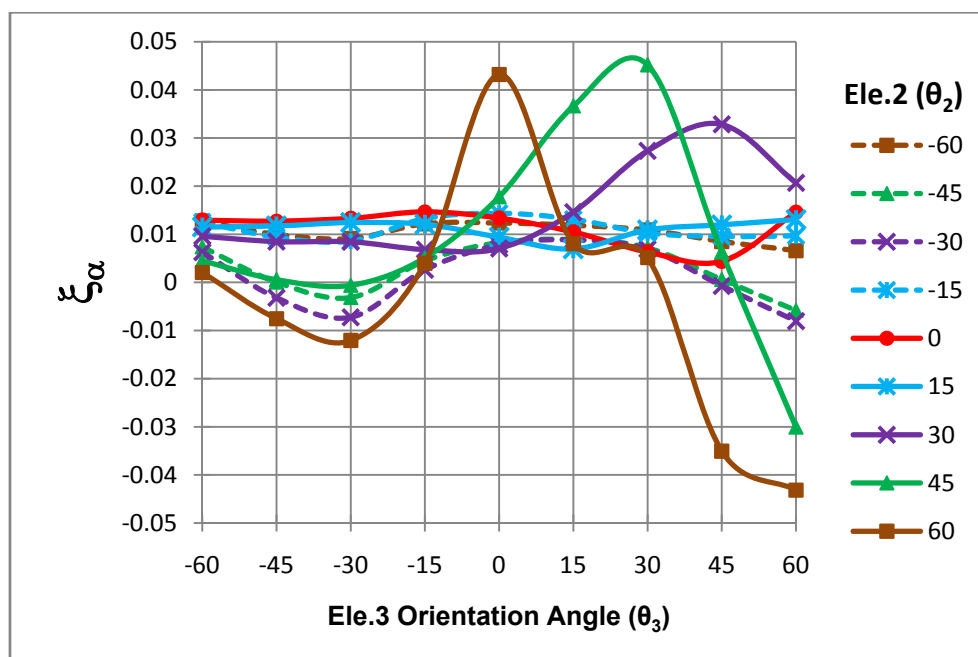
Figure 5.11: Pitch damping ratio; Elements 2&3 combinations.

The orientation of element two (θ_2) of -60°, -15°, 0° and 15° produce positive pitch damping ratios all over the range of the element three (θ_3) orientations.

Case VI

The plunge damping ratio behaviours for the elements 1 & 3 combinations shown in Figure (5.12) follow the behaviour of the element 1 & 2 case. This is expected since element one appears to be the most influential location.
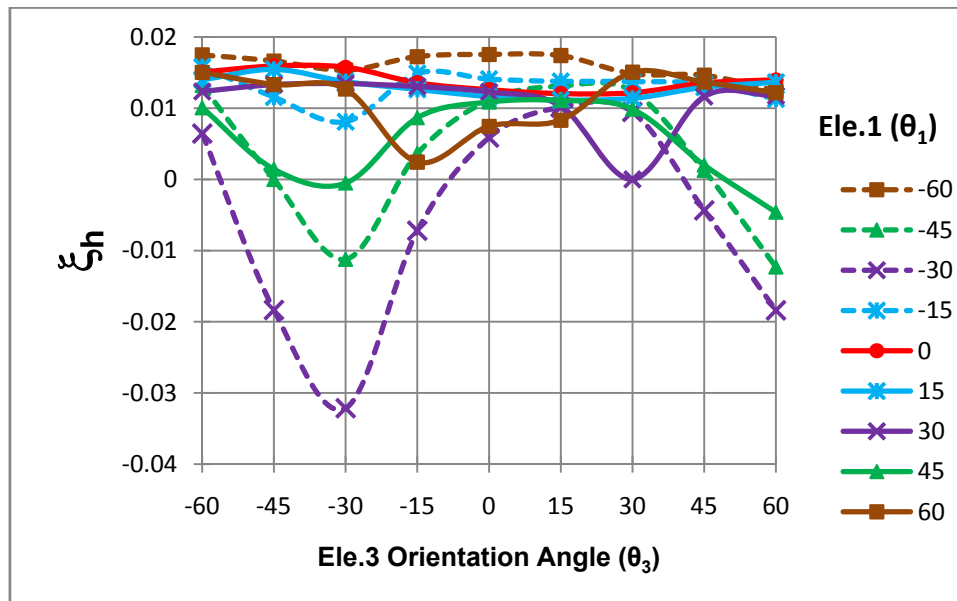
Figure 5.12: Plunge damping ratio; Elements 1&3 combinations.

Most of the combinations produce stable behaviour except for the element orientation angles of -30° and 45°. These have unstable (negative ratios) portions. However, these instabilities are reduced in comparison with the case of elements 1 & 2. This indicates that element three actuation has introduced a better stabilizing regime compared to that from element two. This could be due to the gap between the two actuated elements.
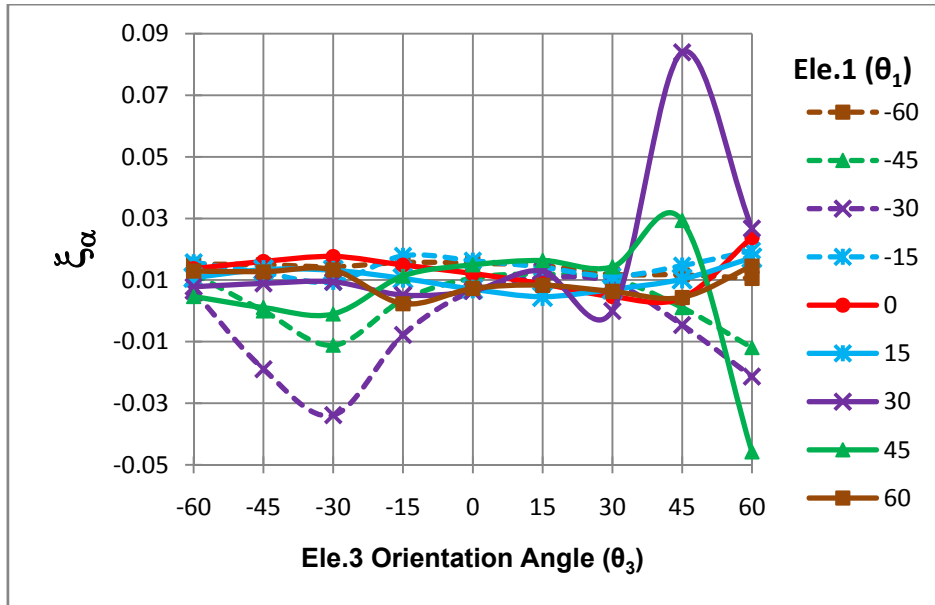
Figure 5.13: Pitch damping ratio; Elements 1&3 combinations.

The same reduction effect on the unstable portions appears in the pitch ratio behaviour. However, the stable (positive ratio) portion of the $45^°$ behaviour line of element one experienced a reduction too. This indicates that element three actuation introduces a divergent and not a stabilizing effect to the system compared to that for element two actuations.

Overall, most of the behaviour lines of the plunge damping ratio follow the trend depicted in Figure (5.10). This is clear in both the single actuator and double actuators configurations. The same can be mentioned for the pitch damping ratio behaviour lines but with more irregular behaviours especially for the case of the element 2 & 3 combinations.

Multi-actuation of piezos has a more pronounced effect on flutter speed when compared with the individual ones. Figure (5.14) shows the gain in flutter speed due to the actuation of a sample combination of elements one and two of $(-30^°,\theta_2^°)$ when compared with the individual actuator cases. The figure shows a similar profile with a shift of the maximum flutter speed achieved from $15^°$ of the individuals to $30^°$ for the multi-actuation case. However, the comparison between the inactivated and activated curves of the elements one and two combination shows that the flutter speed increased only at two angles namely, $15^°$ and $30^°$ while it occurs over a range of angles for individual cases ($-60^°$, $-15^°$, $0^°$, $15^°$ and $30^°$).
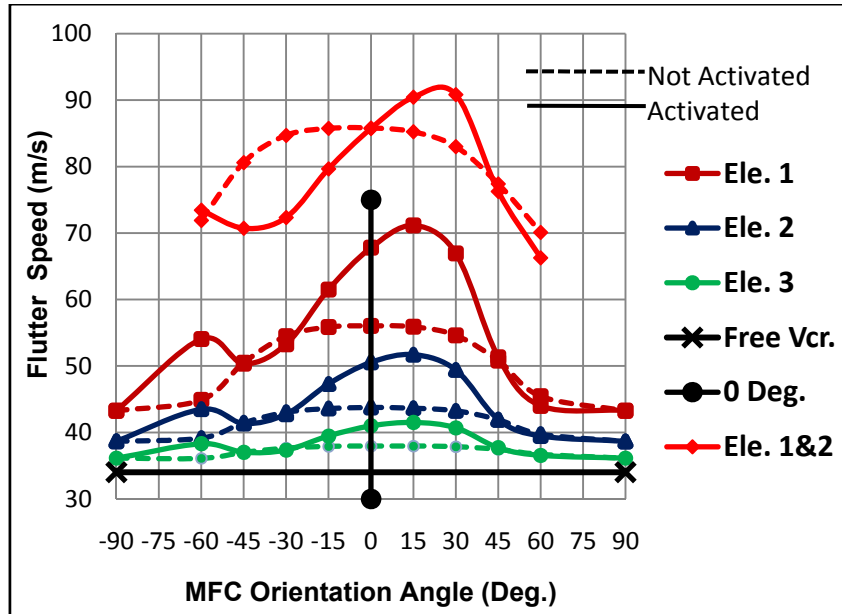
Figure 5.14: Flutter speed comparison between the individual and multi actuation.

To gain more insight on the effect of the actuator orientation on the pitch angle of the beam, the span-wise Effective Pitch Angle (EPA) for each case is shown in the following figures. Figures (5.15) to (5.18) illustrate different profiles of the span-wise EPA for cases I, II, III, IV, V and VI respectively. For the first three cases, it is clear that the profile changes at the element with the piezoelectric patches. However, the three have similar profiles with different EAP variation magnitudes. Also, the positive and negative orientations are kind of symmetrical around $0^{°}$ for most of them. This symmetry becomes clear as the piezos move away from the beam root. Another observation is that the minimum EPA is raised as the piezos moves away from the root; there are negative EPAs in Element 1 but in Element 3, all are positives.
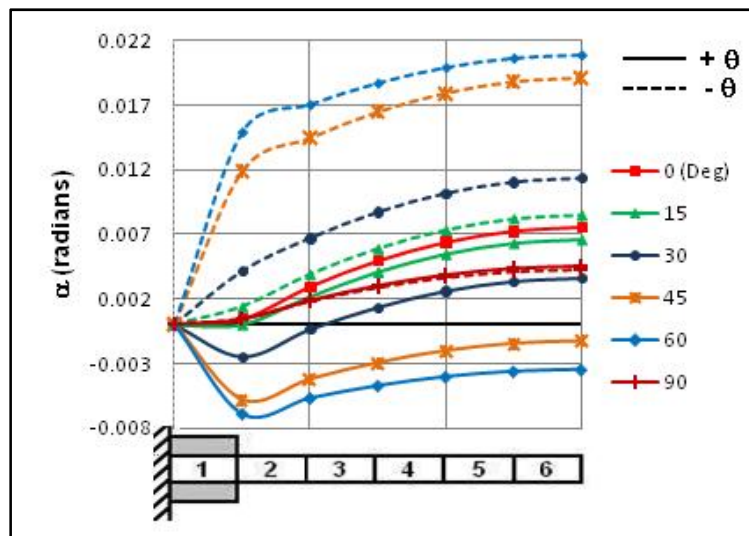
Figure 5.15: Span-wise EPA due to Ele. 1 actuation.
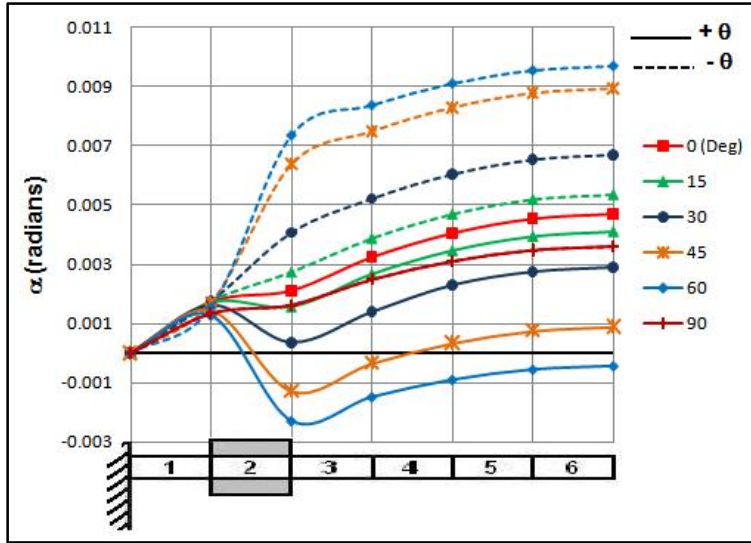
Figure 5.16: Span-wise EPA due to Ele. 2 actuation.
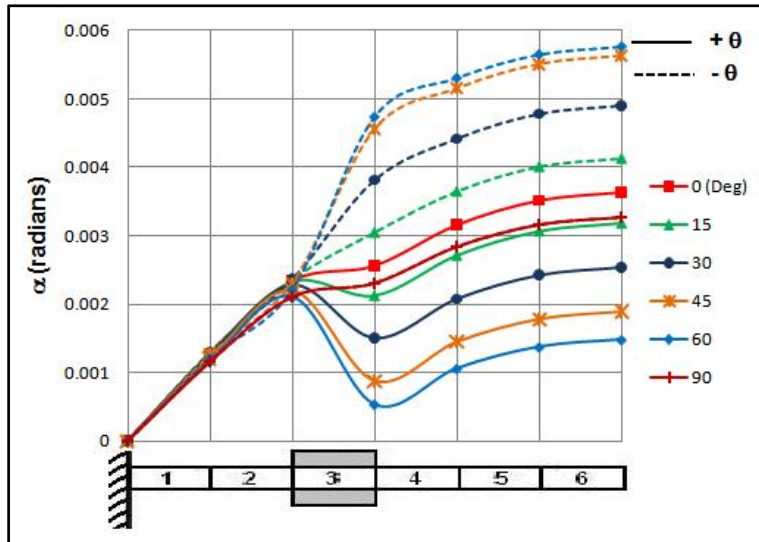
Figure 5.17: Span-wise EPA due to Ele. 3 actuation.
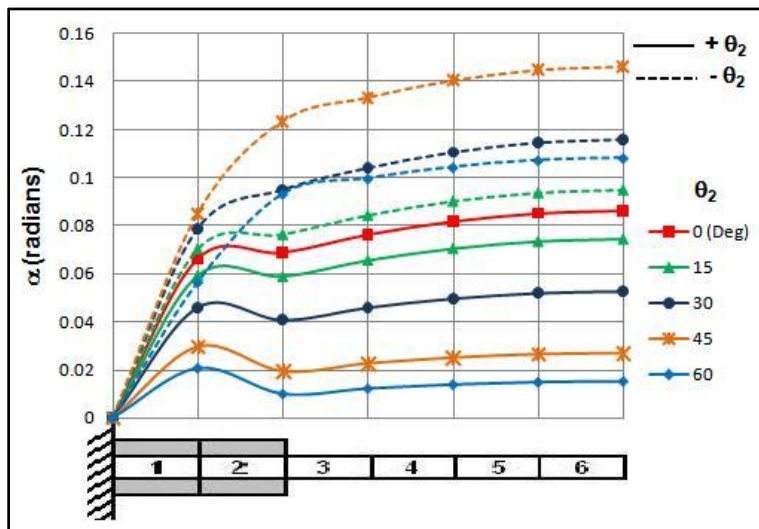
Figure 5.18: Span-wise EPA due to combination (-60,θ_2) actuation.
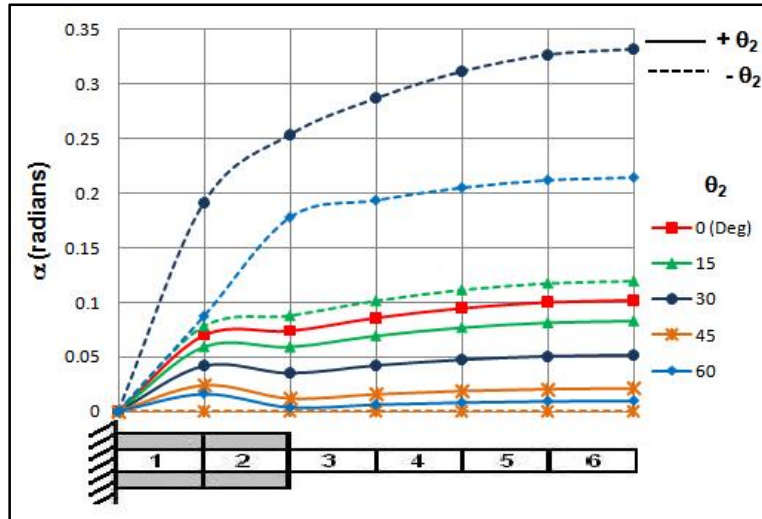
Figure 5.19: Span-wise EPA due to combination (-45,θ₂) actuation.

Figures (5.17) and (5.18) show two combinations of $(-60^{°},\theta_2^{°})$ and $(-45^{°},\theta_2^{°})$ of case IV as examples of multi-actuation cases.

A closer look at the actual piezo actuation effects is obtained by evaluating the Δ(EPA) through subtracting the inactivated EAP values from the activated ones to exclude the mechanical effects of the piezos. Figures (5.19) to (5.23) show the actual Δ(EPA) exerted by activating the corresponding actuator of each case. Although the Δ(EPA) is small, they vary from case to case and from one combination to another. These EAP variations highlight the controllability of a main player in aerodynamic forces which is the Angle of Attack.
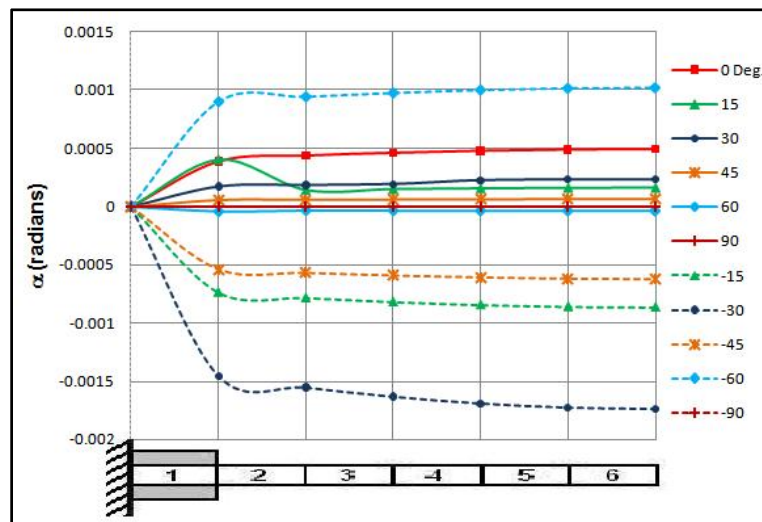
Figure 5.20: Span-wise Δ(EPA) due to Ele.1 actuation.
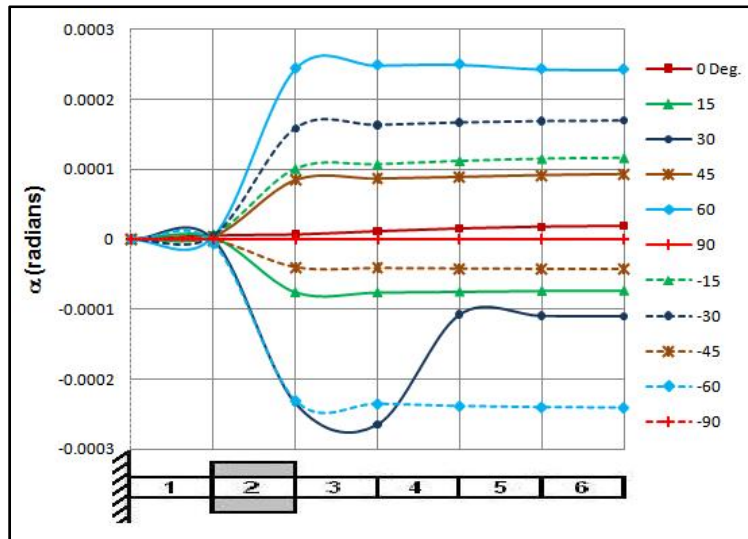
Figure 5.21: Span-wise Δ(EPA) due to Ele.2 actuation.

Figure 5.22: Span-wise Δ(EPA) due to Ele.3 actuation.

Figure 5.23: Span-wise Δ(EPA) due to combination (-60,θ₂) actuation.
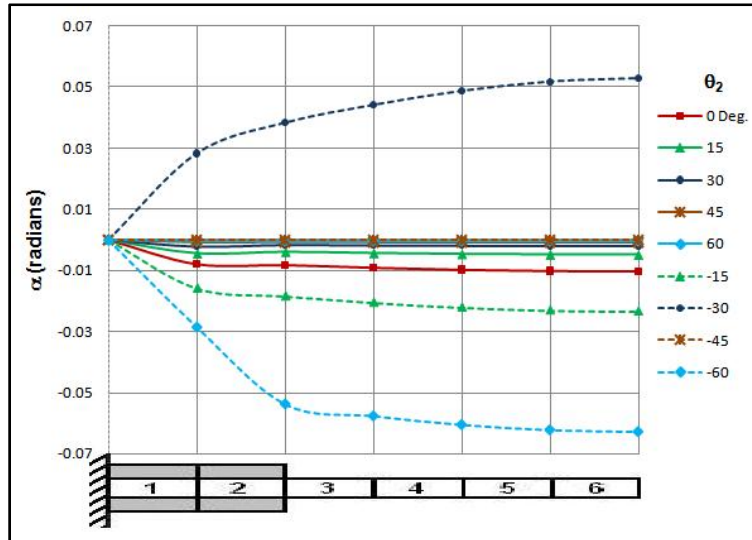
Figure 5.24: Span-wise Δ(EPA) due to combination (-45,θ₂) actuation.

5.5. Summary

The control law and model of flutter control case of a cantilever beam using piezoelectric patches are presented in this chapter. A six-element beam model is developed to permit various configurations of the piezo-patch location along the beam. A multi-control capability is also incorporated in the model. This model is based on the Finite Element model developed in Chapter 4 which incorporates the capability of aligning the piezoelectric patches in different orientations. This gave more flexibility in investigating a wide range of orientations and location configurations. The obtained results of such configurations provided more insight on the behaviour of the flutter onset and its control. The results also show that there is a room for more investigation especially on the control law.

Chapter 6.   CONCLUSION AND RECOMMENDATIONS

The conclusions from this work are clearly made on the basis of the work done on Shape Memory Alloys (SMAs) on the modelling of the Aeroelastic characteristics of a beam with embedded piezoelectric patches.

6.1. Control of Structures using SMAs

The use of SMA wires to alter the natural frequencies of composite plates has been investigated. Two configurations of surface mounted (fastened) SMA wires are mathematically modelled using Rayleigh-Ritz method and the evaluated results are compared with the experimentally obtained results. The comparison showed a good match between the two results. On the other hand, a mismatch between the percentage changes is observed. It is assumed that the composite plates made for the experiments had undergone some tensile pre-straining during the fabrication which caused the mismatch. Even with this tensile pre-straining, some shift in the natural frequencies was observed especially for modes 4 and higher. The effective change of natural frequencies by using only two SMAs or a single SMA wire may help in developing the configuration of the actuators to receive the optimum response. This phenomenon minimises the number of SMA wires used and the energy spent for actuation can be reduced. This study demonstrates that the alteration of dynamic structural properties using SMAs is possible, even though the changes observed in this study are rather small. This strategy for control can be analytically modelled as shown by the reasonable match between the analytical and experimental results. This is a good portent for prospective mathematical modelling of the optimisation of control features of SMAs with regards to its configuration and location on the structure.

This study shows for low frequency cases, the use of SMA's in or on polymeric composite structures might be effective in inducing a momentary shift in natural frequencies when a reduction in the amplitude of vibration is required. The SMA configuration studies here also showed that simple linear spatial arrangement on or in a structure can be adequate in inducing a dynamic structural change.

Modeling of the SMA actuation was established but thermal effects might need further attention. Also, the handling of the SMA wires requires adequate instrumentation to obtain reliable results.

6.2. Control of Aeroelastic Flutter

In the second part, the utilization of the piezoelectric patches in controlling structural flutter has been demonstrated. A finite element model for bending-torsion case is developed with the capability of multi-element actuation with the concurrent ability to vary the orientation (skew angle) of the AFC patches. This study has demonstrated some level of confidence in the formulative analytical equations derived for a beam structure subjected to harmonic loading conditions for the determination of the critical flutter speed. The effect of the piezoelectric actuation on flutter has been demonstrated through two control strategies; open loop in-plane forces control and closed loop moments control. In the open loop in-plane forces control, the 0 degree piezoelectric orientation proved to be the most effective in shifting the flutter speed. In the other hand, the 45 degree piezoelectric orientation appeared to have the most effect on the amplitude on the twist angle.

The closed loop control is obtained using the LQR technique. The flutter speed and the damping are seen to be maximized at actuator orientation of 15 degrees. Multi-element Piezo actuation is also trending in the same direction as the single element actuation. Some piezo orientations have been shown to be totally unsuitable for multi-mode control such as 60 degrees for the 2nd element actuation. Overall, the wide range of pitch angles has been obtained from the variation of the orientation and combination of the actuators. Twist (torsional movement) angle appears to be promising as an effective flutter control parameter. Multi-element actuation will need optimization for situation-specific control – based on geometric and loading complexities.

6.3. Recommendations for Future work

1. Based on the work undertaken in this research, it might be worth conceiving a real hybrid control system consisting of both SMAs and piezoelectric sensors and actuators.   The control methodology could consist of passive one involving temperature movements for the control of the SMAs such as in jet engine exhaust flows and an algorithmic one involving the piezoelectric actuators and sensors. This might introduce the concept of effective control based on the transduction process (of the sensor) and the frequency range of the anticipated application.

2. Experimental validation of the developed analytical models of the control of Aeroelastic flutter. This will be further validate the numerical simulations shown in this study, especially for the optimal placement of the piezoelectric patches and the corresponding optimal orientation.

3. Increase the complexity (and hence realism) of the model by introducing added geometric complexity, such as an aerofoil configuration. This will augment the models in this study where loading complexities were introduced. This will also increase the dimensional complexity from the 1-D problem to a 2-and 3-D problem.

REFERENCES

[1]   in *Encyclopedia of Smart Materials*, M. Schwartz, Ed. New York: J. Wiley & Sons, 2002.

[2]   A. Yousefi-Koma and D. G. Zimcik, "Applications of Smart Structures to Aircraft for Performance Enhancement," *Canadian Aeronautics and Space Journal,* vol. 49, pp. 163-172, 2003.

[3]   V. Giurgiutiu, "Active-Materials Induced-Strain Actuation for Aeroelastic Vibration Control," *The Shock and Vibration Digest,* vol. 32, pp. 355-368, 2000.

[4]   M. V. Gandhi and B. S. Thompson, *Smart Materials and Structures*. London: Chapman & Hall, 1992.

[5]   S. B. Choi, Y. K. Park, and T. Fukuda, "A Proof-of-Concept Investigation on Active Vibration Control of Hybrid Smart Structures," *Mechatronics,* vol. 8, pp. 673-689, SEP 1998.

[6]   V. Balamurugan and S. Narayanan, "Active-passive Hybrid Damping in Beams with Enhanced Smart Constrained Layer Treatment," *Engineering Structures,* vol. 24, pp. 355-363, 2002.

[7]   H. T. Banks, R. C. Smith, and Y. Wang, *Smart Material Structures : Modeling, Estimation, and Control*. Chichester ; New York : Paris: Wiley ; Masson, 1996.

[8]   C. A. Rogers and V. Giurgiutiu, "Concepts of Adaptronic Structures," in *Adaptronics and Smart Structures: Basics, Materials, Design and Applications*, H. Janocha, Ed. Berlin: Springer, 1999.

[9]   V. K. Wadhawan, *Smart Structures: Blurring the Distinction Between the Living and the Nonliving*. Oxford: Oxford University Press, 2007.

[10]   D. Sahoo and C. E. S. Cesnik, "Roll Maneuver Control of UCAV Wing Using Anisotropic Piezoelectric Actuators," in *43rd AIAA/ASME/ASCE/AHS/ASC Structures, Structural Dynamics, and Materials*, Denver, CO, USA, pp. 3867-3877, 2002.

[11]   B. Sanders, F. E. Eastep, and E. Forster, "Aerodynamic and Aeroelastic Characteristics of Wings with Conformal Control Surfaces for Morphing Aircraft," *Journal of Aircraft,* vol. 40, pp. 94-99, 2003.

[12]   M. Mesaric and F. Kosel, "Unsteady Airload of an Airfoil with Variable Camber," *Aerospace Science and Technology,* vol. 8, pp. 167-174, 2004.

[13] Al-Fin, "Material: Heal Thyself! The Brave New World of Synthetic Materials That Self-Heal ", http://alfin2100.blogspot.com/2008/12/material-heal-thyself-brave-new-world.html

[14] B. Culshaw, *Smart Structures and Materials*. Boston: Artech House, 1996.

[15] W. Cao, "Multifunctional Materials - the Basis for Adaptronics," in *Adaptronics and Smart Structures: Basics, Materials, Design and Applications*, H. Janocha, Ed. Berlin: Springer, 1999.

[16] A. V. Srinivasan and D. M. McFarland, *Smart Structures : Analysis and Design*. Cambridge: Cambridge University Press, 2001.

[17] M. Hariri, B. Veeramamachaneni, and S. John, "Vibration Control of Polymeric Composite Plates Using Shape Memory Alloys," in *Smart Structures and Materials 2006: Smart Sensor Monitoring Systems and Applications*, San Diego, USA, p. 616710, 2006.

[18] C. A. Rogers, C. Liang, and D. K. Barker, "Dynamic Control Concept using Shape Memory Alloy Reinforced Plates," in *Smart Materials Structures and Mathematical Issues, US Army Research Office Workshop*, Norfolk, pp. 39-62, 1988.

[19] C. A. Rogers, C. Liang, and J. Jia, "Structural Modification of Simply-Supported Laminated Plates Using Embedded Shape Memory Alloy Fibers," *Computers & Structures,* vol. 38, pp. 569-580, 1991.

[20] A. Baz, K. Imam, and J. Mccoy, "Active Vibration Control of Flexible Beams Using Shape Memory Actuators," *Journal of Sound and Vibration,* vol. 140, pp. 437-456, AUG 8 1990.

[21] Z. Chaudhry and C. A. Rogers, "Bending and Shape Control of Beams Using SMA Actuators," *Journal of Intelligent Material Systems and Structures,* vol. 2, pp. 581-602, 1991.

[22] A. V. Srinivasan, D. G. Cutts, and L. M. Schetky, "Thermal and Mechanical considrations in Using Shape Memory Alloys to Control Vibrations in Flexible Structures," *Metallurgical Transactions A,* vol. 22A, pp. 623-627, 1991.

[23] R. G. Ballas, (2007), *Piezoelectric Multilayer Beam Bending Actuator: Static and Dynamic Behavior and Aspects of Sensor Integration*, [Online], Available: http://dx.doi.org/10.1007/978-3-540-32642-7

[24] Piezo Systems Inc., "History of Piezoelectricity", October 2008; http://www.piezo.com/tech4history.html

[25] Piezo Systems Inc., "Introduction to Piezo Transducers", October 2008; http://www.piezo.com/catalog7B.pdf%20files/Cat7B.20,21,22,23,23,60,61&62.pdf

[26] A. R. Faria and S. F. M. Almeida, "Enhancement of Pre-Buckling Behavior of Composite Beams with Geometric Imperfections Using Piezoelectric Actuators," *Composites: Part B,* vol. 30, pp. 43-50, 1999.

[27] D. A. Saravanos and A. P. Christoforou, "Low-Energy Impact of Adaptive Cylindrical Piezoelectric-Composite Shells," *International Journal of Solids and Structures,* vol. 39, pp. 2257-2279, APR 2002.

[28] M. V. Donadon, S. F. M. Almeida, and A. R. de Faria, "Stiffening Effects on the Natural Frequencies of Laminated Plates with Piezoelectric Actuators," *Composites Part B-Engineering,* vol. 33, pp. 335-342, 2002.

[29] H. Waisman and H. Abramovich, "Variation on Natural Frequencies of Beams Using the Active Stiffening Effect," *Composites Part B-Engineering,* vol. 33, pp. 415-424, 2002.

[30] R. Sedaghati, A. Zabihollah, and M. Ahari, "Sensitivity Analysis and Optimal Design of Smart Piezolaminated Composite Beams," *AIAA Journal,* vol. 44, pp. 2987-2996, 2006.

[31] Z. K. Kusculuoglu, B. Fallahi, and T. J. Royston, "Finite Element Model of a Beam with a Piezoceramic Patch Actuator," *Journal of Sound and Vibration,* vol. 276, pp. 27-44, 2004.

[32] A. Suleman, "Adaptive Composites Modelling and Application in Panel Flutter and Noise Suppression," *Computers and Structures,* vol. 76, pp. 365-378, 2000.

[33] S. Narayanan and V. Balamurugan, "Finite element modelling of piezolaminated smart structures for active vibration control with distributed sensors and actuators," *Journal of Sound and Vibration,* vol. 262, pp. 529-562, 2003.

[34] S. H. Moon and S. J. Kim, "Suppression of nonlinear composite panel flutter with active/passive hybrid piezoelectric networks using finite element method," *Composite Structures,* vol. 59, pp. 525-533, MAR 2003.

[35] S. Raja, A. A. Pashilkar, R. Sreedeep, and J. V. Kamesh, "Flutter Control of a Composite Plate with Piezoelectric Multilayered Actuators," *Aerospace Science and Technology,* vol. 10, pp. 435-441, 2006.

[36] A. A. Bent, N. W. Hagood, and J. P. Rodgers, "Anisotropic Actuation with Piezoelectric Fiber Composites," *Journal of Intelligent Material Systems and Structures,* vol. 6, pp. 338-349, 1995.

[37] L. J. Nelson, "Smart Piezoelectric Fibre Composites," *Materials Science and Technology,* vol. 18, pp. 1245-1256, 2002.

[38] M. C. Ray and N. Malik, "Finite Element Analysis of Smart Structures Containing Piezoelectric Fibre-Reinforced Composite Actuator," *AIAA Journal,* vol. 42, pp. 1398-1405, 2004.

[39] R. B. Williams, G. Park, D. J. Inman, and W. K. Wilkie, "An Overview of Composite Actuators with Piezoceramic Fibers," in *IMAC-XX: Conf. on Structural Dynamics*, Los Angeles, CA, 2002.

[40] W. K. Wilkie, R. G. Bryant, J. W. High, R. L. Fox, R. F. Hellbaum, A. Jalink, B. D. Little, and P. H. Mirick, "Low-Cost Piezocomposite Actuator for Structural Control Applications," in *SPIE's 7th Annual International Symposium on Smart Structures and Materials* Newport Beach, California, 2000.

[41] H. Y. Zhang and Y. P. Shen, "Vibration suppression of laminated plates with 1–3 piezoelectric fiber-reinforced composite layers equipped with interdigitated electrodes," *Composite Structures,* vol. 79, pp. 220-228, 2007.

[42] M. S. Azzouz, C. Mei, J. S. Bevan, and J. J. Ro, "Finite Element Modeling of MFC/AFC Actuators and Performance of MFC," *Journal of Intelligent Material Systems and Structures,* vol. 12, pp. 601-612, 2001.

[43] H. F. Tiersten, *Linear Piezoelectric Plate Vibrations: Elements of the Linear Theory of Piezoelectricity and the The Vibrations of Piezoelectric Plates*. New York: Plenum Press, 1969.

[44] "IEEE Standard on Piezoelectricity; ANSI/IEEE Std. 176-1987," The Institute of Electrical and Electronics Engineering Inc., New York 1988.

[45] E. H. Dowell, R. Clark, D. Cox, H. C. Curtiss, J. W. Edwards, K. C. Hall, D. A. Peters, R. Scanlan, E. Simiu, F. Sisto, and T. W. Strganac, *A Modern Course in Aeroelasticity*, 4 ed. Dordrecht: Springer Science & Business Media, 2005.

[46] L. A. Wood, *Aircraft vibration and flutter*. Melbourne: Sir Lawrence Wackett Centre for Aerospace Design Technology, Dept. of Aerospace Engineering, RMIT, 1998.

[47] Y. C. Fung, *An Introduction to the Theory of Aeroelasticity*, Dover Phoenix ed. New York: Dover Publications, 1995.

[48] T. Theodorsen, "General Theory of Aerodynamic Instability and the Mechanism of Flutter," National Advisory Committe for Aerounautics, NACA Report 496, 1949.

[49] H. Haddadpour and R. D. Firouz-Abadi, "Evaluation of Quasi-steady Aerodynamic Modeling for Flutter Prediction of Aircraft Wings in Incompressible Flow," *Thin-Walled Structures,* vol. 44, pp. 931-936, 2006.

[50] S. N. Singh and W. Yim, "State Feedback Control of an Aeroelastic System with Structural Nonlinearity," *Aerospace Science and Technology,* vol. 7, pp. 23-31, 2003.

[51] M. R. Moosavi, A. R. Naddaf Oskouei, and A. Khelil, "Flutter of Subsonic Wing," *Thin-Walled Structures,* vol. 43, pp. 617-627, 2005.

[52] S. Gujjula, S. N. Singh, and W. Yim, "Adaptive and Neural Control of a Wing Section using Leading- and Trailing-edge Surfaces," *Aerospace Science and Technology,* vol. 9, pp. 161-171, 2005.

[53] S. Na, L. Librescu, M. Kim, I. Jeong, and P. Marzocca, "Robust Aeroelastic Control of Flapped Wing Systems Using a sliding Mode Observer," *Aerospace Science and Technology,* vol. 10, pp. 120-126, 2006.

[54] V. M. Rao, A. Behal, P. Marzocca, and C. M. Rubillo, "Adaptive Aeroelastic Vubration Suppression of a Supersonic Airfoil with Flap," *Aerospace Science and Technology,* vol. 10, pp. 309-315, 2006.

[55] E. F. Sheta, R. W. Moses, and L. J. Huttsell, "Active Smart Material Control system for Buffet Alleviation," *Journal of Sound and Vibration,* vol. 292, pp. 854-868, 2006.

[56] A. P. Costa, P. A. Moniz, and A. Suleman, "Experimental Aeroelastic Control Using Adaptive Wing Model Concepts," in *Smart Structures and Materials 2001: Industrial and Commercial Applications of Smart Structures Technologies*, CA, USA, pp. 37-47, 2001.

[57] J. Heeg, "Analytical and Experimental Investigation of Flutter Suppression by Piezoelectric Actuation," Hampton, Virginia: NASA Technical Paper 3241, 1993.

[58] A. McGowan, "The Piezoelectric Aeroelastic Response Tailoring Investigation," in *The 4th Annual Workshop: Advances in Smart Materials for Aerospace Applications*, USA, pp. 191-195, 1996.

[59] S. H. Moon and J. S. Hwang, "Panel Flutter Suppression with an Optimal Controller Based on the Nonlinear Model Using Piezoelectric Materials," *Composite Structures,* vol. 68, pp. 371-379, 2005.

[60] C. E. S. Cesnik, M. Ortega-Morales, and M. J. Patil, American Institute of Aeronautics and Astronautics, "Active Aeroelastic Tailoring of High Aspect Ratio Composite Wing", September 2008; http://www.aoe.vt.ed/~mpatil/conference/SDM00AAT.pdf

[61] S. Varadarajan, K. Chandrashekhara, and S. Agrawal, "LQG/LTR-Based Robust Control of Composite Beams with Piezoelectric Devices," *Journal of Vibration and Control,* vol. 6, pp. 607-630, 2000.

[62] M. T. Valoor, K. Chandrashekhara, and S. agrawal, "Active Vibration Control of Smart Composite Plates Using Self-adaptive Neuro-controller," *Journal of Smart Materials and Structures,* vol. 9, pp. 197-204, 2000.

[63] Y. X. Shen and A. Homaifar, "Vibration Control of Flexible Structures with PZT Sensors and Actuators," *Journal of Vibration and Control,* vol. 7, pp. 417-451, MAR 2001.

[64] M. Tadi, "Compensator Design for a Supersonic Panel Flutter," *Composite and Structures,* vol. 80, pp. 989-999, 2002.

[65] N. Bhoir and S. N. Singh, "Output Feedback Nonlinear Control of an Aeroelastic System with Unsteady Aerodynamics," *Aerospace Science and Technology,* vol. 8, pp. 195-205, 2004.

[66] J. Han, J. Tani, and J. Qiu, "Active Flutter Suppression of a Lifting Surface Using Piezoelectric Actuation and Modern Control Theory," *Journal of Sound and Vibration,* vol. 291, pp. 706-722, 2006.

[67] K. K. Reddy, J. Chen, A. Behal, and P. Marzocca, "Multi-Input/Multi-Output Adaptive Output Feedback Control Design for Aeroelastic Vibration Suppression," *Journal of Guidance, Control, and Dynamics,* vol. 30, pp. 1040-1048, 2007.

[68] M. Kim, Q. Li, J.-K. Huang, and C. Mei, "Active Control of Nonlinear Panel Flutter Using Aeroelastic Modes and Piezoelectric Actuators," *AIAA Journal,* vol. 46, pp. 733-743, 2008.

[69] J. N. Reddy, *Mechanics of Laminated Composite Plates and Shells: Theory and Analysis*, 2nd ed. Boca Raton: CRC Press, 2003.

[70] J. N. Reddy, *Theory and Analysis of Elastic Plates*. Philadelphia, PA: Taylor & Francis, 1999.

[71] J. M. Whitney, *Structural Analysis of Laminated Anisotropic Plates*. Lancaster, PA: Technomic, 1987.

[72] S. John and M. Hariri, "Effect of Shape Memory Alloy Actuation on the Dynamic response of Polymeric composite Plates," *Composites Part A: Applied Science and Manufacturing,* vol. 39, pp. 769-776, 2008.

[73] X. Dong, G. Meng, and J. Peng, "Vibration Control of Piezoelectric Smart Structures Based on System Identification Technique: Numerical Simulation and Experimental Study," *Journal of Sound and Vibration,* vol. 297, pp. 680-693, 2006.

[74] S. H. Moon, "Finite Element Analysis and Design of Control System with Feedback Output Using Piezoelectric sensor-Actuator for Panel Flutter Suppression," *Finite Element in Analysis and Design,* vol. 42, pp. 1071-1078, 2006.

[75] J. N. Reddy, "On Laminated Composite Plates with Integrated Sensors and Actuators," *Engineering Structures,* vol. 21, pp. 568-593, 1999.

[76] J. N. Reddy, *An Introduction to the Finite Element Method*, 3rd ed. New York, NY: McGraw-Hill Higher Education, 2006.

[77] P. Trivailo, *Vibrations : Theory & Aerospace Applications*, 3rd ed. vol. I & II. Melbourne: RMIT, Dept. of Aerospace Engineering, 2005.

[78] S. S. Rao, *The finite element method in engineering*, 4th ed. Amsterdam: Elsevier Butterworth Heinemann, 2005.

[79] Y. W. Kwon and H. C. Bang, *The Finite Element Method Using MATLAB*, 2nd ed. Boca Raton, FL: CRC Press, 2000.

[80] F. Fairman, W., *Linear Control Theory: The State Space Approach*. Chichester: Wiley, 1998.

[81] C. De Marqui Jr, E. M. Belo, and F. D. Marques, "A Flutter Suppression Active Controller," *Proc. IMechE, Part G: J. Aerospace Engineering,* vol. 219, pp. 19-33, 2005.

[82] J. Ko and T. W. Strganac, "Adaptive Feedback Linearization for the Control of a Typical Wing Section with Structural Nonlinearity," *Nonlinear Dynamics,* vol. 18, pp. 289-301, 1999.

[83] C. R. Fuller, S. J. Elliott, and P. A. Nelson, *Active Control of Vibration*. London: Academic Press, 1997.

[84] B. Bandyopadhyay, T. C. Manjunath, and M. Umapathy, (2007), *Modeling, Control and Implementation of Smart Structures: A FEM-State Space Approach*, [Online], Available: http://dx.doi.org/10.1007/978-3-540-48394-6

[85] P. Donthireddy and K. Chandrashekhara, "Modeling and Shape Control of Composite Beams with Embedded Piezoelectric Actuators," *Composite Structures,* vol. 35, pp. 237-244, 1996.

[86] M. Goland, "The Flutter of a Uniform Cantilever Wing," *Journal of Applied Mechanics,* vol. 12, pp. A-197-A208, 1945.

APPENDICES

A1. Nodal Forces due to Linear Varying Loading (For Chapter 4)
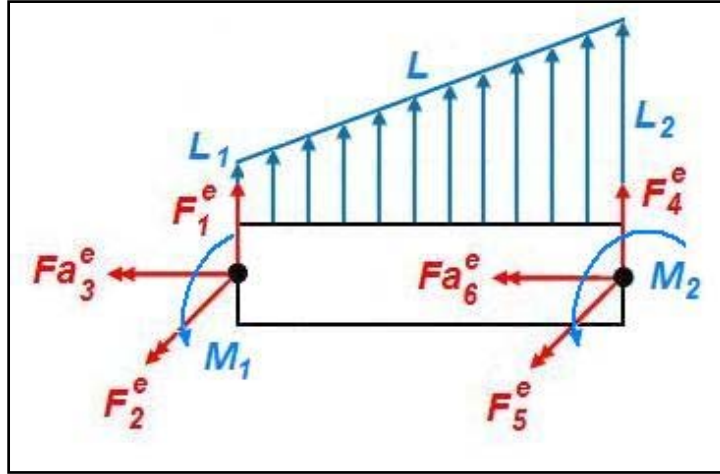
Figure A1.00.1: Nodal forces due to linear varying loading

By letting;

L_1 is the force acting at the element start (node 1) and,

L_2 is the force acting at the end of the element (node 2).

Therefore,

$$L(x) = L_1 + \frac{x}{l}(L_2 - L_1) \tag{A1.1}$$

For

$$F_i^e = \int_0^l L\, \psi_i dx$$

Using Eqn. (4.63) for i = 1, 2, 4 & 5;

$$F_1^e = \int_0^l \left[L_1 + \frac{x}{l}(L_2 - L_1)\right]\left[1 - \frac{3x^2}{l^2} + 2\frac{x^3}{l^3}\right] dx$$

Integration evaluation gives;

$$F_1^e = -\frac{l}{20}(7L_1 + 3L_2)\,,\ F_2^e = -\frac{l}{60}(3L_1 + 2L_2)$$

$$F_4^e = -\frac{l}{20}(3L_1 + 7L_2)\,,\ F_5^e = \frac{l}{20}(2L_1 + 3L_2) \tag{A1.2}$$

For the pitching moments;

M_1 is the moment acting at the element start (node 1) and,

M_2 is the moment acting at the end of the element (node 2).

Therefore,

$$M(x) = M_1 + \frac{x}{l}(M_2 - M_1) \tag{A1.3}$$

For

$$Fa_i^e = \int_0^l M \, \phi_i dx$$

Using Eqn. (4.64) for $i = 3$ & 6;

$$Fa_3^e = \int_0^l \left[M_1 + \frac{x}{l}(M_2 - M_1) \right] \left[1 - \frac{x}{l} \right] dx$$

$$Fa_6^e = \int_0^l \left[M_1 + \frac{x}{l}(M_2 - M_1) \right] \left[\frac{x}{l} \right] dx$$

Integration evaluation gives;

$$Fa_3^e = -\frac{l}{6}(2M_1 + M_2) \, ,$$

$$Fa_3^e = -\frac{l}{6}(M_1 + 2M_2) \tag{A1.4}$$

And hence, the global actuator matrix is;

$$\begin{bmatrix} F_1^e \\ F_2^e \\ Fa_3^e \\ F_4^e \\ F_5^e \\ Fa_6^e \end{bmatrix} = -\frac{l}{60} \begin{bmatrix} 3(7L_1 + 3L_2) \\ l(3L_1 + 2L_2) \\ 10(2M_1 + M_2) \\ 3(3L_1 + 7L_2) \\ -l(2L_1 + 3L_2) \\ 10(M_1 + 2M_2) \end{bmatrix} \tag{A1.5}$$

A2. Aeroelastic Model Computer Code Validation Using Galerkin's Method (For Chapter 5)

A2.1 Goland's Wing Flutter Speed

Goland's Wing Properties

$l := 20$ $\qquad$ $c := 6$ $\qquad$ $ycg := .1$

$m := .746$ $\qquad$ $\rho := .07651$ $\qquad$ $Ia := 1.943$

$EI := 23.6 \cdot 10^6$ $\qquad$ $GJ := 2.39 \cdot 10^6$

$a := \frac{1}{2} \cdot \rho \cdot c^3 \cdot \frac{\pi}{8}$

$ea := .33$ $\qquad$ $ea1 := ea - .25$ $\qquad$ $ea2 := .75 - ea$

$Sa := m \cdot ycg \cdot c$ $\qquad$ $Sa = 0.448$

$AR := \frac{(2l)^2}{2l \cdot c}$ $\qquad$ $AR = 6.667$

$ARR := \frac{AR}{AR + 2}$ $\qquad$ $ARR = 0.769$

$Cla := 2 \cdot \pi \cdot ARR$ $\qquad$ $Cla = 4.833$

$q := \frac{1}{2} \cdot \rho \cdot c \cdot Cla$ $\qquad$ $q = 1.109$

Shape Functions

$k := \frac{.4597 \cdot \pi}{l}$

$H(x) := .73 \cdot [\cosh(k \cdot x) - \cos(k \cdot x) - 0.734(\sinh(k \cdot x) - \sin(k \cdot x))]$

$A(x) := .15 \sin\left(\pi \cdot \frac{x}{2l}\right)$
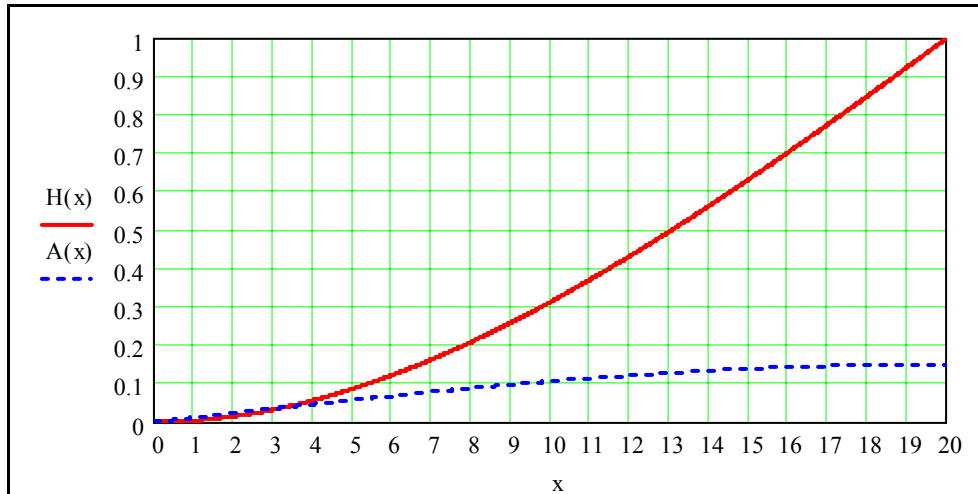
Figure 0: Shape functions presentation along the half-span.

$$a11 := EI \cdot \int_0^l \left(\frac{d^2}{dx^2} H(x) \right)^2 dx \qquad a22 := GJ \cdot \int_0^l \left(\frac{d}{dx} A(x) \right)^2 dx$$

$$b12 := \int_0^l -q \cdot H(x) \cdot A(x)\, dx \qquad b22 := \int_0^l -c \cdot q \cdot ea1 \cdot (A(x))^2 dx$$

$$c11 := \int_0^l m \cdot (H(x))^2 dx \qquad c12 := -\int_0^l Sa \cdot H(x) \cdot A(x)\, dx$$

$$c21 := c12 \qquad c22 := \int_0^l Ia \cdot (A(x))^2 dx$$

$$d11 := \int_0^l q \cdot (H(x))^2 dx \qquad d12 := \int_0^l -q \cdot c \cdot ea2 \cdot H(x) \cdot A(x)\, dx$$

$$d21 := \int_0^l q \cdot c \cdot ea1 \cdot H(x) \cdot A(x)\, dx \qquad d22 := \int_0^l -\left(q \cdot c^2 \cdot ea1 \cdot ea2 - a \right) \cdot (A(x))^2 dx$$

$$a11 = 8.869 \times 10^3 \qquad a22 = 3.317 \times 10^3$$

$$b12 = -1.087 \qquad b22 = -0.12$$

$$d11 = 5.228 \qquad d12 = -2.74 \qquad d21 = 0.522 \qquad d22 = 0.428$$

$$c11 = 3.516 \qquad c12 = -0.439 \qquad c21 = -0.439 \qquad c22 = 0.437$$

120

$A1 := -c21 \cdot c12 + c11 \cdot c22$ $A1 = 1.344$

$B1 := d11 \cdot c22 + c11 \cdot d22 - c12 \cdot d21 - c21 \cdot d12$ $B1 = 2.818$

$C1 := a11 \cdot c22 + a22 \cdot c11$ $C1 = 1.554 \times 10^4$

$C2 := c11 \cdot b22 + d11 \cdot d22 - c21 \cdot b12 - d12 \cdot d21$ $C2 = 2.771$

$D1 := a11 \cdot d22 + d11 \cdot a22$ $D1 = 2.114 \times 10^4$

$D2 := d11 \cdot b22 - d21 \cdot b12$ $D2 = -0.059$

$E1 := a11 \cdot a22$ $E1 = 2.942 \times 10^7$

$E2 := a11 \cdot b22$ $E2 = -1.063 \times 10^3$

$S := D2 \cdot (B1 \cdot C2 - A1 \cdot D2)$ $S = -0.463$

$R := B1 \cdot C1 \cdot D2 + B1 \cdot C2 \cdot D1 - 2 \cdot A1 \cdot D1 \cdot D2 - B1^2 \cdot E2$ $R = 1.742 \times 10^5$

$V := B1 \cdot C1 \cdot D1 - B1^2 \cdot E1 - A1 \cdot D1^2$ $V = 9.118 \times 10^7$

$U1 := \dfrac{\left(-R + \sqrt{R^2 - 4 \cdot S \cdot V}\right)}{2 \cdot S}$ $U2 := \dfrac{\left(-R - \sqrt{R^2 - 4 \cdot S \cdot V}\right)}{2 \cdot S}$

$U1 = -522.628$ $U2 = 3.767 \times 10^5$

$U111 := \sqrt{U1}$ $U222 := \sqrt{U2}$

$U111 = 22.861i$ $U222 = 613.72$

$M := \dfrac{U222}{1130}$ $M = 0.543$

$w1 := \sqrt{\dfrac{D1 + D2 \cdot U1}{B1}}$ $w2 := \sqrt{\dfrac{D1 + D2 \cdot U2}{B1}}$

$w1 = 86.682$ $w2 = 18.707i$

$Hz := \dfrac{w1}{2 \cdot \pi}$ $Hz = 13.796$

A2.2 Uniform Beam Aeroelastic Model Flutter Speed

Beam Properties

$l := .6$ $\qquad\qquad$ $c := .1$ $\qquad\qquad$ $t := .002$

$\rho mat := 2700$ $\qquad\qquad$ $Ia := 8.642$

$E := 69 \cdot 10^9$ $\qquad\qquad$ $G := 27 \cdot 10^9$

$ea := .4$

$I := c \cdot \dfrac{t^3}{12}$ $\qquad\qquad$ $J := c \cdot \dfrac{t^3}{3}$

$m := \rho mat \cdot c \cdot t$ $\qquad$ $m = 0.54$ $\qquad$ $\rho := 1.2$

$EI := E \cdot I$ $\qquad\qquad$ $EI = 4.6$

$Iy := \dfrac{1}{3} \cdot \rho mat \cdot \left(1 - 3 \cdot ea + 3 \cdot ea^2\right) \cdot c^3 \cdot t$ $\qquad\qquad$ $Iy = 5.04 \times 10^{-4}$

$GJ := G \cdot J$ $\qquad\qquad$ $GJ = 7.2$

$Iz := \dfrac{1}{12} \cdot \rho mat \cdot c \cdot t^3$ $\qquad$ $Iz = 1.8 \times 10^{-7}$

$ycg := .5 - ea$

$Ia := (Iy + Iz)$ $\qquad\qquad$ $Ia = 5.042 \times 10^{-4}$

$ea1 := ea - .25$ $\qquad\qquad$ $ea2 := .75 - ea$

$Sa := m \cdot ycg \cdot c$ $\qquad\qquad$ $Sa = 5.4 \times 10^{-3}$

$a := \dfrac{1}{2} \cdot \rho \cdot c^3 \cdot \dfrac{\pi}{8}$

$AR := \dfrac{(2l)^2}{2l \cdot c}$ $\qquad\qquad$ $AR = 12$

$ARR := \dfrac{AR}{AR + 3.}$ $\qquad\qquad$ $ARR = 0.8$

$Cla := 2 \cdot \pi \cdot ARR$ $\qquad\qquad$ $Cla = 5.027$

$q := \dfrac{1}{2} \cdot \rho \cdot c \cdot Cla$ $\qquad\qquad$ $q = 0.302$

Shape Functions

$$k := \frac{.97 \cdot \pi}{l}$$

$$H(x) := [\cosh(k \cdot x) - \cos(k \cdot x) - 0.734(\sinh(k \cdot x) - \sin(k \cdot x))]$$

$$A(x) := \sin\left(\pi \cdot \frac{x}{2l}\right)$$
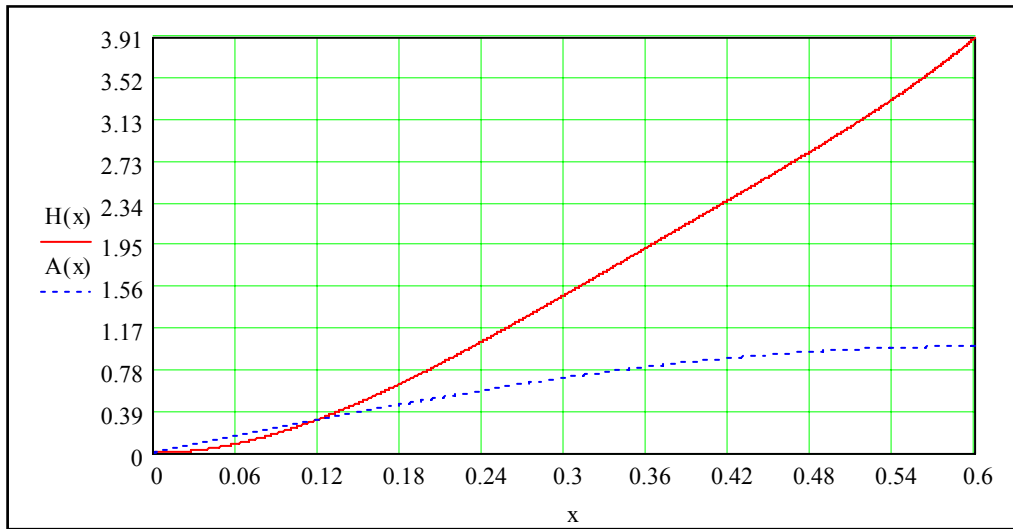
Figure 0.2: Shape functions for beam model.

$$a11 := EI \cdot \int_0^l \left(\frac{d^2}{dx^2} H(x)\right)^2 dx \qquad a22 := GJ \cdot \int_0^l \left(\frac{d}{dx} A(x)\right)^2 dx$$

$$b12 := \int_0^l -q \cdot H(x) \cdot A(x) \, dx \qquad b22 := \int_0^l -c \cdot q \cdot ea1 \cdot (A(x))^2 \, dx$$

$$c11 := \int_0^l m \cdot (H(x))^2 \, dx \qquad c12 := -\int_0^l Sa \cdot H(x) \cdot A(x) \, dx$$

$$c21 := c12 \qquad c22 := \int_0^l Ia \cdot (A(x))^2 \, dx$$

$$d11 := \int_0^l q \cdot (H(x))^2 \, dx \qquad d12 := \int_0^l -q \cdot c \cdot ea2 \cdot H(x) \cdot A(x) \, dx$$

$$d21 := \int_0^l q \cdot c \cdot ea1 \cdot H(x) \cdot A(x) \, dx \qquad d22 := \int_0^l -\left(q \cdot c^2 \cdot ea1 \cdot ea2 - a\right) \cdot (A(x))^2 \, dx$$

$a11 = 1.543 \times 10^3$ 　　　　　　　　　$a22 = 14.804$

$b12 = -0.247$ 　　　　　　　　　　　$b22 = -1.357 \times 10^{-3}$

$d11 = 0.716$ 　　　　　　　　　　　$d12 = -8.639 \times 10^{-3}$

$d21 = 3.702 \times 10^{-3}$ 　　　　　　　$d22 = 2.318 \times 10^{-5}$

$c11 = 1.282$ 　　　　　　　　　　　$c12 = -4.419 \times 10^{-3}$

$c21 = -4.419 \times 10^{-3}$ 　　　　　　$c22 = 1.513 \times 10^{-4}$

$A1 := -c21 \cdot c12 + c11 \cdot c22$ 　　　　$A1 = 1.743 \times 10^{-4}$

$B1 := d11 \cdot c22 + c11 \cdot d22 - c12 \cdot d21 - c21 \cdot d12$ 　　$B1 = 1.162 \times 10^{-4}$

$C1 := a11 \cdot c22 + a22 \cdot c11$ 　　　　$C1 = 19.209$

$C2 := c11 \cdot b22 + d11 \cdot d22 - c21 \cdot b12 - d12 \cdot d21$ 　　$C2 = -2.782 \times 10^{-3}$

$D1 := a11 \cdot d22 + d11 \cdot a22$ 　　　　$D1 = 10.634$

$D2 := d11 \cdot b22 - d21 \cdot b12$ 　　　　$D2 = -5.77 \times 10^{-5}$

$E1 := a11 \cdot a22$ 　　　　　　　　　$E1 = 2.284 \times 10^4$

$E2 := a11 \cdot b22$ 　　　　　　　　　$E2 = -2.094$

$S := D2 \cdot (B1 \cdot C2 - A1 \cdot D2)$ 　　　$S = 1.807 \times 10^{-11}$

$R := B1 \cdot C1 \cdot D2 + B1 \cdot C2 \cdot D1 - 2 \cdot A1 \cdot D1 \cdot D2 - B1^2 \cdot E2$ 　　$R = -3.323 \times 10^{-6}$

$V := B1 \cdot C1 \cdot D1 - B1^2 \cdot E1 - A1 \cdot D1^2$ 　　　　　$V = 3.709 \times 10^{-3}$

$U1 := \dfrac{\left(-R + \sqrt{R^2 - 4 \cdot S \cdot V}\right)}{2 \cdot S}$ 　　　　$U2 := \dfrac{\left(-R - \sqrt{R^2 - 4 \cdot S \cdot V}\right)}{2 \cdot S}$

$U1 = 1.828 \times 10^5$ 　　　　　　　$U2 = 1.123 \times 10^3$

$U11 := \sqrt{U1}$ 　　　　　　　　　$U222 := \sqrt{U2}$

$U11 = 427.569$ 　　　　　　　　　$U222 = 33.51$

　　　　　　　　　　　　　　　$M := \dfrac{U222}{343}$ 　　　　$M = 0.098$

$w1 := \sqrt{\dfrac{D1 + D2 \cdot U1}{B1}}$ 　　　　$w2 := \sqrt{\dfrac{D1 + D2 \cdot U2}{B1}}$

w1 = 27.12

$$Hz := \frac{w1}{2 \cdot \pi}$$

Hz = 4.316

w2 = 301.615

$$Hz2 := \frac{w2}{2 \cdot \pi}$$

Hz2 = 48.004

A3. MATLAB Program Flowchart and Listing (For Chapter 5)

A3.1 Program Flowchart
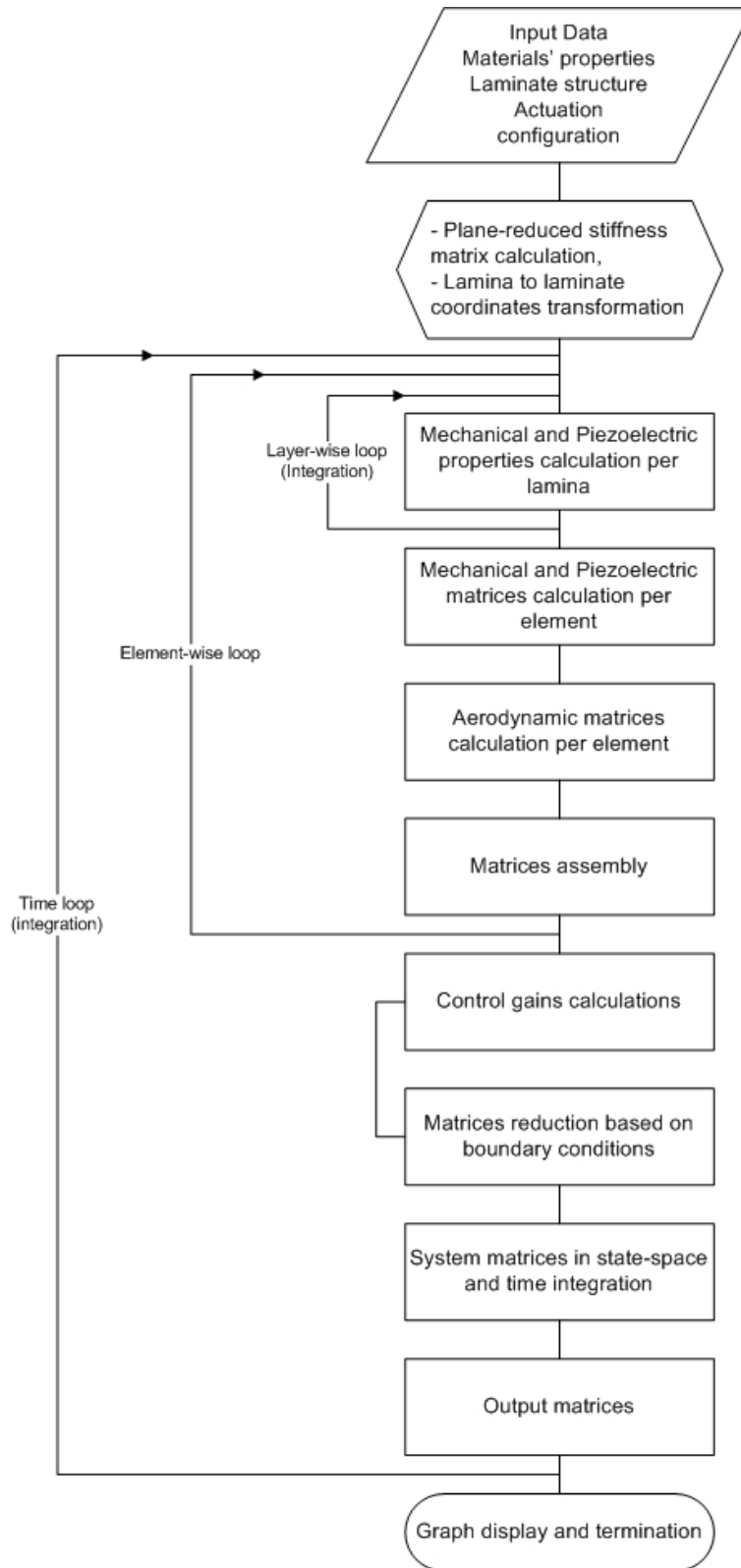
A3.2 Program Listing

The Main Program

```
% ==========================================================================
% Time responce of damped Fluttering Wing.
% ### Incorporates LQR full state feedback controller
% ### Variables renamed for final version:
% ###            Qs ==> ELs : External Load -s: system matrix, before
% ###                          applying boundary conditions.
% ###            Qa ==> ELa : External Load -a: actual; after applying
% ###                          boundary conditions.
% ###        Also Q  ==> EL, Qm ==> ELm
% ###
% ###    _8: THE CONTROL IS VARIABLE FOR EACH ACTUATOR (MULTI-CONTROL
% ###        INPUTS)
% ==========================================================================


clc
clear all
global ks m c Mxps bc mxSMD mxM vectQ Mxpa ELs ELa AFs AFa

% ==== Enter the system parameters ====
nel = 6;                          % Number of elements.
nnel = 2;                         % Number of nodes per element.
ndof = 3;                         % Number of degree of freedom at each node.
tnnod = (nnel-1)*nel+1;           % Total number of nodes.
sdof = ndof*tnnod;                % System degree of freedom
edof = nnel*ndof;
% ==============
% Beam Properties
width = .1;%1.8288;%.0254;
% Eb = 144.8*10^12;
Eb1= 69*10^9;%144.8*10^9;
Eb2= 69*10^9;%144.8*10^9;%9.65*10^9;
Gb12= 27*10^9;%7.1*10^9;
Nub12= 0.32;
MPb=[Eb1 Eb2 Gb12 Nub12]';
blength = .6;%0.254;
tb = 0.002;%.007233;%0.00127;
rhob = 2700;
Vb=0;
% ==================
% Piezo's Properties
% rhopti = 7600          % Subscript "pt" : Top Piezo,
% Epti = 63*10^9;            % Subscript "pb" : Bottom Piezo.
% tpt = 0.0002;
rhop = 7552;%7600;
%Ep = 63*10^9;
Ep1= 36.5*10^9;%63*10^9;
Ep2= 7.6*10^9;%63*10^9;
Gp12=14.6*10^9;%24.8*10^9;
Nup12=0.25;%0.28;
MPp= [Ep1 Ep2 Gp12 Nup12]';
```

```matlab
tp = 0.001;%0.0002;
pzndx=zeros(nel,2);
Vp=0;
Vpmax=0;%10^4;
d31= 530*10^-12; %-166*10^-12;
d32= -210*10^-12;%-166*10^-12;
dp = [d31 d32 0]';
% ================
% Node data
l= blength/nel;
%I = width*tb^3/12;
% ===================
% Laminate Data
% nk=3;                              % Number of the laminate layers.
LOs= [-60 0 -60 0 0 0;
      0 0 0 0 0 0;
      -60 0 -60 0 0 0];%[0 0 90 90 0 0]';         % Structure laminate
orientation
Lorb = [0 1 0];%[0 1 1 1 1 0]';            % Beam laminating order
Lorp = [1 0 1];%[1 0 0 0 0 1]';            % PZT laminating order
nla=length(Lorb);                          % Number of the laminate
layers.
Vorps= [1  1  1  0  0  1;...
        0  0  0  0  0  0;...
        -1  -1  -1  0  0  -1];%[1 0 0 0 0 -1]';      % Voltage polarity
order for PZT wafers
pzndx= [1 1 0 0 0 0;...
        1 1 0 0 0 0];
% ===============================
% Proportional Damping coefficients
a= 0.02137;                % 2 elem ==> .02171, 4 ele ==> .02143, 6 ele ==>
.02137
b= 0.02137;
% =======================
% Boundary Conditions
bc=ones(sdof,1); %[0 0 1 1 1 1];
bc(1)=0;
bc(2)=0;
bc(3)=0;
bc;
% ===========================================

%------------------------------------------------------------------------
% ==== Initialization
%---------------
ks = zeros(sdof,sdof);                     % initialization of system
stiffness matrix
m = zeros(sdof,sdof);                 % initialization of system mass
matrix
c = zeros(sdof,sdof);                 % initialization of system mass
matrix
E = zeros(nla,0);

invm=zeros(sdof,sdof);
kinvm=zeros(sdof,sdof);
cinvm=zeros(sdof,sdof);
ndx=zeros(nnel*ndof,1);                % initialization of index vector
% nsndx=zeros(sdof,1);
Mxps=zeros(sdof,1);
ELs=zeros(sdof,1);
AFe=zeros(sdof,1);
```

```matlab
AFs=zeros(sdof,1);
F=zeros(2*tnnod,1);
%x0=[0;0;0;0;0;0;0;0];
EL=0;
Q1=0;
Q2=0;
Q3=0;
Q4=0;
Q5=0;
Q6=0;
tt=0;                     % Total laminate thickness
LS=zeros(nla,1);          % Layer thickness structure/order
h=0;                      % Structure/Laminate thickness
zk=zeros(nla+1,1);
D11=0;
Fxp = 0;
Mxp=0;
Vpb=0;
Vpt=0;
Vb=0;
Vair=0;
Io=0;
I2=0;
L=0;
M=0;
alfae=0;
alfat=0;
hdot=0;
alfadot=0;


EFt=zeros(nel,1);


% ==========================================================
% ---- Matrices Indexing based on BC's ----

[nsndx,sndof]= bcndx(sdof,bc);
sdof;
sndof;

x0=zeros(2*sndof,1);
xs=zeros(2*sdof,1);
xe=zeros(edof,1);
a0=zeros(2*sndof,1);


% ------------------------------
%   Temporary

LOs= [-30 60 0 0 0 0;
       0 0 0 0 0 0;
      -30 60 0 0 0 0];%[0 0 90 90 0 0]';  % Structure laminate orientation
% ------------------------------

tmax= 1;
tstep = .001;


Vair=66.28;


Vpmax=10^4;
```

```matlab
% Vpmax=0;


zk;
all_x=[x0]; all_t=[0]; all_Q5=[0]; all_Q2=[0];
t1Q5=0.1; t2Q5=0.11; t1Q2=0.2; t2Q2=0.4; t3Q2=0.6;
all_Vpt=[0];all_Vpb=[0];all_F=[F];all_Vp=[0];all_u=[0];
CTRL=zeros(nel,1);
all_L0=[0];all_L1=[0];all_L2=[0];all_L3=[0];all_L4=[0];all_L5=[0];all_L6=[0
];
all_T0=[0];all_T1=[0];all_T2=[0];all_T3=[0];all_T4=[0];all_T5=[0];all_T6=[0
];
all_B0=[0];all_B1=[0];all_B2=[0];all_B3=[0];all_B4=[0];all_B5=[0];all_B6=[0
];
all_H0=[0];all_H1=[0];all_H2=[0];all_H3=[0];all_H4=[0];all_H5=[0];all_H6=[0
];
all_R0=[0];all_R1=[0];all_R2=[0];all_R3=[0];all_R4=[0];all_R5=[0];all_R6=[0
];
all_A0=[0];all_A1=[0];all_A2=[0];all_A3=[0];all_A4=[0];all_A5=[0];all_A6=[0
];
all_Va1=[0];all_Va2=[0];all_Va3=[0];all_Va4=[0];all_Va5=[0];all_Va6=[0];
all_M0=[0];all_M1=[0];all_M2=[0];all_M3=[0];all_M4=[0];all_M5=[0];all_M6=[0
];
% ====================================================================
% ==== Solving by time integration
for cur_time=0:tstep:tmax-tstep

    disp(sprintf('Time = %6.3f [s]', cur_time))
    disp(sprintf('Air Velocity = %6.3f [m/s]', Vair))
%     if cur_time > t2Q5
%         %Vpt= 1*cos(10*pi*cur_time);
%         Vpt=-0.05*x0(sndof-1);
%         Vpb=0.05*x0(sndof-1);
%     else
%          Vpt=0;
%          Vpb=0;
%     end
%     Vpt = 50;
%     Vpb = -50;
    x0;
%     for iel=1:nel
%         nel;
%         iel;
%         a0(iel*3)=2*pi/180;
%
%         %x0(iel*3)=x0(iel*3)+2*pi/180
%     end
%     x0 = x0 + a0;
    ks  = zeros(sdof,sdof);
    KCs = zeros(sdof,sdof);
    m   = zeros(sdof,sdof);
    MCs = zeros(sdof,sdof);
    c   = zeros(sdof,sdof);
    CCs = zeros(sdof,sdof);
    mxps=zeros(sdof,1);
    Mxps=zeros(sdof,1);
    AFs= zeros(sdof,1);
    Fas= zeros(sdof,1);
    Bs = zeros(sdof,nel);          % PZT control matrix


% =============================================================
% ==== Calculate the matrices in the state-space equation ====
```

```matlab
% ============================================================
%     pzndx(1,1)=0;
%     pzndx(1,2)=0;
%     pzndx(2,1)=0;
%     pzndx(2,2)=0;
%     for iel = 1:2
%         for iiel =1:nel
%             pzndx(iiel,iel)=0;
%         end
%     end
%     pzndx= [1 0 0 0 0 0;...
%             1 0 0 0 0 0];
    Condx=pzndx;
% ==================================================================
% ==== Calculations of the laminated structure in element level


% ----------------------------------------------------------
% ---- Calculating the laminated structure properties

%       [QS,epS]=WF_LamStr(MPb,MPp,LO,Lorb,Lorp,dp);        % Calculating
Q11,Q12,Q22 ... in structure coordinate system

    for iel=1:nel

        LO = LOs(:,iel);
        iel;
        [QS,epS]=WF_LamStr(MPb,MPp,LO,Lorb,Lorp,dp);        % Calculating
Q11,Q12,Q22 ... in structure coordinate system


        Vorp = Vorps(:,iel);
        iel;
        Lt=zeros(nla,1);
        h=0;
        rho=zeros(nla,1);
        EF=zeros(nla,1);
        % ------------------------------
        % ---- Piezoelectric Indexing ----

        Lorpndx=Lorp;
        Lorpndx(1)=pzndx(1,iel);
        Lorpndx(nla)=pzndx(2,iel);
        Lorpndx=Lorpndx + Lorb;

        Vorpndx = Vorp;
        Vorpndx(1)= Vorp(1)*Condx(1,iel);
        Vorpndx (nla)= Vorp(nla)*Condx(2,iel);
        Vorpndx;

        EFp=Vpmax/tp;                                       % PZT Electric
Field

        QSx=QS;
%         QSx(1)=pzndx(1,iel);
%         QSx(nla)=pzndx(2,iel);
%         QSx
        for ila = 1:nla
```

```matlab
            Lt(ila)=tb*Lorb(ila)+tp*Lorp(ila)*Lorpndx(ila);          %
Lamina/layer thickness
            h=h+Lt(ila);                                             %
Laminate thickness
            rho(ila)=rhob*Lorb(ila)+rhop*Lorp(ila)*Lorpndx(ila);     %
Lamina/layer density
            %EF(ila)=EFp*Vorpndx(ila);                               %
Lamina/layer Electric Field
        end
        rho;
        EF*tp;
        Lt;
        h;
        zk(1)=-h/2;
        for ila = 2:nla+1
            zk(ila)=zk(ila-1)+Lt(ila-1);
        end
        zk;
%         rhopt=rhop*pzndx(1,iel);
%         rhopb=rhop*pzndx(2,iel);
%
%         Ept=Ep*pzndx(1,iel);
%         Epb=Ep*pzndx(2,iel);


        % ------------------------------------------------
        % ---- Calculate laminated element properties ----
        D11=0; D12=0; D22=0; D16=0; D26=0; D66=0;
        npx=0; npy=0; npxy=0;
        Npx=0; Npy=0; Npxy=0;
        I00=0; I01=0; I02=0; I20=0; I21=0; I22=0;
        mpx=0; mpy=0; mpxy=0;
        Mpx=0; Mpy=0; Mpxy=0;


        ea = 0.4;


        for k=1:nla
%             tt= tt+t(k);
            zk(k);
            zk(k+1);
            zk(k)^3;
            zk(k+1)^3;
            k;
            EF*tp;
            epS(k,1);
            width;

            D11 = D11 + QS(k,1)/3*(zk(k+1)^3-zk(k)^3);%*Lorpndx(k)
            D12 = D12 + QS(k,2)/3*(zk(k+1)^3-zk(k)^3);%*Lorpndx(k);
            D22 = D22 + QS(k,3)/3*(zk(k+1)^3-zk(k)^3);%*Lorpndx(k);
            D16 = D16 + QS(k,4)/3*(zk(k+1)^3-zk(k)^3);%*Lorpndx(k);
            D26 = D26 + QS(k,5)/3*(zk(k+1)^3-zk(k)^3);%*Lorpndx(k);
            D66 = D66 + QS(k,6)/3*(zk(k+1)^3-zk(k)^3);%*Lorpndx(k);

            npx = npx + width*epS(k,1)*(zk(k+1)-zk(k))*Vorp(k);
            npy = npy + width*epS(k,2)*(zk(k+1)-zk(k))*Vorp(k);
            npxy = npxy + width*epS(k,3)*(zk(k+1)-zk(k))*Vorp(k);

            mpx = mpx + width/2*epS(k,1)*(zk(k+1)^2-zk(k)^2)*Vorp(k);
            mpy = mpy + width/2*epS(k,2)*(zk(k+1)^2-zk(k)^2)*Vorp(k);
            mpxy = mpxy + width/2*epS(k,3)*(zk(k+1)^2-zk(k)^2)*Vorp(k);
```

```matlab
                I00 = I00 + width*rho(k)*(zk(k+1)-zk(k));
                I01 = I01 + width^2*rho(k)*(0.5-ea)*(zk(k+1)-zk(k));
                I02 = I02 + rho(k)*width^3/3*(1-3*ea+3*ea^2)*(zk(k+1)-zk(k));
                I20 = I20 + width*rho(k)/3*(zk(k+1)^3-zk(k)^3);
                I21 = I21 + rho(k)*(0.5-ea)*width^2/3*(zk(k+1)^3-zk(k)^3);
                I22  =  I22  +  rho(k)*(1-3*ea+3*ea^2)*width^3/9*(zk(k+1)^3-
zk(k)^3);

            end

        DD=[D11 D12 D22 D16 D26 D66];
%          EFf = EFt(iel)
%          Npx = EFf*npx;
%          Npy = EFf*npy;
%          Npxy = EFf*npxy;
%          Np=[Npx Npy Npxy]

        mp=[mpx mpy mpxy];

        Y0=width;
        Y1 = width^2*(0.5-ea);
        Y2 = width^3*(1-3*ea+3*ea^2)/3;

%
[Km,Gm,Mm,mxpm,ELe]=WF_7_eleSMD(DD,Np,mp,I00,I01,I02,I20,I21,I22,EL,l,Y0,Y1
,Y2);

[Km,G1,G2,G3,Mm,mxpm,ELe]=WF_8_eleSMD(DD,mp,I00,I01,I02,I20,I21,I22,EL,l,Y0
,Y1,Y2);

%          Ge = G1*Npx+G2*Npxy+G3*Npy
        ge = G1*npx+G2*npxy+G3*npy;
        Ge = EFt(iel)*ge;
        iel;
        EFt;
% -------------------------------------
        % ---- Calculating Aerodynamic Forces ----
        Mac = 0;

        rhoair =1.2;
%          Vair = 56;%52.84;%34
        q = 0.5 * rhoair * Vair^2;
        Cla = 0.8*2*pi;
        alpha0=2*pi/180;
        ea1 = ea-0.25;
        ea2 = 0.75-ea;
        xs;
% ---- Create ELEMENT stiffness, mass & damping matrices  ----


[Kae,Cae,Fa0,Mae]=WF_6_eleAero_a(l,alpha0,rhoair,Cla,width,Vair,ea1,ea2);

        for ij=1:edof
            xe(ij)=xs(iel*3-3+ij);
        end
        xe;
        AFe = Fa0;
        ll=[1 1 1 1 1 1]';
```

```matlab
        Fae=(Kae+Cae)*xe+Fa0;
        %AL = Kae*
% ---------------------------------------------------------
% ---- System stiffness, mass, damping in element level

        ke=Km-Ge+Kae;
        me=Mm+Mae;


% Proportional Damping
        [Cm]=a*Km+b*Mm;
        Cm;
        Cae;
        ce = Cm+Cae;
% --------------------------------------------------
% ---- Calculate Control System Matrices

        KCe = Km;%ke;
        MCe = Mm;%me;
        CCe = Cm;%ce;
        Be  = mxpm'+ge*xe;


% ---------------------------------------------------------
% ---- Assemblying stiffness, mass and damping matrices ----

        ndx = fedofndx(iel,nnel,ndof);
        ks  = SB_mxasmbl(ks,ke,ndx);
        KCs = SB_mxasmbl(KCs,KCe,ndx);
        m   = SB_mxasmbl(m,me,ndx);
        MCs = SB_mxasmbl(MCs,MCe,ndx);
        c   = SB_mxasmbl(c,ce,ndx);
        CCs = SB_mxasmbl(CCs,CCe,ndx);
%        Gs  = SB_mxasmbl(Gs,Ge,ndx);
        Bs= B_Ctrlmxasmbl(Bs,Be,ndx,iel);



[mxps,ELs,AFs,Fas]=WF_7_mxasmbl1D(mxps,ELs,AFs,Fas,mxpm,ELe,AFe,Fae,ndx);
        c;
        mxps;
    end


% ---------------------------------------------------------
% ---- Reduce control matrices based on boundary conditions

    [KCa,CCa,MCa,mxpa,Faa,Ba]                                          =
WF_8_mxred(KCs,CCs,MCs,mxps,Fas,Bs,nsndx,sndof,nel);
    mxpa;
    Ba;
% ------------------------------------
% ---- Calculate Control gain using LQR

    invMC=inv(MCa);

    A    = [zeros(sndof,sndof), eye(sndof,sndof);-invMC*KCa -invMC*CCa];
    mxMC = [zeros(sndof,sndof);invMC];
    B    = 5000*mxMC*Ba;%mxpa;
    Q    = eye(2*sndof,2*sndof);
    R    = eye(1,1);
    [G,S]=felqr(A,B,Q,R);
    G;
```

```matlab
    u    = G*x0;
    EE=Vpmax/tp;
    EFt = EE*u;
% ------------------------------------------------------------
    mxps;
%    Mxpe = EFt*mxpm;
    Mpx = EFt*mpx;
    Mpy = EFt*mpy;
    Mpxy = EFt*mpxy;
     Mxps = Bs*EFt;
%        Np=[Npx Npy Npxy];
%        Mp=[Mpx Mpy Mpxy];
% ============================================================
% ====      Applying boundary conditions ====
% ============================================================
% = To reduce the matrices dimensions based on boundary
% = conditions.
% ============================================================

% ---- Matrices Indexing based on BC's ----

%[nsndx,sndof]= bcndx(sdof,bc);
% ------------------------------------------------------------

% ---- Matrices reduction ----
ka=zeros(sndof,sndof);
ca=zeros(sndof,sndof);
ma=zeros(sndof,sndof);
Mxpa=zeros(sndof,1);
sndof;
ELa=zeros(sndof,1);
[ka,ca,ma,Mxpa,ELa,AFa] = WF_mxred(ks,c,m,Mxps,ELs,AFs,nsndx,sndof);
ka;
ca;
ma;
ELa;
AFa;
%[V,D]=eig(ka,ma);
invm=inv(ma);
ka;
invm*ka;
[s] = sprintf('%6.4f' , ka);
mxSMD = [zeros(sndof,sndof), eye(sndof,sndof);-invm*ka -invm*ca];
mxM = [zeros(sndof,sndof);invm];
Mxpa;
AFa;
sndof;
%mxSMD = [zeros(sdof,sdof), eye(sdof,sdof);-invm*k -invm*c];
%mxM = [zeros(sdof,sdof);invm];

% ==== Describe the excitation forces ====
   % disp(sprintf('Time = %6.6f [s]', cur_time))
 ELa ;
 Mxpa;
    if cur_time > t1Q5 & cur_time <= t2Q5
        ELa(sndof-2)=0*sin(pi*(cur_time-t1Q5)/(t2Q5-t1Q5))^2; % change to
La(sndof-2)
    else
        ELa(sndof-2)=0;
    end;
```

```matlab
    ELa(sndof-2);

   %if cur_time <= t1Q2
    %    Q2 = 0;
    %elseif cur_time > t1Q2 & cur_time < t2Q2
    %    Q2 = -50000*(cur_time-t1Q2);
    %elseif cur_time > t2Q2 & cur_time < t3Q2
    %    Q2 = -50000*(t2Q2-t1Q2)+50000*(cur_time-t2Q2);
    %elseif cur_time > t3Q2
    %    Q2 = 0;
    %end
   %vectQ=[Q3;Q4;Q5;Q6];

   cur_time;
   %ELa'
   tstep;
  x0;
   % ==== Integrate equations of motion in the loop ====
  [t,x] = ode23(@WF_7_stsp_xdot,[cur_time cur_time+tstep],x0);
  [ii,jj]=size(x);
  x0=x(ii,:)';
  %x0(sndof)*180/pi;

   for iel=1:nel
       nel;
       iel;
       a0(iel*3)=0*pi/180;

       %x0(iel*3)=x0(iel*3)+2*pi/180
    end
  x0 = x0 + a0;

  %    xe(3)=0;
  for jj = 4:sdof
      jj;
      xs(jj) = x0(jj-3);
  end
  for jj = sdof+4:2*sdof
      jj;
      xs(jj) = x0(jj-6);
  end
  x0;
  xe;

%
===========================================================================
===============

   all_x=[all_x,x0];
   all_t=[all_t,cur_time+tstep];
   all_Q5=[all_Q5,ELa(sndof-2)];
   all_Vpt=[all_Vpt,EF(1)*tp];
   all_Vpb=[all_Vpb,Mxpa(2)];
%    all_Vp=[all_Vp,EFt*tp];
   all_F=[all_F,F];
%    all_u=[all_u,u];
   %all_Q2=[all_Q2,Q2];
% -------------------------------------------------------------------------
   all_H0=[all_H0,xs(1)];    all_H1=[all_H1,xs(4)];              %  Vertical
Displacement
```

```matlab
    all_H2=[all_H2,xs(7)];  all_H3=[all_H3,xs(10)];
    all_H4=[all_H4,xs(13)];
    all_H5=[all_H5,xs(16)]; all_H6=[all_H6,xs(19)];

    all_R0=[all_R0,xs(2)];     all_R1=[all_R1,xs(5)];          %  Rotational
Displacement
    all_R2=[all_R2,xs(8)];  all_R3=[all_R3,xs(11)];
    all_R4=[all_R4,xs(14)];
    all_R5=[all_R5,xs(17)]; all_R6=[all_R6,xs(20)];

    all_A0=[all_A0,xs(3)];     all_A1=[all_A1,xs(6)];          %  Torsional
Dispalcement
    all_A2=[all_A2,xs(9)];  all_A3=[all_A3,xs(12)];
    all_A4=[all_A4,xs(15)];
    all_A5=[all_A5,xs(18)]; all_A6=[all_A6,xs(21)];

% -------------------------------------------------------------------------

    all_L0=[all_L0,Fas(1)];    all_L1=[all_L1,Fas(4)];         %  Aerodynamic
vertical forces (Lift)
    all_L2=[all_L2,Fas(7)];  all_L3=[all_L3,Fas(10)];
    all_L4=[all_L4,Fas(13)];
    all_L5=[all_L5,Fas(16)]; all_L6=[all_L6,Fas(19)];

    all_B0=[all_B0,Fas(2)];    all_B1=[all_B1,Fas(5)];         %  Aerodynamic
bending forces
    all_B2=[all_B2,Fas(8)];  all_B3=[all_B3,Fas(11)];
    all_B4=[all_B4,Fas(14)];
    all_B5=[all_B5,Fas(17)]; all_B6=[all_B6,Fas(20)];

    all_T0=[all_T0,Fas(3)];    all_T1=[all_T1,Fas(6)];         %  Aerodynamic
torsional forces (Pitch)
    all_T2=[all_T2,Fas(9)];  all_T3=[all_T3,Fas(12)];
    all_T4=[all_T4,Fas(15)];
    all_T5=[all_T5,Fas(18)]; all_T6=[all_T6,Fas(21)];

% -------------------------------------------------------------------------


% -------------------------------------------------------------------------

    all_Va1=[all_Va1,EFt(1)*tp];     all_Va2=[all_Va2,EFt(2)*tp];          %
Actuator Voltage.
    all_Va3=[all_Va3,EFt(3)*tp];  all_Va4=[all_Va4,EFt(4)*tp];
    all_Va5=[all_Va5,EFt(5)*tp];  all_Va6=[all_Va6,EFt(6)*tp];

end

All_H=[all_H0; all_H1; all_H2; all_H3; all_H4; all_H5; all_H6];
All_R=[all_R0; all_R1; all_R2; all_R3; all_R4; all_R5; all_R6];
All_A=[all_A0; all_A1; all_A2; all_A3; all_A4; all_A5; all_A6];

All_L=-[all_L0; all_L1; all_L2; all_L3; all_L4; all_L5; all_L6];
All_T= [all_T0; all_T1; all_T2; all_T3; all_T4; all_T5; all_T6];
All_B= [all_B0; all_B1; all_B2; all_B3; all_B4; all_B5; all_B6];

All_Va= [all_Va1; all_Va2; all_Va3; all_Va4; all_Va5; all_Va6];
```

```matlab
% ==== Plot the system excitation force Q5 ====
% figure
% %subplot(211)
% contour(all_F)
% %plot(all_t,all_F(tnnod,:),'r-')
% grid on
% ylabel('L, [N]')
% title('Lift Forces')

% ==== Plot the system excitation force Q2 ====
%subplot(212)
%plot(all_t,all_Q2,'r--')
%grid on
%ylabel('Q2, [N]')
%xlabel('Time, [s]')
sndof-1;
% ==== Plot beam tip translation displacement ====
sndof-2;
figure
subplot (211)
% plot(all_t,all_x(1,:),'b-');
plot(all_t,all_x(sndof-2,:),'b-')
%hold on
%plot(all_t,all_x(7,:),'r--')
grid on
xlabel('Time, [s]')
ylabel('h[m]')
title('Tip Traslation Displacement')
%legend('q4: Displacemnt');
2*sndof-1;
% ==== Plot beam tip velocity ====
2*sndof-2;
%figure
% subplot(222)
% plot(all_t,all_x(2*sndof-2,:),'r-')
% %hold on
% %plot(all_t,all_x(4,:),'r--')
% %grid on
% xlabel('Time, [s]')
% ylabel('Vtip [m/s]')
% title('Tip Velocity')
% %legend('q5dot','q2dot');
% ==== Plot beam tip Twist angle ====
sndof;
%figure
subplot(212)
plot(all_t,all_x(sndof,:),'b-')
%hold on
%plot(all_t,all_x(7,:),'r--')
grid on
xlabel('Time, [s]')
ylabel('Alfa [Rad]')
title('Tip Twist Angle')
%legend('q4: Displacemnt');
% ===============================
% figure
% subplot(211)
% plot(all_t,all_Vp,'r-')
% %hold on
% %plot(all_t,all_x(4,:),'r--')
% grid on
```

```matlab
% xlabel('Time, [s]')
% ylabel('Vpt[Volts]')
% title('Voltage')
% %legend('q5dot','q2dot');
% subplot(212)
% plot(all_t,all_u,'r--')
% %hold on
% %plot(all_t,all_x(4,:),'r--')
% grid on
% xlabel('Time, [s]')
% ylabel('Vpb [Volts]')
% title('Voltage')
% %legend('q5dot','q2dot');
% =============================================
% ==== FFT
%figure
Ztip=all_x(sndof-2,:);
Ttip=all_x(sndof,:);
Dtip=Ztip+Ttip;
% Y = fft(Ztip,512);
% Pyy = Y.* conj(Y) / 512;
% H = fft(Ttip,512);
% hyy = H.*conj(H)/512;
% % ==== Graph the first 257 points (the other 255 points are redundant) on
a meaningful frequency axis:
% f = 1000*(0:256)/512;
% subplot(222)
% plot(f,Pyy(1:257))
% title('Frequency content of y')
% xlabel('frequency (Hz)')
% % =============
% f = 1000*(0:256)/512;
% subplot(224)
% plot(f,hyy(1:257))
% title('Frequency content of y')
% xlabel('frequency (Hz)')

L=length(Ztip);
Fs=1/tstep;
NFFT = 2^nextpow2(L); % Next power of 2 from length of y
Y = fft(Ztip,NFFT)/L;
f = Fs/2*linspace(0,1,NFFT/2);

% Plot single-sided amplitude spectrum.
% subplot(222)
% plot(f,2*abs(Y(1:NFFT/2)))
% title('Single-Sided Amplitude Spectrum of y(t)')
% xlabel('Frequency (Hz)')
% ylabel('|Y(f)|')

L=length(Ttip);
Fs=1/tstep;
NFFT = 2^nextpow2(L); % Next power of 2 from length of y
Y = fft(Ttip,NFFT)/L;
f = Fs/2*linspace(0,1,NFFT/2);

% Plot single-sided amplitude spectrum.
% subplot(224)
% plot(f,2*abs(Y(1:NFFT/2)))
% title('Single-Sided Amplitude Spectrum of y(t)')
```

```matlab
% xlabel('Frequency (Hz)')
% ylabel('|Y(f)|')
```

Boundary Conditions Indexing

```matlab
function [nsndx,sndof]= bcndx(sdof,bc)
sdof=sdof;
sndof=0;


% --------------------------------------------------------------
% ---- Matrices indexing based on BC's ----
%  Purpose:
%      To Calculate the new system degree of freedom baced on
%      the boundary conditions.
%
%  Variable Description:
%      bc(i) - Boundary conditions matrix (1=free, 0=fixed)
%      sdof  - System degree of freedom
%      sndof - System new degree of freedom after applying B.C's.
%      nsndx - New system index
%
%--------------------------------------------------------------
for i=1:sdof
    sndof=sndof+bc(i);
end

ii=1;
for j= 1:sdof

    if bc(j)==1
        nsndx(ii)=j;
        ii=ii+1;
    end
end
```

Plane Stress-reduced Stiffness

```matlab
function [QS,epS]=LamStr(MPb,MPp,LO,Lorb,Lorp,dp)

%--------------------------------------------------------------
%  Purpose:
%      To Calculate the Plane stress-reduced stiffness (Q11,Q12,Q22 & Q66)
%      from the material properties.
%      And to transform the lamina properties into structure properties (ES)
%  Variable Description:
%      ES    - Array of the laminated structure
%      MPb   - Material properties for the beam
%      MPp   - Material properties for the PZT
%      Lorb  - Beam laminating order
%      Lorp  - PZT laminating order
%      LPb   - Plane stress-reduced stiffness of the beam
%              [Q11 Q12 Q22 Q66]'b
%      LPp   - Plane stress-reduced stiffness of the PZT
```

```matlab
%            [Q11 Q12 Q22 Q66]'p
%      SPb  - Beam stiffness in laminated coordinates
%            [Q11S Q12S Q22S Q66S]
%      SPp  - PZT stiffness in laminated coordinates
%
%--------------------------------------------------------------
kk= length(LO);
dp;
% ==== Calculating the Plane stress-reduced stiffness
%
% ----- Laminated beam
MPb;
Nu12= MPb(4);
Nu21 = Nu12*MPb(2)/MPb(1);
Nub= 1/(1-Nu12*Nu21);

Tranb= [ Nub      0     0  0;...
          0   Nu12*Nub  0  0;...
          0      Nub    0  0;...
          0       0     1  0];
LPb = Tranb*MPb;

% ----- Laminated PZT
MPb;
Nu12= MPp(4);
Nu21 = Nu12*MPp(2)/MPp(1);
Nup= 1/(1-Nu12*Nu21);

Tranp= [ Nup      0     0  0;...
          0   Nu12*Nup  0  0;...
          0      Nup    0  0;...
          0       0     1  0];
LPp = Tranp*MPp;

% =======================================================
% ==== Transforming stiffnesses from laminate coordinate system into
%      structure coordinate system
LO;
kk=length(LO);
theta= LO*pi/180;

    for ii=1:kk
        ta=theta(ii);
        Tran= [       (cos(ta))^4                2*(sin(ta))^2*(cos(ta))^2
(sin(ta))^4                4*(sin(ta))^2*(cos(ta))^2;...
             (sin(ta))^2*(cos(ta))^2              (sin(ta))^4+(cos(ta))^4
(sin(ta))^2*(cos(ta))^2       -4*(sin(ta))^2*(cos(ta))^2;...
                (sin(ta))^4                2*(sin(ta))^2*(cos(ta))^2
(cos(ta))^4                4*(sin(ta))^2*(cos(ta))^2;...
             sin(ta)*(cos(ta))^3                                      -
sin(ta)*(cos(ta))^3+(sin(ta))^3*cos(ta)       -(sin(ta))^3*cos(ta)      -
2*sin(ta)*(cos(ta))^3+2*(sin(ta))^3*cos(ta);...
             (sin(ta))^3*cos(ta)                                      -
(sin(ta))^3*cos(ta)+sin(ta)*(cos(ta))^3       -sin(ta)*(cos(ta))^3      -
2*(sin(ta))^3*cos(ta)+2*sin(ta)*(cos(ta))^3;...
             (sin(ta))^2*(cos(ta))^2             -2*(sin(ta))^2*(cos(ta))^2
(sin(ta))^2*(cos(ta))^2 (sin(ta))^4+(cos(ta))^4-2*(sin(ta))^2*(cos(ta))^2];
        ii;
        Tran;
        SPb= Tran*LPb;
```

```
        SPp= Tran*LPp;

        for jj=1:6
            QS(ii,jj)=SPb(jj)*Lorb(ii)+SPp(jj)*Lorp(ii);
        end;
QS;
% ---------------------------------------------------------
% ---- The Stiffness Matrix in Structure/laminate coordinates

        QQ(1,1)=SPb(1)*Lorb(ii)+SPp(1)*Lorp(ii);
        QQ(1,2)=SPb(2)*Lorb(ii)+SPp(2)*Lorp(ii);
        QQ(1,3)=SPb(4)*Lorb(ii)+SPp(4)*Lorp(ii);
        QQ(2,1)=QQ(1,2);
        QQ(2,2)=SPb(3)*Lorb(ii)+SPp(3)*Lorp(ii);
        QQ(2,3)=SPb(5)*Lorb(ii)+SPp(5)*Lorp(ii);
        QQ(3,1)=QQ(1,3);
        QQ(3,2)=QQ(2,3);
        QQ(3,3)=SPb(6)*Lorb(ii)+SPp(6)*Lorp(ii);

        QQ;


% --------------------------------------------------------------------
% ---- Transforming PZT strain coefficient d (m/volt) from laminate
% ---- coordinate system into structure coordinate system

        Trand = [  (cos(ta))^2        (sin(ta))^2      0;...
                   (sin(ta))^2        (cos(ta))^2      0;...
                  cos(ta)*sin(ta)  -cos(ta)*sin(ta)  0];

        dpS= Trand*dp;

% ----------------------
% ---- PZT e=Q*d

        eS = QQ*dpS;


        for jj=1:3
            epS(ii,jj)=eS(jj)*Lorp(ii);    % matrix of "e" for all layers
        end
    end
    epS;
```

Elemental stiffness and Mass Matrices

```
function
[Km,G1,G2,G3,Mm,mxpm,ELe]=eleSMD(DD,mp,I00,I01,I02,I20,I21,I2
2,EL,l,Y0,Y1,Y
2)

%-----------------------------------------------------------
%  Purpose:
%      To Calculate the stiffness and mass matrices for beam element with
displacement
%      degrees of freedom only
%
```

```matlab
%  Variable Description:
%     ke    - element stiffness matrix
%     me    - element mass matrix
%     E     - elastic modulus
%     sh    - shear modulus
%     l     - element length
%     thick - element thickness
%     width - width of the beam element
%     rho   - mass density of the beam element (mass per unit volume)
%             lumped mass matrix only
%------------------------------------------------------------
% ==== Element Stiffness Matrix
D11=DD(1);
D12=DD(2);
D22=DD(3);
D16=DD(4);
D26=DD(5);
D66=DD(6);


mpx=mp(1);
mpy=mp(2);
mpxy=mp(3);


 Khh=(D11*Y0)/l^3;
 JA=(4*Y0*D66)/l;
 KA=(2*Y0*D12)/l;
 Kaa=JA+KA;
 kha=(4*Y0*D16)/l;
 kah=(2*Y0*D16)/l;
    Kmt= [ 12*Khh    6*l*Khh    0*kha     -12*Khh     6*l*Khh     0*kha;...
           6*l*Khh   4*l^2*Khh   kha      -6*l*Khh    2*l^2*Khh    -kha;...
            0*kah      kah       Kaa       0*kah      -kah         -Kaa;...
           -12*Khh   -6*l*Khh   0*kha      12*Khh     -6*l*Khh    0*kha;...
           6*l*Khh   2*l^2*Khh   -kha     -6*l*Khh    4*l^2*Khh     kha;...
            0*kah     -kah       -Kaa      0*kah       kah          Kaa];



 % ----------------------------------------
 % ==== Geometric Stiffness Matrix
 % Fxp = width * Fp , where Fp is Piezoelectric plane forse
g1 = 1/(30*l);
g2 = Y0/12;
g3 = Y0*l/6;

G1= g1*[ 36*Y0      3*l*Y0       30*Y1      -36*Y0       3*l*Y0      -30*Y1;...
          3*l*Y0    4*l^2*Y0       0        -3*l*Y0     -l^2*Y0         0;...
          30*Y1       0          30*Y2      -30*Y1        0         -30*Y2;...
         -36*Y0     -3*l*Y0      -30*Y1      36*Y0      -3*l*Y0       30*Y1;...
          3*l*Y0    -l^2*Y0        0        -3*l*Y0     4*l^2*Y0        0;...
         -30*Y1       0          -30*Y2      30*Y1        0           30*Y2];


 G2= g2*[  0      0     -6      0     0     -6;...
           0      0      l      0     0     -l;...
          -6     -l      0     -6     l      0;...
           0      0      6      0     0      6;...
           0      0     -l      0     0      l;...
           6      l      0      6    -l      0];


 G3= g3*[  0      0      0      0     0      0;...
           0      0      0      0     0      0;...
```

```matlab
            0        0        2        0        0        1;...
            0        0        0        0        0        0;...
            0        0        0        0        0        0;...
            0        0        1        0        0        2];

% ---------------------------------------------
% ==== Total Stiffness Matrix =====
  Km=Kmt;%-Gm;


% ===============================================
% ==== Mass Matrix

   mIo=zeros(6,6);
   mI2=zeros(6,6);
   AM = I00*l/420;
   BM = I20/(30*l);
   IA = (I02+I20)*l/6;
   Mah = I01*l/60;
   Mha = Mah;
   CM = I21/l;
   DM = I22/l;
   mIo = [156*AM    22*l*AM    21*Mha    54*AM     -13*l*AM   9*Mha;...
          22*l*AM   4*l^2*AM   3*l*Mha   13*l*AM   -3*l^2*AM  2*l*Mha;...
          21*Mah    3*l*Mah    2*IA      9*Mah     -2*l*Mah   IA;...
          54*AM     13*l*AM    9*Mha     156*AM    -22*l*AM   21*Mha;...
          -13*l*AM  -3*l^2*AM  -2*l*Mha  -22*l*AM  4*l^2*AM   -3*l*Mha;...
          9*Mah     2*l*Mah    IA        21*Mah    -3*l*Mah   2*IA];


    mI2= [36*BM     3*l*BM     CM    -36*BM     3*l*BM    -CM;...
          3*l*BM    4*l^2*BM   0     -3*l*BM    -l^2*BM     0;...
           CM         0        DM     -CM         0       -DM;...
          -36*BM    -3*l*BM    -CM    36*BM     -3*l*BM    CM;...
          3*l*BM    -l^2*BM    0     -3*l*BM    4*l^2*BM    0;...
           -CM        0        -DM     CM         0        DM];

      Mm=mIo+mI2;


% ===============================================
% ==== Piezoelectric Force Matrix

 mxpm = [0  -mpx  -2*mpxy   0   mpx   2*mpxy];
 %Mxpe=Mxpetemp*Mxp;


 % ===============================================
 % ==== Element Nodal Forces


 ELetemp=[1 1 1 1 1 1];   % Check this with the
 ELe=ELetemp*EL;
```

The Aerodynamic Stiffness and Mass Matrices

```matlab
function [Kae,Cae,Fa0,Mae]=eleAero(l,alpha0,rhoair,Cla,width,Vair,ea1,ea2)

%-------------------------------------------------------------
%  Purpose:
%      To Calculate the Aerodynamic stiffness and mass matrices for beam
```

```matlab
%      element with displacement degrees of freedom only
%
%  Variable Description:
%     Kae    - element Aerodynamic stiffness matrix
%     Cae    - element Aerodynamic damping matrix
%     Mae    - element Aerodynamic mass matrix
%      l     - element length
%     thick  - element thickness
%
%-------------------------------------------------------------
% ==== Element Aerodynamic Stiffness Matrix
q = 0.5 * rhoair * Vair^2;

Ae = -q*width*Cla*l/60;

    Kae= Ae*[ 0    0        21        0    0               9;...
              0    0        3*l       0    0             2*l;...
              0    0    20*width*ea1  0    0    10*width*ea1;...
              0    0         9        0    0              21;...
              0    0       -2*l       0    0            -3*l;...
              0    0    10*width*ea1  0    0    20*width*ea1];

 Kae;


 % ----------------------------------------
 % ==== Element Aerodynamic Damping Matrix


  a = width*pi/8;
  CA = -l*q*width*Cla/(60*Vair);
  aa = (width*ea1*ea2-a/Cla);

    Cae= CA*[      21          0      21*width*ea2          9          0
9*width*ea2;...
                  3*l          0      3*l*width*ea2        2*l         0
2*l*width*ea2;...
             20*width*ea1  0        20*width*aa       10*width*ea1   0
10*width*aa;...
                   9          0       9*width*ea2         21          0
21*width*ea2;...
                 -2*l         0    -2*l*width*ea2       -3*l          0    -
3*l*width*ea2;...
             10*width*ea1  0        10*width*aa       20*width*ea1   0
20*width*aa];

% ==== CL0 component ==================

  FA= -l/60*q*width*Cla;

  Fa0= FA*alpha0*[ 30;...
                   5*l;...
                   30*width*ea1;...
                   30;...
                   -5*l;...
                   30*width*ea1];
% -------------------------------------
 Mae=0;
```

Indexing

```
function [index]=fedofndx(iel,nnel,ndof)

edof = nnel*ndof;
start = (iel-1)*(nnel-1)*ndof;
%
for i = 1:edof
    index(i) = start+i;
end
```

Matrix Assembly

```
function [k]=mxasmbl(k,ke,ndx)
%-------------------------------------------------------
%  Purpose:
%     Assembly of element matrices into the system matrix
%
%  Synopsis:
%     [k]=mxasmbl1(k,ke,ndx)
%
%  Variable Description:
%     k   - system matrix
%     ke  - element matri
%     ndx - d.o.f. vector associated with an element
%-------------------------------------------------------


 edof = length(ndx);
 for i=1:edof;
   ii=ndx(i);
   for j=1:edof
     jj=ndx(j);
     k(ii,jj)=k(ii,jj)+ke(i,j);
   end
 end
```

Vector Assembly

```
function
[mxps,ELs,AFs,Fas]=mxasmbl1D(mxps,ELs,AFs,Fas,mxpm,ELe,AFe,Fae,ndx)
%-------------------------------------------------------
%  Purpose:
%     Assembly of element matrices into the system matrix
%
%  Synopsis:
%     [k]=mxasmbl1(k,ke,ndx)
%
%  Variable Description:
%     k   - system matrix
%     ke  - element matri
%     ndx - d.o.f. vector associated with an element
```

```matlab
%---------------------------------------------------------



 edof = length(ndx);
 for i=1:edof;
     ii=ndx(i);
%    Mxps(ii);
   %for j=1:edof
    %  jj=ndx(j);
     mxps(ii)=mxps(ii)+mxpm(i);
     ELs(ii) =ELs(ii)+ELe(i);
     AFs(ii) =AFs(ii)+AFe(i);
     Fas(ii) =Fas(ii)+Fae(i);
   %end
end
```

Control Matrix Reduction

```matlab
function                                       [KCa,CCa,MCa,mxpa,Faa,Ba]=
mxred(KCs,CCs,MCs,mxps,Fas,Bs,nsndx,sndof,nel)



sndof;
nsndx;
for i=1:sndof
    for j=1:sndof
        KCa(i,j)=KCs(nsndx(i),nsndx(j));
        CCa(i,j)=CCs(nsndx(i),nsndx(j));
        MCa(i,j)=MCs(nsndx(i),nsndx(j));
    end
    mxpa(i,1)=mxps(nsndx(i),1);
    Faa(i,1) =Fas(nsndx(i),1);

    for jj =1:nel
        Ba(i,jj)=Bs(nsndx(i),jj);
    end
end
```

LQR Control (Matlab™ Library)

```matlab
function [G,S]=felqr(A,B,Q,R);
%-----------------------------------------------------------------------
----------------
%  Purpose:
%     The function subroutine felqr.m calculates the feedback gain matrix
by
%     Linear Quadratic Regulator(LQR) technique. The given system is
%
%                        xdot = Ax + Bu,     u = -Gx
%
%     and the cost function to be minimized is defined as
%
%                    J=(1/2)integral(x^TQx+u^TRu)dt
%  Synopsis:
```

```matlab
%       [G,S]=flqr(A,B,Q,R)
%
%  Variable Description:
%      Input arguments   - A, B, Q, R
%      Output parameters - G = R^G^TS : feedback gain matrix
%                          S : Solution of the Algebraic Ricatti Equation
(ARE)
%                                  AS+A^TS-SBR^S+Q=0
%  Notes:
%      i) (A,B) should be controllable.
%      ii) Q is at least positive semi-definite.
%          R is at least positive definite.
%-----------------------------------------------------------------------
---------------


H=[A -B*inv(R)*B';                              %  Build the Hamiltonian
matrix
   -Q         -A'];

[V,D]=eig(H);                                   %  Solve eigenvalue problem

n=size(A); twon=max(size(H));


% Normalized each eigenvector to unity magnitude

av=abs(V);
magav=av'*av;

dmagav=diag(magav);

V=V*sqrt(inv(diag(dmagav)));                     %   Normalize the
eigenvector
%-----------------------------------------------------------------------
-----------------
%  Sort the eigenvalues with stable real parts
%-----------------------------------------------------------------------
-----------------

rel=real(diag(D));

nindex=[];pindex=[];

for i=1:twon

if(rel(i)<=0)
nindex=[nindex i];
else
pindex=[pindex i];
end

end

V=V(:, [pindex,nindex]);                         % Rearrange the eigenvector
order
```

```matlab
%------------------------------------------------------------------------
----------------
%    Compute the feedback gain matrix and Riccati Matrix
%------------------------------------------------------------------------
----------------

S=real(V(n+1:twon,n+1:twon)*inv(V(1:n,n+1:twon)));

G=real(inv(R)*B'*S);
%------------------------------------------------------------------------
----------------
```

Matrix Reduction

```matlab
function [KCa,CCa,MCa,mxpa,Faa]= mxred(KCs,CCs,MCs,mxps,Fas,nsndx,sndof)


sndof;
nsndx;
for i=1:sndof
    for j=1:sndof
        KCa(i,j)=KCs(nsndx(i),nsndx(j));
        CCa(i,j)=CCs(nsndx(i),nsndx(j));
        MCa(i,j)=MCs(nsndx(i),nsndx(j));
    end
    mxpa(i,1)=mxps(nsndx(i),1);
    Faa(i,1) =Fas(nsndx(i),1);

end
```

State Space EoM's

```matlab
% ==== Integration ====
function xdot=stsp_xdot(cur_time,x)
global mxSMD mxM vectQ Mxpa Qa AFa

xdot = mxSMD*x+mxM*Qa-mxM*Mxpa-mxM*AFa;
```